MHD IN DIVERGENCE FORM: A COMPUTATIONAL METHOD FOR ASTROPHYSICAL FLOW

Thesis by
Maurice H.P.M. van Putten

In Partial Fulfillment of the Requirements
for the Degree of
Doctor of Philosophy

California Institute of Technology
Pasadena, California
1992
(Defended May 18, 1992)

To my parents

Acknowledgement

It is a great pleasure to thank Professor E. Sterl Phinney for the opportunity to work in Theoretical Astrophysics. The academic freedom granted under his supervision allowed for the liberty to the pursuit of the ideas as outlined in this thesis.

I am greatly indebted to Applied Mathematics for their computational support and for their stimulating environment without which this work would not have been possible. I also would like to express much gratitude to Professor S.-T Yau, Professor Kip S. Thorne and Professor A.T. de Hoop for their interest and encouragement in my work. I would also like to give special mention to Professor Tim de Zeeuw, Dr. Tasso J. Kaper and Professor John Hawley for very stimulating discussions in the early stages of this work, and to Professor Eusebius Doedel for his support in the very last stage of this work.

I am delighted to thank my parents for all of their continued support. Their optimistic views have always been very encouraging which contributed much to this result. I am very greatful to my friend Linda Ji for all of her encouragement and insight during many stages of this work. I have been fortunate to have met Petr Pich who encouraged me wisely to engaging in numerous activities which made my studies much more pleasant and fruitful. Their input has been truly generous and left a clear mark on this thesis.

This research was supported through grants from NSF, AST 84-51725, and NASA, NAGW-2394.

Abstract

The equations of MHD in curved space-time are presented in divergence form for the purpose of numerical implementation. This result follows from a covariant divergence form of the single fluid theory of electro-magneto-hydrodynamics in curved space-time with general constitutive relations.

Some one- and two-dimensional shock computations are given. A pseudo-spectral method with weak smoothing is used in all of our computations. The pseudo-spectral method is constructed by consideration of Riemann problems in one dimension. The power of MHD in divergence form is brought about by using uniform grid-spacing and explicit time-stepping. The problems considered are shock-tube problems in transverse MHD with analytical comparison solution and a coplanar Riemann problem as discussed for nonrelativistic MHD in Brio and Wu [37]. In a limit of nonrelativistic velocities comparison is made of the results of the latter with those in [37]. In two dimensions cylindrically symmetric problems are considered for test of isotropy, independence of coordinate system and convergence (using comparison results in polar coordinates). We conclude with a computation of a shock induced vortex in jet flow with $\Gamma \approx 2.35$, a relativistic jet computation with $\Gamma \approx 3.25$ and, finally, computations on magnetic pressure dominated stagnation points in a 2D shock problem in nontransverse MHD.

This work is proposed for numerical study of astrophysical flows, and in particular as a "vehicle" towards the origin of jets.

Contents

List of Figures

List of Tables

Chapter 1

Introduction

Today's radio astronomy has provided us with detailed images of jet flow near active galactic nuclei (AGN). These images resolve jets on the kiloparsec scale and less using aperture synthesis, *e.g.* Westerbork and Merlin, and very long baseline interferometry (VLBI) techniques. The radio emission from these flows is portrayed with remarkable detail. Jets appear to provide energy transport from AGN to remote lobes and "hot spots" (see, *e.g.* [47]). The observed synchrotron radiation is believed to come mainly from particles accelerated in shocks in the jets. Furthermore, jets are subject to nonlinear instabilities which tend to form shocks and eddies which are suggested by their radio images.

AGN with dual opposing jets constitute the classical double radio sources. Fanaroff and Riley classified these sources according to their intensity in Class I and Class II sources, the second class containing the stronger sources ($> 10^{25}$W/Hz at 178 MHz) [14]. The source 3C273 forms an apparent exception with a single jet-lobe structure emanating from a bright quasar. Jets propagate as a beam of high-energy particles through the interstellar or in-

tergalactic medium over large distances (kiloparsecs). In FR II sources the jets terminate largely by thermalization in the radio lobe, while jets in FR I sources also appear to lose much of their energy in the propagation process. In FR II sources, the jet is believed to terminate either through a strong shock or dissipative magnetic reconnection (see, *e.g.*, [39] and references therein). The energy thus extracted from the nucleus may well exceed the luminosity of the nucleus by one order of magnitude. Moreover, the energy carried away by the jet may exceed the external energy obtained through accretion [21]. It follows that the energy transported away by jets is intrinsic energy of the nucleus in some cases. This *energy extraction problem* and the collimation of jets have become pressing issues in Astrophysics.

Numerical simulations have become a viable tool in understanding these unsteady, nonlinear flows. Current large scale simulations are being performed in the approximation of nonviscous and nonrelativistic fluids. The presence of magnetic fields is accounted for by taking the limit of magnetohydrodynamics (MHD). These simulations have been highly successful in the study of propagation of jets [39]. The origin is one of the most speculative aspects of jets, as it lies below the resolution of current observations. It is also of considerable interest, because generation of jets may actually be a signature of general relativistic effects as can expected near very compact objects such as black holes [21]. Most jets are believed to be relativistic to ultra-relativistic near the origin on the parsec scale and less. This has made quantitative simulations so far prohibitively difficult, as it requires numerical implementation of the equations of general relativistic MHD. Successful

numerical implementation of the equations of general relativistic MHD may well be regarded as a "vehicle" towards the origin of jets.

The preceding discussion forms the motivation for the formulation of the problem in this thesis as follows.

SEEK: *A computational method for simulation of MHD flow in the presence of shocks and in the presence of a general background metric. The method is to be consistent in the sense of extending nonrelativistic simulations and preserving divergence free magnetic fields.*

This thesis describes a formulation of the equations of fully relativistic MHD which is amenable to numerical implementation. The theory of MHD describes a hyperbolic system of equations. From classical computational fluid dynamics we may learn that a divergence formulation constitutes a good starting point for numerical implementation. Taking this strategy, we are led to seek a divergence form of relativistic MHD. We begin by introducing a formulation of electrodynamics of moving matter with general constitutive equations on hyperbolic Riemannian manifolds in divergence form. This work is based on the formulation of Lichnerowiz [6]. His formulaton of the initial value problem for electrodynamics of moving matter in curved space-time is a mixed partial differential-algebraic system of equations. The algebraic equations form the well-known constraints on the electric and magnetic field. These constraints impose the condition that in the rest frame of the fluid the electromagnetic fields are purely spatial and contain no time component. We will show

Theorem 1.0.1 *Maxwell's equations in general media can be reformulated*

in covariant form as a system of divergence equations without constraints.

This is the main result of Chapter 2. We use this theorem to formulate MHD in divergence form. This formulation of Maxwell's equations allows for further analytical analysis of hyperbolicity for single fluid theories in some generality. A covariant expression for the characteristic determinant, whose roots are the characteristic eigenvalues, is derived. This expression is of some interest in the analysis of discretized versions of these equations, as they arise in numerical implementations. The special case of locally adiabatic ideal magneto-hydrodynamics is of main interest in numerical applications. A first numerical study of this divergence formulation of Maxwell's equations is performed in the problem of ultra-relativistic wave-breaking. An analytical comparison solution for simple waves of one-dimensional transverse magneto-hydrodynamics is derived for the purpose of an exact error analysis. The results are presented with $\Gamma \approx 8$. Using leapfrog time-stepping on a uniform grid the results are obtained with second order accuracy.

MHD flows of astrophysical interest are especially those in which shocks occur. Computation of the entropy change in shocks in a shock capturing scheme requires a correct formulation of the energy equation. We will show

Theorem 1.0.2 *The equations of locally adiabatic ideal magneto- hydrodynamics including the flux-freezing constraint (MHD) can be stated in divergence form with the property that the standard jump conditions across surfaces of discontinuity for this system are the physical jump conditions of conservation of energy-momentum, baryon number and those of Maxwell's equations.*

Together with the description of a pseudo- spectral method for its numerical implementation, this is the main result of Chapter 3. We emphasize that in the limit of zero magnetic field, this theorem yields a divergence formulation of relativistic hydrodynamics which may be competitive with existing formulations of relativistic hydrodynamics.

The evolution of MHD flow in the presence of shocks is considered first in one-dimensional coplanar shock tube problems in flat space-time. The computations are performed using a pseudo-spectral method. This pseudo-spectral method is a weak smoothing method in that its smoothing operator is effectively a small perturbation of the identity (its transfer function is real and bounded below by 0.80). The method is studied in transverse MHD by an exact error analysis. In transverse MHD we compare numerical to analytical results in a restricted class of shock-tube problems. The implementation is then applied in various ways. The relativistic generalization of Brio and Wu's coplanar Riemann problem of classical MHD is computed and in the limit of nonrelativistic velocities the results are compared with those in [37]. This coplanar Riemann problem is studied also in the limit of a small and vanishing longitudinal magnetic field. The results illustrate that strong transverse flow may occur in the order of the strength of the transverse magnetic field, even when the longitudinal magnetic field becomes arbitrarily small (the limit of small longitudinal magnetic field constitutes a singular limit of coplanar MHD; see, *e.g.* [50] for a recent discussion in nonrelativistic MHD). Furthermore, the stability of the shock in compound waves in the relativistic version of Brio and Wu's coplanar Riemann problem is studied. A perturbed

coplanar Riemann problem is considered, and some tentative indications on this shock being slow and no longer intermediate (as it is in the classical case) are found. As this analysis takes us also to the limits of our implementation, these conclusions are to be considered tentative and suggestive for further study. Finally, some comments on numerical evaluation of the intermediate shocks in classical MHD are made.

We continue to demonstrate MHD in divergence form in two spatial dimensions. An extension of the 1D numerical method mentioned above enables us to compute 2D shock problems in relativistic MHD. Several problems are considered. The purpose of these examples is two-fold: to test the 2D implementation of the numerical scheme and to illustrate some aspects of jet flow as these can be expected to arise in astrophysical applications. In cylindrically symmetric problems, tests of isotropy, independence of coordinate system, and convergence are considered. We further present a calculation of a shock induced vortex in flow with $\Gamma \approx 2.35$, an ultra-relativistic jet simulation in slab geometry with $\Gamma \approx 3.25$ and calculations on magnetic pressure dominated stagnation points in 2D shock problems in nontransverse MHD. The latter problem further illustrates that the magnetic field is preserved divergence free in higher dimensions.

We conclude this introduction with stating MHD in divergence form as we propose this for numerical implementation:

$$
\begin{aligned}
&\nabla_a T^{ab} = 0, \\
&\nabla_a (u^{[a} h^{b]} + g^{ab} c_1)(U) = 0, \\
&\nabla_a (r u^a) = 0, \\
&\nabla_a \{(u^c u_c + 1)\xi^a\} = 0.
\end{aligned}
$$

Its meaning will become clear as the reader travels along his/her time-like world-line through this thesis.

Chapter 2

MAXWELL'S EQUATIONS IN DIVERGENCE FORM

(Appeared in *Communications of Mathematical Pysics*, 141:63-77, 1991, as "Maxwell's Equations in Divergence Form for General Media with Applications to MHD.")

2.1 Introduction

Maxwell's equations appear in a wide variety of problem settings in general relativity. We will consider them as they appear in general relativistic formulations of electro-magneto-fluid problems. They appear in their natural form as an underdetermined system of divergence equations. Lichnerowicz [7] showed that implementation of constitutive relations of a particular medium yields a pair of scalar constraints. Thus, electromagnetic fields in general media are determined completely by a mixed partial differential-algebraic system of equations.

Numerical treatment of electro-magneto-fluid problems by standard meth-

ods requires these problems to be formulated as a system consisting purely of partial differential equations with no constraints. Of course, the constraints as they appear in Lichnerowicz's formulation are avoided when taking the electromagnetic field variables as 3-vectors (cf. [16, 32]). The electromagnetic fields in general media are then determined by a quasi-linear system of differential equations in an explicit space-time split.

In this paper, we will show that the constraints from Lichnerowicz's formulation can become conserved quantities in a new system of partial differential equations in which the electromagnetic field variables remain 4-vectors. Thus, we will arrive at a system consisting purely of partial differential equations with no constraints. We will show

Theorem 1 *Maxwell's equations in general media can be reformulated in covariant form as a system of divergence equations without constraints.*

Theorem 1 enables us to formulate general electro-magneto-fluid problems as hyperbolic systems in divergence form. The divergence form is well-known to be a good starting point for numerical implementation. Advanced numerical methods have been developed in classical fluid dynamics for hyperbolic systems of this form. Theorem 1 thus allows general electro-magneto-fluid problems to be approached numerically by existing numerical methods from computational fluid dynamics (see, e.g., [48]). In divergence form, it now also becomes possible to treat electro-magneto-fluid problems numerically in the weak formulation. It is well-known that weak formulations of systems in divergence form uniquely determine the jump conditions across shocks (cf. [24]). The shock structure of Maxwell's solutions in the new formulation will

be discussed in detail.

To illustrate this theorem from an analytical perspective, we apply it to the classical MHD problem and show that MHD can be reformulated as a system of divergence equations without constraints. In this form, the MHD problem can now be treated numerically by any of the standard numerical methods from classical fluid dynamics.

The Theorem also allows for a general formulation of the problem of characteristics for a large class of electro-magneto-fluid problems. The associated questions of hyperbolicity and wave structure are central in relativistic magneto-fluid dynamics [57, 58, 6, 7, 8] [2, 1, 31]. Our Theorem permits us to formulate this problem of characteristics in terms of vector fields and scalars. We derive a general expression for the characteristic form of the associated system of partial differential equations.

To illustrate this approach, we show how the principle of covariance imposes the general structure on the infinitesimally small wave equations in MHD.

In Section 2, we prove the Theorem, and in Section 3 we discuss the shock structure of the new formulation. In Section 4, we reformulate MHD as a system in divergence form. We present our general theory of characteristics in Section 5. Our derivation of characteristics for MHD is discussed in Section 6, and our numerical study of ultra-relativistic wave breaking is presented in Section 7.

2.2 Maxwell's equations in divergence form

In this section we prove our Theorem, showing that Maxwell's equations in general media can be written in divergence form without constraints. Maxwell's equations can be stated in terms of a pair of divergences of 2-forms $\boldsymbol{H}$, the electric field-magnetic induction tensor, and $\boldsymbol{G}$, the electric induction-magnetic field tensor, [7] as

$$\begin{aligned} \nabla^a * H_{ab} &= 0, \\ \nabla^a G_{ab} &= -j_b, \end{aligned} \tag{2.1}$$

where $\boldsymbol{j}$ is the electric current 1-form. Here, $*$ denotes the Hodge star operator defining the dual $*\boldsymbol{\alpha}$ of a p-form $\boldsymbol{\alpha}$ on an n-dimensional Riemannian manifold as

$$*\alpha_{i_1 \ldots i_{n-p}} \equiv \frac{1}{p!} \alpha^{j_1 \ldots j_p} \epsilon_{j_1 \ldots j_p i_1 \ldots i_{n-p}},$$

where ϵ is the Levi -Civita tensor. Throughout this paper we use the convention that roman indices run from 0 to 3. The constitutive relations for a medium yield two scalar constraints. Before proceeding to prove the Theorem, we show how these constraints arise.

In a medium with velocity four-vector $\boldsymbol{u}$, we have [1]

$$(e_a, b_a) := (u^b H_{ab}, -u^b * H_{ab}), \tag{2.2}$$

$$(d_a, h_a) := (u^b G_{ab}, -u^b * G_{ab}) \tag{2.3}$$

for the electric field, $\boldsymbol{e}$, magnetic induction, $\boldsymbol{b}$, electric induction, $\boldsymbol{d}$, and magnetic field, $\boldsymbol{h}$, respectively. We remark that as a consequence of the

[1] Eqs. (2.2)-(2.3) and (2.6)-(2.7) contain sign corrections to those in *Comm. Math. Phys.*, 141, 63-77, 1991.

antisymmetry of $\boldsymbol{H}$ and $\boldsymbol{G}$, we have the algebraic identities

$$u^b e_b = u^b h_b = 0, \tag{2.4}$$

$$u^b d_b = u^b b_b = 0. \tag{2.5}$$

The 2-forms $\boldsymbol{H}$ and $\boldsymbol{G}$ can now be expressed as [7, 9]

$$\boldsymbol{H} = \boldsymbol{u} \wedge \boldsymbol{e} + *(\boldsymbol{u} \wedge \boldsymbol{b}), \tag{2.6}$$

$$\boldsymbol{G} = \boldsymbol{u} \wedge \boldsymbol{d} + *(\boldsymbol{u} \wedge \boldsymbol{h}). \tag{2.7}$$

Here, the velocity four-vector $\boldsymbol{u}$ actually enters as its dual one-form, but we will not make this explicit.

Thus, Maxwell's equations are a set of evolution equations for the family of tensor fields $U = (\boldsymbol{e}, \boldsymbol{d}, \boldsymbol{h}, \boldsymbol{b}, \boldsymbol{u}, \boldsymbol{g}, q)$ with given $\boldsymbol{g}$, where $\boldsymbol{g}$ is the metric. The scalar variable q (which corresponds to the electric charge density) arises as an extra degree of freedom so that the following familiar relationship holds:

$$0 \equiv d^2 * \boldsymbol{G} = d * \boldsymbol{j}. \tag{2.8}$$

Here, d denotes the exterior derivative. We remark that there can be no confusion between the d for the exterior derivative and that for the electric induction, because the latter always explicitly appears as a tensor.

In this form, Maxwell's equations can be closed by local constitutive relations of the form

$$\begin{aligned} \boldsymbol{d} &= \tilde{\boldsymbol{d}}(\boldsymbol{e}, \boldsymbol{h}, \boldsymbol{u}, \boldsymbol{g}, q), \\ \boldsymbol{b} &= \tilde{\boldsymbol{b}}(\boldsymbol{e}, \boldsymbol{h}, \boldsymbol{u}, \boldsymbol{g}, q), \\ \boldsymbol{j} &= \tilde{\boldsymbol{j}}(\boldsymbol{e}, \boldsymbol{h}, \boldsymbol{u}, \boldsymbol{g}, q) \end{aligned} \tag{2.9}$$

with $\partial\tilde{\boldsymbol{j}}(U)/\partial q \neq 0$ and such that the identities

$$u^a \tilde{d}_a(U) = u^a \tilde{b}_a(U) = 0 \tag{2.10}$$

hold as algebraic implications of (4). For example, in the familiar case of linear, isotropic media this reduces to

$$\tilde{\boldsymbol{d}}(U) = \epsilon \boldsymbol{e}, \quad \tilde{\boldsymbol{b}}(U) = \mu \boldsymbol{h}, \tag{2.11}$$

where ϵ is the electric permittivity and μ is the magnetic permeability. Furthermore, using the fact that $\boldsymbol{u}$ is nowhere vanishing, it is consistent to take

$$\tilde{\boldsymbol{j}}(U) = q\boldsymbol{u} + \sigma \boldsymbol{e} \tag{2.12}$$

with σ as the electric conductivity. In this case, q is precisely the electric charge density.

As a result, Maxwell's equations are stated as a set of evolution equations for $V = (\boldsymbol{e}, \boldsymbol{h}, q)$ (and $\boldsymbol{u}$) in the family variables $U = (V, \boldsymbol{u}, \boldsymbol{g})$ as a mixed partial differential-algebraic system of equations as [7]

$$\begin{cases} \nabla^a {*H}_{ab}(U) = 0, \\ \nabla^a G_{ab}(U) = -\tilde{j}_b(U), \\ c_1(U) := u^a h_a = 0, \\ c_2(U) := u^a e_a = 0. \end{cases} \tag{2.13}$$

This comprises a set of 10 equations for the 9 variables V. In the degenerate case of MHD when the medium is linear, isotropic with σ infinite, this reduces to

$$\begin{cases} \nabla^a u_{[a} b_{b]} = 0, \\ u^a b_a = 0, \end{cases} \tag{2.14}$$

in view of $\boldsymbol{e} \equiv \boldsymbol{d} \equiv 0$. This comprises a set of five equations for the four unknowns $\boldsymbol{b}$.

The sets of equations above evidently consist of systems of the type

$$K : \begin{cases} \nabla^a \omega_{ab} = j_b, \\ c = 0, \end{cases} \tag{2.15}$$

where ω is a 2-form, $\boldsymbol{j}$ is a 1-form, and $c = 0$ forms a scalar constraint. Now consider a Cauchy-problem for K on a smooth space-like hypersurface Σ in a hyperbolic Riemannian space $(\mathbf{M}, \boldsymbol{g})$ with given metric $\boldsymbol{g}$. Cauchy-data for K must satisfy a compatibility condition. This can be made precise as follows. Let $\boldsymbol{\nu}$ be a unit vector field normal to Σ. Decomposing ∇ on the space-like Σ orthogonally as

$$\nabla_a = -\nu_a(\nu^c \nabla_c) + (\nabla_\Sigma)_a,$$

where ∇_Σ is interior to Σ, we can rewrite K on Σ as

$$-\nu^a(\nu^c \nabla_c)\omega_{ab} + (\nabla_\Sigma)^a \omega_{ab} = j_b.$$

Next, we observe that

$$\nu^a \nu^b (\nu^c \nabla_c)\omega_{ab} \equiv 0,$$

because $\boldsymbol{\omega}$ is antisymmetric. Therefore, the Cauchy-data on Σ must satisfy the two compatibility conditions

$$\begin{cases} \nu^b \{(\nabla_\Sigma)^a \omega_{ab} - \nu^b j_b\} = 0, \\ c = 0. \end{cases} \tag{2.16}$$

We have, in the context of classical $C^2(\mathbf{M})$ solutions,

Lemma 2.2.1 *A Cauchy- problem for K on Σ can be reformulated as a Cauchy-problem for*

$$K' : \begin{cases} \nabla^a(\omega_{ab} + g_{ab}c) = j_b, \\ \nabla^a j_a = 0 \end{cases} \tag{2.17}$$

on Σ with the same Cauchy-data in the sense that if a solution exists to one then it exists to the other and the solutions agree in the future domain of dependence of Σ.

Proof: Clearly, we need only show that a classical solution to the new formulation with Cauchy-data compatible with K yields a classical solution to the original K-formulation. We will do so by showing that c satisfies the canonical wave equation with vanishing Cauchy-data:

$$\begin{cases} \Box c = 0 & \text{in } D^+(\Sigma), \\ c = 0 & \text{on } \Sigma, \\ \nu^a \nabla_a c = 0 & \text{on } \Sigma. \end{cases}$$

Here, $\Box = g^{ab}\nabla_a\nabla_b$ is the Laplace-Beltrami wave operator [10], $D^+(\Sigma)$ denotes the future domain of dependence of Σ (cf. [38, 10]), and $\boldsymbol{\nu}$ is a vector field normal to Σ. This can be derived in two steps.

Step (a): Recall that for p-forms $\boldsymbol{\alpha}$ on Riemannian manifolds the following identity holds [15]

$$(p-1)!(-1)^{p+1} *^{-1} d * \boldsymbol{\alpha} = \nabla^a \alpha_{a i_1 \ldots i_{p-1}} \boldsymbol{dx}^1 \wedge \ldots \wedge \boldsymbol{dx}^{p-1}.$$

Consequently, we have

$$\nabla^b \nabla^a \omega_{ab} = *^{-1} d^2 * \boldsymbol{\omega} = 0.$$

Therefore, $\nabla^b j_b = 0$ implies

$$0 = \nabla^b\{\nabla^a(\omega_{ab} + g_{ab}c) - j_b\} = g^{ab}\nabla_a\nabla_b c \equiv \Box c.$$

Step(b): Now consider a classical solution to the new formulation with Cauchy-data on Σ which satisfy the compatibility conditions for K. Then using

$$\nabla_a = -\nu_a(\nu^c\nabla_c) + (\nabla_\Sigma)_a$$

as before, we have

$$\begin{aligned} 0 &= \nu^b\{\nabla^a(\omega_{ab} + g_{ab}c) - j_b\} \\ &= -\nu^b\nu^a(\nu^c\nabla_c)\omega_{ab} + \nu^b\{(\nabla_\Sigma)^a\omega_{ab} - j_b\} + \nu^b\nabla_b c \\ &= \nu^b\nabla_b c, \end{aligned}$$

because ω is antisymmetric.

Together, Step (a) and Step (b) show that c satisfies the wave equation with vanishing Cauchy-data. This forces $c \equiv 0$ in $D^+(\Sigma)$ (cf. [38, 10]), and the proof is complete. □

This allows us to obtain Maxwell's equations in precisely the number of variables in V, because the Lemma directly yields:

Theorem 2.2.1 *The equations of Maxwell can be reformulated as a system of divergence equations as*

$$\begin{cases} \nabla^a(*H_{ab} + g_{ab}c_1)(U) = 0, \\ \nabla^a(G_{ab} + g_{ab}c_2)(U) = -\tilde{j}_b(U), \\ \nabla^a\tilde{j}_a(U) = 0 \end{cases} \tag{2.18}$$

in the sense as described in the Lemma.

The constraints in Maxwell's equations have thus been given a conservative implementation. We emphasize that the new formulation imposes no compatibility conditions on the Cauchy-data on Σ. With arbitrary Cauchy-data we may construct solutions to the new formulation in which c is no longer vanishing. It is only when the compatibility conditions for K are satisfied that, as we have shown above, c will remain zero, and the solution will be a Maxwell's solution. In the case of a charged fluid a solution with $c_2(U) = u^a e_a \neq 0$ leads to forces along world lines. For this reason, solutions with $c_1, c_2 \neq 0$ will be regarded as nonphysical.

In this sense the new formulation features a larger class of solutions than the original formulation of Maxwell's equations. Therefore, a detailed discussion of Maxwell's solutions with shocks in the new formulation is required.

2.3 Shock structure

We will discuss the shock structure of the new formulation of Maxwell's equations in terms of K'. Consider a solution to K' which possesses a smooth, time-like shock surface S. Let $\boldsymbol{\nu}$ denote a vector field normal to S. Then the following jump conditions must hold

$$\begin{cases} 0 = \nu^a[\omega_{ab} + g_{ab}c] = \nu^a[\omega_{ab}] + \nu_b[c], \\ 0 = \nu^a[j_a]. \end{cases} \tag{2.19}$$

Here, $[f] = (f)^+ - (f)^-$ denotes the jump across S. Consequently,

$$0 = \nu^a \nu_a [c], \tag{2.20}$$

by antisymmetry of $\boldsymbol{\omega}$, and hence of $[\boldsymbol{\omega}]$. Since S is not null, it follows that

$$[c] = 0. \tag{2.21}$$

Thus, we obtain

Lemma 2.3.1 *The jump conditions for K across a smooth shock surface S,*

$$\begin{cases} \nu^a[\omega_{ab}] = 0, \\ \nu^a[j_a] = 0, \end{cases} \tag{2.22}$$

are preserved in the new formulation K'.

Now consider an open neighborhood Ω of S. Let Ω^- and Ω^+ denote the subregions of Ω lying at either side of S. Let $I^-(S)$ denote the chronological past of S (cf. [38]). We have

Lemma 2.3.2 *A solution to K' in Ω which satisfies K in Ω^- is a solution to K in $\Omega \bigcap I^-(S)$.*

Proof: We consider a solution to K' which is C^2 in each of Ω^+ and Ω^-, and which is C^1 in each of $\Omega^+ \bigcup S$ and $\Omega^- \bigcup S$. Notice that this forces

$$c \equiv 0 \text{ in } \Omega^-.$$

We will show that c satisfies the canonical wave equation with vanishing Cauchy-data in Ω^+:

$$\begin{cases} \Box c = 0 \text{ in } \Omega^+, \\ (c)^+ = 0 \text{ on } S, \\ \nu^a(\nabla_a c)^+ = 0 \text{ on } S. \end{cases}$$

Of course, we have already demonstrated in the proof of Lemma 2.3.1 that c satisfies the wave equation in Ω^+. It remains to derive the Cauchy-data. We will do so in two steps.

Step (a): From the discussion preceding Lemma 2.3.1, we have

$$0 = [c] = (c)^+ - (c)^- = (c)^+,$$

since $c \equiv 0$ in Ω^-.

Step (b): Decompose ∇ on S as

$$\nabla_a = \nu_a(\nu^c \nabla_c) + (\nabla_S)_a.$$

By Lemma 2.3.1 and smoothness of S, we have

$$0 = (\nabla_S)^a \nu^b [\omega_{ab}] = \nu^b (\nabla_S)^a [\omega_{ab}] + [\omega_{ab}](\nabla_S)^a \nu^b.$$

Let $\{x^\alpha\}_{\alpha=1}^3$ denote a coordinate system for Σ, and $\mathbf{e}_{(\alpha)} = \partial/\partial x^\alpha$. By Lemma 2.3.1, $\nu^a[\omega_{ab}] = 0$ so that

$$[\omega_{ab}](\nabla_S)^a \nu^b = [\omega_{\alpha\beta}] \nabla^\alpha \nu^\beta.$$

The symmetry of the extrinsic curvature tensor, $\mathbf{K}$, [15] in

$$-\nabla_\alpha \nu^\beta = \mathbf{K}(\mathbf{e}_{(\alpha)}, \mathbf{e}_{(\beta)})\boldsymbol{\nu}$$

further implies

$$[\omega_{\alpha\beta}] \nabla^\alpha \nu^\beta = 0.$$

We, therefore, have

$$\nu^b (\nabla_S)^a [\omega_{ab}] = 0.$$

This and the second jump condition from Lemma 2.3.1 together imply

$$\begin{aligned} 0 &= \nu^b (\nabla_S)^a [\omega_{ab}] - \nu^b [j_b] \\ &= \nu^b \{(\nabla_S)^a (\omega_{ab})^+ - (j_b)^+\} - \nu^b \{(\nabla_S)^a (\omega_{ab})^- - (j_b)^-\} \\ &= \nu_b \{(\nabla_S)^a (\omega_{ab})^+ - (j_b)^+\}, \end{aligned}$$

since the solution to K' is assumed to be a smooth solution to K in $\Omega^- \bigcup S$. Therefore, the solution to K' satisfies

$$\begin{aligned} 0 &= \nu^b\{\nabla^a(\omega_{ab} + g_{ab}c) - j_b\}^+ \\ &= \nu^b\{(\nabla_S)^a(\omega_{ab})^+ - (j_b)^+\} + \nu^b(\nabla_b c)^+ \\ &= \nu^b(\nabla_b c)^+, \end{aligned}$$

using the assumption that the solution to K' is C^1 in $\Omega^+ \bigcup S$. We remark that a proof for this result in a weak formulation can also be given.

Together, Step (a) and Step (b) show that c satisfies the canonical wave equation in Ω^+ with vanishing Cauchy-data. This forces $c \equiv 0$ in $\Omega \bigcap I^-(S)$ by Holmgren's Uniqueness Theorem (cf. [44]). □

We have therefore demonstrated

Proposition 2.3.1 *Maxwell's solutions are preserved across smooth shock surfaces in the divergence formulation of Theorem 2.1 in the sense as described in Lemma 2.3.2.*

2.4 MHD in divergence form

In this section, ideal MHD is formulated as a system of divergence equations with no constraints. Consider a perfectly conducting fluid with unit velocity four-vector $\boldsymbol{u}$ in a background with metric $\boldsymbol{g}$. The fluid is described by a stress-energy tensor [12]

$$\boldsymbol{T}^M = rf\boldsymbol{u} \otimes \boldsymbol{u} + P\boldsymbol{g}, \tag{2.23}$$

where r is the proper restmass density, f is the specific enthalpy and P is the fluid pressure. Physically, f appears as $f = f(r, S)$ with entropy S. However, one usually takes $r = r(f, S)$ in view of

$$dP = rdf - rTdS \tag{2.24}$$

as the implicit definition of the temperature T. The electromagnetic field is described by

$$\boldsymbol{T}^{EM} = \boldsymbol{b}^2(\boldsymbol{u} \otimes \boldsymbol{u} + \boldsymbol{g}/2) - \boldsymbol{b} \otimes \boldsymbol{b}, \tag{2.25}$$

where $\boldsymbol{b}$ is the magnetic induction. Write

$$\boldsymbol{T} = \boldsymbol{T}^{M} + \boldsymbol{T}^{EM} \tag{2.26}$$

for the total stress energy tensor. The standard governing equations for MHD comprise a mixed partial differential-algebraic system of equations of the form [57, 7, 8, 36]

$$\begin{cases} \nabla^a T_{ab} = 0, \\ \nabla^a u_{[a} b_{b]} = 0, \\ \nabla^a (r u_a) = 0, \\ u^a \nabla_a S = 0, \\ u^a b_a = 0, \\ u^a u_a = -1. \end{cases}$$

It is well known that $u^a u_a = -1$ is conserved along streamlines, so that MHD is a problem with essentially one constraint: $u^a b_a = 0$. Anile and Pennisi [36] reformulated this standard form of MHD as a quasi-linear system of partial differential equations. They obtained their result by a detailed study of the equations. However, their final system is not in divergence form.

Our Theorem allows us to obtain:

Corollary 2.4.1 *The equations of ideal MHD can be reformulated as a system of divergence equations without constraints as*

$$\begin{cases} \nabla^a T_{ab} = 0, \\ \nabla^a (u_{[a} b_{b]} + g_{ab} u^c b_c) = 0, \\ \nabla^a (r u_a) = 0, \\ \nabla^a (r S u_a) = 0 \end{cases} \tag{2.27}$$

in the sense as described in the Lemma.

In this form, MHD may now be treated numerically by any of the standard numerical methods for hyperbolic systems in divergence form. To illustrate one of its analytical aspects, we will show that this formulation will naturally yield the well-known characteristics for MHD. To this end, we first put the problem of characteristics in a more general setting.

2.5 A covariant formulation of characteristics

A large class of electro-magneto-fluid problems in general relativity can be formulated in terms of a family of tensor fields $U = (a^1, \cdots, a^p, \boldsymbol{u}^1, \cdots, \boldsymbol{u}^q, \boldsymbol{g})$ which consists entirely of scalars $a^i \in \mathcal{T}^0_0(\mathbf{M})$, vector fields $\boldsymbol{u}^j \in \mathcal{T}^1_0(\mathbf{M})$ and a hyperbolic metric $\boldsymbol{g} \in \mathcal{T}^0_2(\mathbf{M})$. Here, $\mathcal{T}^{r_i}_{s_i}(\mathbf{M})$ are the tensor fields of type (r_i, s_i) on a four-dimensional manifold $\mathbf{M}$. Our Theorem enables us to formulate Maxwell's equations as a system consisting only of partial differential equations with no constraints. For this reason, the class of problems that we will discuss are those for which the evolution equations for a subset $V = (a^1, \cdots, a^{p'}, \boldsymbol{u}^1, \cdots, \boldsymbol{u}^{q'})$ $(p' \leq p, q' \leq q)$ of U can be expressed in the

general form

$$A(U;\nabla)V = f(U). \tag{2.28}$$

Here, $A(U;\nabla) : \mathcal{Y}(\mathbf{M}) := (\mathcal{T}^0_0(\mathbf{M}))^{p'} \times (\mathcal{T}^1_0(\mathbf{M}))^{q'} \to \mathcal{Y}(\mathbf{M})$ is a local, first order quasi-linear differential operator and $f(U)$ is local in V.

The problem of characteristics can be stated in terms of a Cauchy-problem in an open neighborhood $\mathcal{N}(\Sigma)$ of a 3-dimensional initial manifold Σ with prescribed Cauchy-data U^0 as

$$C : \begin{cases} A(U;\nabla)V = f(U) & \text{in } \mathcal{N}(\Sigma), \\ U = U^0 & \text{on } \Sigma. \end{cases} \tag{2.29}$$

The initial hypersurface Σ is now said to be characteristic whenever U^0 on Σ and $U' = (\boldsymbol{u}^{q'+1}, \cdots, \boldsymbol{u}^q, \boldsymbol{g})$ in $\mathcal{N}(\Sigma)$ do not suffice to obtain V away from Σ into $\mathcal{N}(\Sigma)$. We will study this problem pointwise in $\mathbf{M}$ as a function of the orientation of nonnull Σ in $(\mathbf{M},\boldsymbol{g})$. The case when Σ is null is excluded specifically. Null-characteristic hypersurfaces form an intricate problem that we will not touch upon here. For this problem we refer to Muller zum Hagen and Seifert [59] and references therein.

Nonnull characteristics can be defined as follows. We first decompose ∇ as $\nabla_a = \pm\nu_a(\nu^c\nabla_c) + (\nabla_\Sigma)_a$ on Σ, depending on whether Σ is time-like (+) or space-like (-). We obtain C in "Cauchy-Kowalewski" form on Σ as:

$$\pm A(U^0;\boldsymbol{\nu})(\nu^a\nabla_a)V + A(U^0;\nabla_\Sigma)V = f(U). \tag{2.30}$$

The characteristic hypersurfaces are then defined by nonnull $\boldsymbol{\nu}$ such that $A(U;\boldsymbol{\nu})(p)$ is not invertible as a map from the bundle $Y(p) := (T^0_0(p))^{p'} \times$

$(T_0^1(p))^{q'}$ into itself ($p \in \Sigma$). Let us use the standard covariant definition of the determinant of $A(U^0;\boldsymbol{\nu})(p)$ ([42], p. 79), det $A(U^0;\boldsymbol{\nu})(p)$, to define

$$(\det A(U^0;\boldsymbol{\nu}))(p) = \det A(U^0;\boldsymbol{\nu})(p) \ (p \in \mathbf{M}). \tag{2.31}$$

Thus, there exists a natural, covariant definition for the determinant of $A(U^0;\boldsymbol{\nu})$ as a scalar field on Σ. The condition for Σ to be characteristic therefore becomes

$$\det A(U^0;\boldsymbol{\nu}) = 0. \tag{2.32}$$

Such a scalar field possesses a very rigid dependence on its arguments. We have the following general representation for the characteristic form of (2.28)

Proposition 2.5.1 *Let U be as above. If $V = (a^1, \ldots, a^{p'}, \boldsymbol{u}^1, \ldots, \boldsymbol{u}^{q'})$ $(p' \leq p, q' \leq q)$ then*

$$det\ A(U;\boldsymbol{\nu}) = \sum a_{\mu_1 \ldots \mu_{q'}\gamma}(U)(u_a^1\nu^a)^{\mu_1} \ldots (u_a^{q'}\nu^a)^{\mu_{q'}}(\nu_a\nu^a)^{\gamma}, \tag{2.33}$$

where $\mu_1 + \ldots + \mu_{q'} + 2\gamma = p' + 4q'$ and the $a_{\mu_1 \ldots \mu_{q'}\gamma}(U)$ are local scalars in U.

A formal proof of this fact is not difficult but somewhat lengthy. We will merely remark that the basic mathematical ingredients are locality and the theorems of Stone-Weierstrass and Riesz. Using these, the proposition follows from invariance of the physics under diffeomorphisms $\phi : \mathbf{M} \to \mathbf{M}$. If ϕ^*

denotes the pull forward map associated with such ϕ, it suffices to consider the invariances

$$(i)\ \det A(U;\boldsymbol{\nu})(p) = \det A \circ \phi^*(U;\boldsymbol{\nu})(p), \qquad \phi(p) = p,$$
$$(ii)\ \det A(U;\boldsymbol{\nu})(p) = \det A \circ \phi^*(U;\boldsymbol{\nu})(\phi^{-1}(p)), \quad \nabla\phi(p) = \mathrm{id}.$$

The first invariance is known as scalar invariance and isotropy, and the second invariance is known as homogeneity.

We wish to emphasize the following. The set of zeros $\boldsymbol{\nu}_p \in \mathcal{T}^1_0(p)$ for which $A(U^0;\boldsymbol{\nu})(p)$ is singular is called the normal cone at $p \in \mathbf{M}$ [18]. This normal cone contains the normals to the characteristic hypersurfaces. These characteristic hypersurfaces carry the infinitesimally small amplitude waves. As such, these zeros must be invariant by the principle of covariance. Thus, if we somehow knew that the normal cone possesses a full set of N real sheets of zeros we could say that this suffices to establish the covariant expression (2.33), up to a nonzero factor. However, in the general case or, more importantly, in proving that the system possesses a full set of N real, spacelike sheets (algebraic hyperbolicity), we need to go through the full formal arguments above.

A system of partial differential equations is regular in the sense of Cauchy-Kowalewski if its characteristic form is not identically zero [15]. Systems involving Maxwell's equations (2.13) without incorporation of the constraints are not regular in this sense. Systems impose uniqueness, and, therefore, may be given a direct numerical implementation, only when regular in the sense of Cauchy -Kowalewski. It is easy to see that the divergence formulation (2.18) regularizes Maxwell's equations (2.13). This is also exemplified in Section 2.6.

The usefulness of such a general form lies in the possibility of *a priori* partial factorization by using elementary facts about the problem at hand. The problem can be considered in terms of blocks $A^{(i)}(U;\nabla)$ each corresponding to a specific subset of tensors from V. Considering these blocks individually, we can consider the rank of each of them. Usually, there will be one or more blocks with known degeneracies, *i.e.*, simple scalar conditions which imply a change in the rank of $A^{(i)}(U^0;\boldsymbol{\nu})$, and a vanishing of det $A(U^0;\boldsymbol{\nu})$. By Proposition 5.1, we can then arrive at a partial factorization of det $A(U^0;\boldsymbol{\nu})$. This will be illustrated in our treatment of ideal MHD. We will call this the method of *uncoupled factors*. This can result in a dramatic reduction of the characteristic determinant. This completes our covariant formulation of the problem of characteristics for problems of type C.

2.6 Infinitesimally small amplitude waves in MHD

The structure of the infinitesimally small amplitude waves will follow from the equations of the characteristics. The characteristics for MHD in Corollary 4.1 as given by Proposition 5.1 are in $V = (\boldsymbol{u}, \boldsymbol{b}, f, S)$ and $U = (V, \boldsymbol{g})$. The evolution of the metric $\boldsymbol{g}$ is described by Einstein's equations

$$\boldsymbol{G} = 8\pi \boldsymbol{T}, \tag{2.34}$$

where the Einstein tensor $\boldsymbol{G}$ depends on $\boldsymbol{g}$ (up to its second derivatives) only, while $\boldsymbol{T}$ is a function of all the tensor fields but none of its derivatives. Furthermore, in MHD only $\boldsymbol{g}$ and none of its derivatives appear. Thus, the

problem of characteristics for Einstein's equations is independent of that of MHD. We will consider the problem of characteristics of MHD only. Alternatively, we could say that we consider MHD in the background of a given, fixed metric.

By Proposition 5.1, we have in this case

$$\det A(U;\boldsymbol{\nu}) = D_N(U;\boldsymbol{\nu}) \equiv \sum \alpha_k(U)(u^a\nu_a)^{\nu_k}(b^a\nu_a)^{\mu_k}(\nu^a\nu_a)^{\gamma_k}, \qquad (2.35)$$

where $\nu_k+\mu_k+2\gamma_k = N$ with $N = 10$. Let us apply the method of uncoupled factors to partially factorize this polynomial in $\boldsymbol{\nu}$. Write $u^a\nabla_a S$ in Cauchy-Kowalewski form on a time-like hypersurface Σ as

$$u^a\nu_a(\nu^c\nabla_c)S + u^a(\nabla_\Sigma)_a S = 0. \qquad (2.36)$$

Thus, $(0,0,0,u^a\nu_a)$ implements $u^c\nabla_c S$ in $A(U;\boldsymbol{\nu})$. Clearly, its rank is zero whenever $u^a\nu_a = 0$. Notice that $\det A(U;\boldsymbol{\nu})$ is even in $\boldsymbol{b}$, and hence also in $\boldsymbol{u}$, by invariance under rotation about $\boldsymbol{u}$ ($\boldsymbol{b}$ is space-like, $\boldsymbol{u}$ is time-like and $u^a b_a = 0$). Indeed, if $\det A(u;\boldsymbol{\nu})$ were odd in $\boldsymbol{b}$, then in going from $\boldsymbol{b}$ to -$\boldsymbol{b}$ by rotation about $\boldsymbol{u}$ $\det A(U;\boldsymbol{\nu})$ would always have a zero, forcing this to be zero for all $\boldsymbol{b}$. But then $\det A(U;\boldsymbol{\nu})$ is also even in $\boldsymbol{b}$. From this we have $(u^a\nu_a)^2$ as a factor. Another uncoupled factor is $\nu^a\nu_a$ due to Maxwell's equations (see the proof of the Lemma). Thus, it must be that

$$\det A(U;\boldsymbol{\nu}) = (u^a\nu_a)^2(\nu^a\nu_a)D_6(U;\boldsymbol{\nu}). \qquad (2.37)$$

By the evenness of D_6 in $\boldsymbol{u}$ and $\boldsymbol{b}$ we have

$$D_6(U;\boldsymbol{\nu}) = R((u^a\nu_a)^2,(b^a\nu_a)^2,\nu^a\nu_a;U). \qquad (2.38)$$

But then R is a homogeneous cubic (in its first three arguments), so that

$$R = PQ, \tag{2.39}$$

where P is linear and Q is homogeneous quadratic. Clearly, each term in $\det A(U;\boldsymbol{\nu})$ contains $(u^a\nu_a)^i(b^a\nu_a)^j$ with $i+j \geq 4$, as follows by inspection of Maxwell's equations. We have, therefore,

$$\begin{aligned} P &= p_1(u^a\nu_a)^2 + p_2(b^a\nu_a)^2, & (2.40)\\ Q &= q_1(u^a\nu_a)^4 + q_2(u^a\nu_a)^2(b^a\nu_a)^2 + q_3(b^a\nu_a)^4 \\ &\quad + q_4(u^a\nu_a)^2(\nu^a\nu_a) + q_5(b^a\nu_a)^2(\nu^a\nu_a). & (2.41) \end{aligned}$$

A mere inspection of the equations now yields the full expressions for the coefficients p_i. It is easy to see that the block $A^{(1,2)}(U;\boldsymbol{\nu})$ in $A(U;\boldsymbol{\nu})$ associated with $(\boldsymbol{u},\boldsymbol{b})$ is of the form

$$A^{(1,2)}(U;\boldsymbol{\nu}) = \begin{bmatrix} (rf^2+b^2)u^a\nu_a & -b^a\nu_a + \boldsymbol{\omega} & * & * \\ \boldsymbol{b}\otimes\boldsymbol{\nu} - b^a\nu_a & u^a\nu_a - \boldsymbol{u}\otimes\boldsymbol{\nu} & * & * \end{bmatrix}, \tag{2.42}$$

where $\boldsymbol{\omega}$ is a linear combination of tensor products from $\boldsymbol{u}$, $\boldsymbol{b}$ and $\boldsymbol{\nu}$. Let $\boldsymbol{e} \neq 0$ such that $e^a u_a = e^a b_a = e^a \nu_a = 0$. Then $e^a\omega_{ab} = 0$. Consideration of $(\lambda\boldsymbol{e}, \mu\boldsymbol{e}, 0, 0)$ as a nullvector of $A^{(1,2)}(U;\boldsymbol{\nu})$ yields immediately

$$P(U;\boldsymbol{\nu}) = (u^a\nu_a)^2(rf+b^2) - (b^a\nu_a)^2. \tag{2.43}$$

The expression for Q is now obtained by straightforward identification, for example by using a symbolic manipulator. It is precisely here where Cauchy-Kowalewski regularity is essential and, also, proved. We have used Macsyma for this purpose and thus rederived the well-known result

$$\begin{aligned} Q(U;\boldsymbol{\nu}) = (f\partial r/\partial f - r)(u^a\nu_a)^4 - (r + b^2\partial r/\partial f r^{-1})(\nu^a\nu_a) \\ (u^a\nu_a)^2 + f^{-1}(\nu^a\nu_a)(b^a\nu_a)^2. \end{aligned} \tag{2.44}$$

We should mention in this context that Macsyma is actually able to give the full factorization at once, when the problem is stated in a specific frame of reference with ν variable. This is quite suprising, considering the fact that we are dealing here with a tenth order polynomial.

The characteristic condition (2.32) thus yields

Proposition 2.6.1 (Bruhat) *MHD possesses two kinds of waves,*

(i) Alfven waves : $P = 0$,
(ii) hydrodynamical waves : $Q = 0$.

It should be mentioned that Bruhat [57, 58] gave the general result with variable metric which includes gravitational waves. This result was derived from a detailed study of the differential equations. We wish to emphasize that the result is largely determined by the principle of covariance. This completes our discussion of waves in ideal MHD.

2.7 On the numerical implementation

An electro-magneto-hydrodynamic (EMHD) problem in a given background metric is completely described by Maxwell's equations and the equations of motion,

$$\nabla_a T^{ab} = f^b.$$

Here, T^{ab} is the stress-energy tensor and f^b is the force density four-vector. The divergence formulation of Maxwell's equations given in Theorem 1 thus enables us to formulate general EMHD problems as hyperbolic systems in divergence form.

A large class of numerical methods exists to treat problems in classical fluid dynamics for such systems in divergence form (see, e.g., [48]). Highly sophisticated schemes have been designed for the computation of solutions of problems in 1D and higher dimensions with shocks (see, e.g., [46, 43, 4, 19]). Our reformulation of EMHD problems to systems in standard form thus allows us to exploit existing numerical methods.

We will give a preliminary demonstration of this advantage below. We will discuss a 1D ultra-relativistic MHD problem until shocks form. We are currently working on a 2D EMHD problem, on which we expect to report in a subsequent paper.

2.7.1 An ultra-relativistic example

We have computed the wave breaking problem for isentropic, transverse MHD in flat space-time. Consideration of simple waves allows for an exact error analysis, since one can compare with an exact, analytical solution. It can easily be shown that the equations for simple waves may be cast in characteristic form as

$$(u^a \pm \alpha^{-1}\beta v^a)\nabla_a(\phi \pm \lambda) = 0,$$

where $u^a = (\cosh\lambda, \sinh\lambda, 0)$, $v^a = \mathrm{d}u^a/\mathrm{d}\lambda$, $\alpha^2 = r^{-1}f\mathrm{d}r/\mathrm{d}f$, $\beta^2 = (1 + k^2\mathrm{d}r/\mathrm{d}f)/(1 + k^2 r/f)$, $\phi(r) = \int^r \alpha^{-1}\beta r^{-1}$ and $k = h/r$, which is constant throughout the fluid. Recall that a monatomic relativistic gas is described by a polytropic equation of state,

$$P = Kr^\gamma,$$

with polytropic index γ between 4/3 (ultra- relativistic limit) and 5/3 (Newtonian limit). In the intermediate case of $\gamma = 3/2$, we find $\alpha^{-1}\beta(r) = \tanh \phi/4$ when $k = 1$ and $K = 2/3$.

Our numerical example concerns a fluid of this type with the Riemann invariant $J = \lambda + \phi$ constant throughout the fluid, and $\gamma = 3/2$. The characteristics along which the solution remains constant are then given by $\mathrm{d}x/\mathrm{d}t = \Lambda = \tanh(5\lambda/4 - J/4)$. With initial data $\lambda(x) = \lambda_0 + \lambda_1 \sin 2\pi x$, the breaking time is: $t_B = \inf(-\mathrm{d}\Lambda/\mathrm{d}x)^{-1}$ (see [41] for a general discussion on breaking times).

The divergence formulation of MHD can be implemented directly using the leapfrog Crank-Nicholson method, until the shock forms. This scheme has second order accuracy, provided that the solution remains smooth. Since the problem has been reformulated in standard form, we expect that the more advanced methods cited before will allow for the computation of solutions in the presence of shocks.

We have computed wave breaking problems in the Newtonian limit, in the relativistic case and in the ultra-relativistic case. We give here results only on the traditionally most difficult case, the ultra-relativistic wave breaking. Figure 2.1 shows the density and velocity distributions at the moment of breaking in a case when the Lorentz factor $\Gamma \approx 8$. Here, $\Gamma = 1/(1-v^2)^{1/2}$, where v is the maximum velocity. In Figure 2.1 the velocity of light is normalized to unity. These results have been obtained without any stabilization process. The numerical and analytical solutions agree to within less than the width of the lines in the figure. The performance of our numerical implemen-

tation is studied by the dependence of the results on the grid size Δt in time and the grid size Δx in space. The numerical solution is compared with the analytical solution in the supremum norm.

Our numerical results show that

(a) the scalar field $c_1 = u^c h_c$ remains identically equal to zero (there is not even a round-off error);

(b) the error in the conserved quantity h/r is in the order of machine round-off error ($\leq 10^{-9}$);

(c) the maximum error between the numerical solution and the analytical solution decays quadratically with grid size, in agreement with the second order accuracy of the numerical scheme. This is shown in Figure 2.2, where the evolution of the error is given for different numbers of grid points, n. This result holds true as long as the wave remains away from breaking. This error is also remarkably independent of $\eta = \Delta t/\Delta x$, $\eta \leq 1$, for velocities, v, satisfying $\Gamma \leq 10$. Significantly smaller timesteps are required for velocities with larger Γ.

In computations of Newtonian and relativistic wave breaking, the numerical results have been the same or better than as given in the observations (a)-(c) above.

Figure 2.2 also shows that for the leapfrog Crank-Nicholson method the error exhibits an exponential growth as a shock develops. The method of Orszag and Tang [48, 13] restores linear error growth away from the moment of breaking. However, this introduces initial errors and fails to reduce the error. It should be mentioned that in these computations the error in the

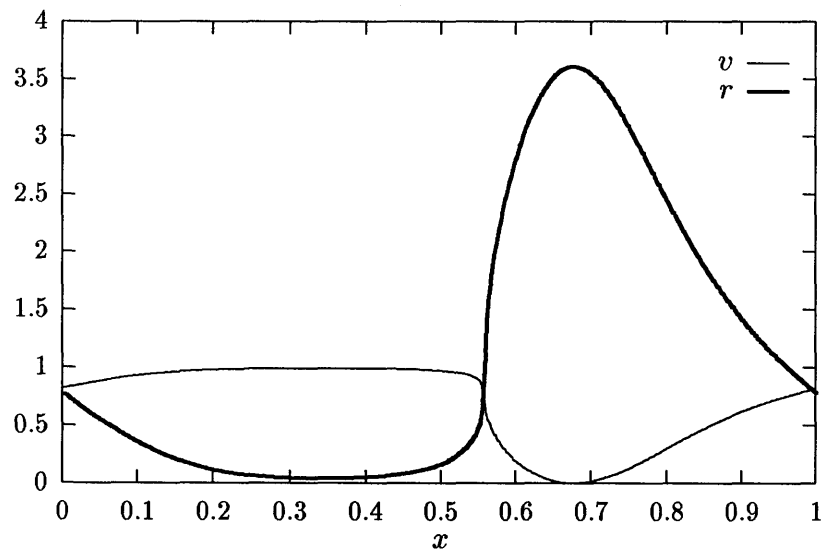

Figure 2.1: The velocity distribution, v, and density distribution, r, at the moment of breaking $t = t_B$. In this example, $\lambda_0 = \lambda_1 = 7/5$, $J = 4.5$ and $t_B = 0.0963$.

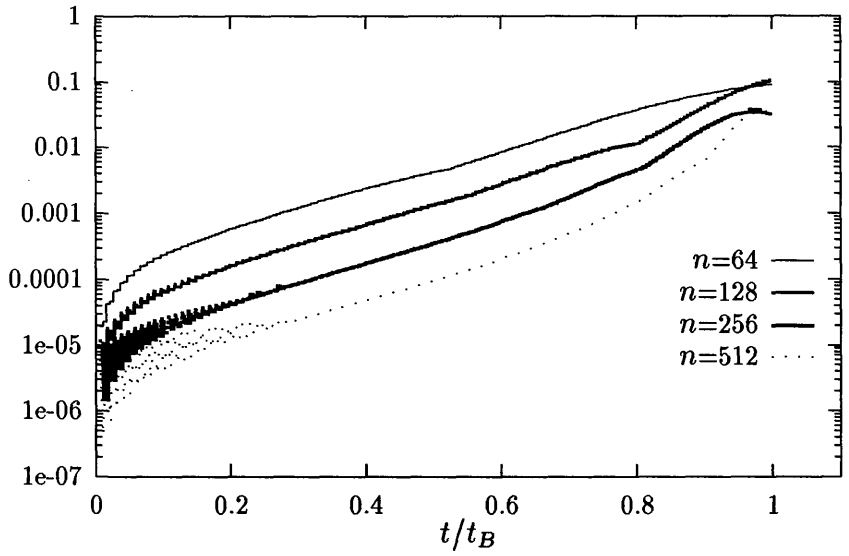

Figure 2.2: The evolution of the error in the example shown in Figure 2.1 for different discretizations. The error is the maximum of the relative error in r and in each of the components u^a and h^a.

Riemann invariant $J = \lambda + \phi$ shows a linear growth in time, and, therefore, remains orders of magnitude smaller than the total error given in Figure 2.2. Advanced numerical schemes should be used for solutions with shocks, as mentioned before.

Acknowledgement. The author expresses his gratitude to Prof. E.S. Phinney for his continued support during the course of this work. Discussions with Prof. T. de Zeeuw during the early stages of this work and critical comments by Mr. Eanna E. Flanagan, Mr. Tasso J. Kaper and Prof. K.S. Thorne are also gratefully acknowledged.

Chapter 3

MHD IN DIVERGENCE FORM

(Submitted to *The Journal of Computational Physics*)

3.1 Introduction

Numerical simulation of hydrodynamics and magneto-hydrodynamics has become increasingly important in the field of astrophysics. Interpretation of the structure, origin and long time evolution of astrophysical flow is approached today succesfully by large scale numerical simulations using nonrelativistic codes [39]. Much of these numerical studies is on the morphology of jets, which show intricate patterns of shocks. Radio-astronomy has provided us with detailed images of these flows on the kiloparsec scale. Lind [29] emphasizes that these simulations are to be regarded as qualitative investigations. In particular, he expresses caution in the interpretation of numerical simulations of jets on the parsec scale, as they are believed to be highly relativistic. Extension of numerical simulations to relativistic hydrodynam-

ics has received much attention by many authors (see, e.g.,[34, 35, 39, 30]). Furthermore, magnetic fields are believed to be present in these flows. Magnetic fields are important in radiative phenomena (Phinney [21]) and in the structure of astrophysical flow [21, 39]. Numerical simulation of relativistic MHD has been considered most notably by Evans and Hawley [16], and most recently by Dubal [40].

In [56] we presented a divergence formulation of locally adiabatic relativistic MHD for the purpose of numerical simulation. We showed that MHD in divergence form allows for numerical simulation of the problem of wave breaking in one dimension up to the moment of breaking. The purpose of this paper is to demonstrate that MHD in divergence form also allows for numerical simulation of more complicated MHD flow with shocks. To this end we seek

(a) MHD in divergence form whose standard jump conditions across surfaces of discontinuity are the physical, enthalpy preserving jump conditions across shocks;

(b) A numerical method for MHD in divergence form for the purpose of shock computations;

(c) A one-dimensional shock-tube problem which features many of the possible MHD shocks.

The first item will be obtained by a rewriting of the result from [56]. The resulting system is equivalent to the former whenever the flow is continuously differentiable.

Several illustrative examples will be computed. Using a pseudo-spectral

method with explicit time-stepping on a uniform grid we further show the effectiveness of the divergence formulation of MHD. Brio and Wu [37] computed the coplanar Riemann problem in classical, nonrelativistic MHD. In this paper, we will study the same problem for relativistic MHD. A pseudo-spectral method is employed which is tested against an analytical solution in a Riemann shock-tube problem in the singular limit of a purely transverse magnetic field. In [37] Brio and Wu showed the existence of a compound wave (a shock wave with attached to it a rarefaction wave of the same family) in nonrelativistic MHD. These results have recently also been computed by Stone *et al.* [51]. We will find that compound waves persist in relativistic MHD as a natural continuation of Brio and Wu's classical, nonrelativistic result.

We remark that our method of taking constraints as conserved quantities may have applications outside the field of MHD. The results in this paper can be taken as demonstration of this method *an sich* in the particular context of MHD.

In Section 2, MHD is formulated in divergence form which allows for the computation of shocks. Our pseudo-spectral method is outlined in Section 3, together with a test on the Riemann shock-tube problem with transverse magnetic field. The relativistic generalization of Brio and Wu's coplanar Riemann problem is presented in Section 4.

3.2 Formulation of the problem

The equations of locally adiabatic ideal magneto-hydrodynamics including the flux-freezing constraint (MHD) can be written in the completely covariant form [56]

$$\begin{cases} \nabla_a T^{ab} = 0, \\ \nabla_a (u^{[a} h^{b]} + g^{ab} u^c h_c) = 0, \\ \nabla_a (r u^a) = 0, \\ \nabla_a (r S u^a) = 0. \end{cases} \tag{3.1}$$

Here, T^{ab} is the total stress-energy tensor. For a fluid with velocity four-vector u^a, $u^c u_c = -1$, magnetic field h^a (magnetic permeability $\mu = 1$) we have

$$T^{ab} = \rho u^a u^b + P^* g^{ab} - h^a h^b, \tag{3.2}$$

where $\rho = rf + h^2$, $P^* = P + h^2/2$, r is the proper restmass density of the fluid, f is the specific enthalpy, P is the pressure. The quantities r, P and f are related to the entropy, S, and the temperature, T, by $dP = rdf - rTdS$. Systems in divergence form uniquely induced jump conditions across surfaces of discontinuity (following a weak formulation, see *e.g.*, [24]). It is these jump conditions that are approximated in simulations by shock-capturing schemes. In the case of (3.1) these jump conditions yield strict adiabaticity, because of the last equation. For this reason, we first rewrite this system so as to obtain a system in divergence form for which these standard jump conditions are the physically correct jump conditions for shocks.

In regions where the flow is smooth, we have

Theorem 3.2.1 *The equations of locally adiabatic MHD can be stated as*

$$\nabla_a F^{aA} \equiv \begin{cases} \nabla_a T^{ab} = 0, \\ \nabla_a (u^{[a} h^{b]} + g^{ab} u^c h_c) = 0, \\ \nabla_a (r u^a) = 0, \\ \nabla_a \{(u^c u_c + 1)\xi^a\} = 0, \end{cases} \tag{3.3}$$

where ξ^a is any prescribed time-like vector field. This system is equivalent to (3.1) in regions where the flow is continuously differentiable. The standard jump conditions across surfaces of discontinuity for this system are those of conservation of energy-momentum, baryon number and Maxwell's equations.

Note that Maxwell's equations imply the identity

$$u_b \nabla_a T^{ab} \equiv u_b \nabla^a (r f u^a u^b + P g^{ab}). \tag{3.4}$$

Consequently, the equation of continuity and the thermodynamic relation $dP = r df - rT dS$ yield

$$u_b \nabla_a T^{ab} \equiv f(r u^a) \nabla_a u^2/2 + (u^2 + 1)(u^a \nabla_a) P + T u^2 (r u^a) \nabla_a S. \tag{3.5}$$

It follows that conservation of either one of the relations

$$\begin{array}{l} u^2 + 1 = 0, \\ u^a \nabla_a S = 0 \end{array} \tag{3.6}$$

implies the other. Thus, for smooth flow the two systems (3.1) and (3.3) are equivalent. The jump conditions across time-like shock surfaces (to which ξ^a is not tangential) as they follow from the second system are evidently those of conservation of energy-momentum and baryon number. The formulation of Maxwell's equations in (3.3) is the same as in (3.1), which yields Maxwell's jump conditions as shown in [56]. We will use this system for our computations of shocks.

We remark that $\xi^a \equiv$ const. yields a quadratically nonlinear system in the hydrodynamical limit to which Roe's linearization (see [52]) can be applied in a straightforward manner. When $h^a \equiv 0$, we obtain

$$\begin{cases} \nabla_a(w^a w^b + sp) = 0, \\ \nabla_a\{(s - \frac{\gamma}{\gamma-1}p)w^a\} = 0, \\ \nabla_a\{(w^c w_c + s^2)\xi^a\} = 0, \end{cases} \tag{3.7}$$

with characteristic determinant (cf. Proposition 5.1 [56])

$$D = (\xi^a \nu_a)(w^a \nu_a)(a_1(w^a \nu_a)^2 - a_2(\nu^a \nu_a)), \tag{3.8}$$

where $a_1 = \frac{2}{\gamma-1}(\gamma p - s)$ and $a_2 = (\frac{\gamma}{\gamma-1}p + s)w^c w_c + (s - \frac{\gamma}{\gamma-1}p)s^2$. Here, $w^a = \sqrt{rf}u^a, s = \sqrt{rf}, p = P/\sqrt{rf}$ and ν_a is a 1-form. Thus, Roe's linearization yields a linear Riemann solver in terms of six null vectors which we have found can readily be implemented. This solver is similar to but not the same as Eulderink's Roe solver [23, 54] which involves five eigenvectors for the Riemann solver. However, a Roe solver for MHD is expected to be rather complex and, by similar arguments, possible in analytic form only when $\gamma = 2$ as in [37]. Therefore, we will not elaborate on this further here.

A pseudo-spectral method is used for all our computations. This method is first applied in a Riemann shock-tube problem with zero longitudinal magnetic field for a fluid with $\gamma = 3/2$ in view of an analytical solution in this case. We will also apply this method to Brio and Wu's coplanar Riemann problem in classical MHD.

3.3 Description of the method

In astrophysical flow, one of the most prominent features of shocks is heating. Shock heating is responsible for emission in violent phenomena such as supernovae [25, 33], accretion flow [45] and jets [39, 29]. In shocks relativistic effects can be significant. Mathematically, relativistic effects appear in the relativistic Rankine-Hugoniot relations for relativistic hydrodynamics (Taub [20]) and relativistic MHD (Lichnerowicz [8]) as singular perturbations of their nonrelativistic counterparts. This is exemplified by the absence of a bound on the ratio on the proper restmass densities (restmass densities in fluid restframe) across shocks, as opposed to the familiar bound $\frac{\gamma+1}{\gamma-1}$ (Bazer and Ericson [27]) for polytropic fluids in the nonrelativistic case. This will be illustrated below. In relation to the change of entropy across shocks this indicates that relativistic effects can be dramatic in the emissivity by shocks in astrophysical flows.

In this Section, we describe a pseudo-spectral method which enables us to study shock computations in our formulation of MHD (3.3) with explicit time-stepping on a uniform grid. In a specific space-time split, $(x^a) = (t, x^\alpha)$, (3.3) may be written as

$$\partial_t F^{tA}(t, x^\alpha) + \partial_\alpha F^{\alpha A}(t, x^\alpha) = 0. \tag{3.9}$$

In all our computations $\xi^a = (\partial_t)^a$. Our pseudo-spectral method is a smoothing method with leapfrog time-stepping of the form

$$(F^{tA})^{m-1} = S_w\{(F^{tA})^{m-1}\} - 2\Delta t \delta_w (F^{xA})^m. \tag{3.10}$$

Here, S_w is a smoothing operator and δ_w an associated spatial derivative operator. Thus, the same smoothing, S_w, is applied to each equation in (3.3).

3.3.1 The operators S_w and δ_w

The smoothing operator S_w will apply to functions $f \epsilon V_N$ on a fixed grid $0 = x_1, \ldots, x_{N+1} = 1$, $N = 2^M$, with uniform grid spacing. Consider smoothing of an element $f \epsilon V_N$ defined by

$$\tilde{f'}_k = \tilde{f}_k \frac{\sin 2\pi kh}{2\pi kh}, \tag{3.11}$$

where $\{\tilde{f}_k\}_{k=-N/2+1}^{N/2-1}$ denotes the discrete Fourier transform. We thus obtain a smoothed function $f' \equiv L_{N,h}(f)$ in V_N. Notice that $L_{N,1/N}$ is Lanczos smoothing [48, 3]. Consider also differentiation with Richardson extrapolation, δ_N^R, on V_N given by

$$\delta_N^R(f)_i = \frac{4}{3}\frac{f_{i+1} + f_{i-1}}{2} - \frac{1}{3}\frac{f_{i+2} - f_{i-2}}{4}. \tag{3.12}$$

The operators S_w and δ_w will now be derived as follows. An element $f \epsilon V_N$ can be taken into V_{2N} by an interpolation, ι_w, of the form

$$\begin{array}{ll} \iota_w(f)_{2i-1} & = f_i, \\ \iota_w(f)_{2i} & = \frac{1}{2(w-1)}\{w(f_{i+1} + f_i) - f_{i+2} - f_{i-1}\}. \end{array} \tag{3.13}$$

Let $\pi : V_{2N} \to V_N$, $\pi(f_{2N})_i = f_{2i-1}$, be the inverse of ι_w. Then $\pi L_{2N,h} \iota_w$ maps V_N into V_N. Smoothing S_w on V_N is now defined as

$$S_w = \pi(\frac{4}{3}L_{2N,\frac{h}{2}} - \frac{1}{3}L_{2N,h})\iota_w, \tag{3.14}$$

where $h = 1/N$. Commensurate with S_w, we take $\delta_w : V_N \to V_N$ as

$$\begin{aligned}\delta_w(f) &= \pi\delta_{2N}^R \iota_w \\ &= (1+\eta)\tfrac{f_{i+1}-f_{i-1}}{2} - \eta\tfrac{f_{i+2}-f_{i-2}}{4},\end{aligned}$$

where $\eta = \frac{\frac{8}{3}}{w-1}$.

Smoothing with S_w is a weak smoothing in the sense that the transfer function $\tilde{S}_w$ of S_w in the spectral domain satisfies $0.80 < \tilde{S}_w \leq 1$. Because the transfer function is relatively flat and does not vanish at the high frequency ends $k = \pm N/2$, S_w represents significantly weaker smoothing than that obtained by Lanczos smoothing. It allows for comparetively smaller and, therefore, more accurate time-stepping.

Finally, we remark that S_w can be easily implemented numerically by integration of $\iota_w\{F^{tA}\}$ using the discrete Fourier transform followed by $\pi\delta_{2N}^R$.

3.3.2 A test problem

We will compute a 1D relativistic Riemann shock-tube problem with purely transverse magnetic field in flat space-time. The problem setting will be in the context of the coplanar Riemann problem for classical MHD by Brio and Wu [37]. The fluid is assumed to be a monatomic gas with polytropic equation of state,

$$P = Kr^\gamma, \tag{3.15}$$

relating the pressure, P, and the restmass density, r, with adiabatic constant K and polytropic constant γ. We have taken $\gamma = 3/2$, in between its ultra-relativistic limit, 4/3, and Newtonian limit, 5/3. Notice that this lies below

the limit established by Taub: $\gamma \leq 5/3$ [20]. The adiabatic constant, K, is taken to be 2/3, uniformly throughout the fluid. We compute the time evolution of fluid on the unit interval, $0 \leq x \leq 1$, which is initially at rest and possesses an initial jump discontinuity, $[r] = r_{right} - r_{left}$, at $x = \frac{1}{2}$. Furthermore, the magnetic flux density, $k = h/r$, where h is the magnetic field strength, also suffers an initial jump at $x = \frac{1}{2}$. In the examples presented below we have taken $k = 1$ for $x < \frac{1}{2}$, and $k = k_R$ for $x > \frac{1}{2}$. Numerically, the initial conditions at $x = \frac{1}{2}$ are chosen to be the mean of the left- and right-states.

A detailed error analysis can be given using a comparison solution obtained by the method of characteristics. Recall that a solution to a Riemann shock-tube problem can be described in three parts: increasing with x we find

(1) A simple wave moving into the uniform state at the left. When $K = 2/3, \gamma = 3/2$ and $k = 1$, and using $u^a = (\cosh(\lambda), \sinh(\lambda), 0, 0)$ the state of the fluid can be expressed analytically as [56]

$$\begin{aligned} &\lambda + \phi(r) = J, \\ &\phi(r) = 4\sinh^{-1}(r^{\frac{1}{4}}), \\ &\Lambda = \tanh(5\lambda/4 - J/4), \end{aligned} \tag{3.16}$$

where $0 \leq \lambda \leq \lambda_2$, the value of the Riemann invariant J is given by $\phi(r_{left})$, and Λ denotes the characteristic velocity;

(2) A uniform state connecting the region with the simple wave solution and the contact discontinuity. Here, the fluid is described simply by $\lambda = \lambda_2$, $r = r_2$ and $h = k_1 r_2 = r_2$ with the continuity condition $\lambda_2 + \phi(r_2) = J$;

(3) A uniform post-shock state in between the contact discontinuity and the shock. Here, the state of the fluid is described by $\lambda = \lambda_2$, $r = r_3$, $P = P_3$ and $h = k_R r_3$ with the jump condition $[F^{aA}(U)]\nu_a(\mu) = 0$ at the shock, where $\nu^a(\mu) = (\sinh\mu, \cosh\mu, 0)$.

For any initial jump $[r]$ this nonlinear problem in $(\lambda_2, r_3, P_3, \mu)$ can be solved by Newton's method.

A test case is considered with zero initial velocity and longitudinal magnetic field h^x, left state $r_L = 1, P_L = 2/3, (h^y)_L = 1$ and right state $r_R = 0.125, P_R = 0.1, (h^y)_R = 0.0625$. The initial hydrodynamical data are those in Sod's shock-tube problem [11] (except for $P_L = 2/3$, which is 1 in Sod's data), following Roe [52] and Brio and Wu [37]. The solution is shown in Fig. 3.1 for $n = 256$. The exact solution of this problem is given by the curve with sharp corners in each of the solution panels. Here, the smoothing by S_w was done with $w = 12$. The evolution of the error with time-step m is shown for the velocity (curve A) and the proper restmass density (curve B) in the postshock region. Averages over the mid one-third of the uniform postshock region are compared with the exact solution. At $m = 516$ the average is over grid points 159-164.

We have also studied the effect of smoothing on the quantities in the postshock region. Various values of w, $\eta \equiv \Delta t/\Delta x$ and leapfrog versus upwind time-stepping have been considered. Generally, smoothing increases with w and decreases with η. Smoothing by w reaches its maximum at $w = 20$ and minimum at $w = 8$. Table 3.1 shows results for various w in the case $n = 512$ at 1032 time-steps with $\eta = 0.10$. Oscillations appear

Quantity	pseudo-spectral			exact
	$w = 8$	$w = 10$	$w = 12$	
r	0.2695	0.2692	0.2687	0.2693
U	0.4574	0.4562	0.4559	0.4566
H	0.1511	0.1513	0.1511	0.1513
P	0.3299	0.3288	0.3284	0.3292
K	2.3587	2.3534	2.3574	2.3554

Table 3.1: Comparison of numerical results by pseudo-spectral method for various smoothing values of w with the exact solution for the Riemann problem shown in Fig.3.1 with discretization $n = 512$. The number of time-steps is $m = 1032$ with time-stepping $\Delta t/\Delta x = 0.10$.

with $w = 8$, a small overshoot remains at the shock when $w = 10$ and no spurious phenomena are present when $w = 12$. Clearly, the results in Table 1 are remarkably independent of w. Smaller time-step sizes $\eta \leq 0.05$ give additional smoothing, while $0.10 \leq \eta \leq 0.15$ yields essentially spurious free results and larger η yield overshoot at the shock. Interestingly, upwind differencing versus leapfrog shows no appreciable change in the results when w assumes intermediate values, $10 \leq w \leq 12$, except for a slight increase in smoothing at the contact discontinuity.

A strong shock computation is shown in Fig. 3.2. The initial data are again with zero initial velocity and longitudinal magnetic field h^x, but now with left state $r_L = 10$, $P_L = 2/3r^{3/2} \approx 21.08$, $(h^y)_L = 10$ and right state $r_R = 1$, $P_R = 0.25$, $(h^y)_R = 0.25$. Stabilization has been obtained by $w = 12$. Notice that the jump in the restmass density across the shock, 5.125 (numerically; 5.140 exact), exceeds the classical bound $\frac{\gamma+1}{\gamma-1} = 5$. Thus, this

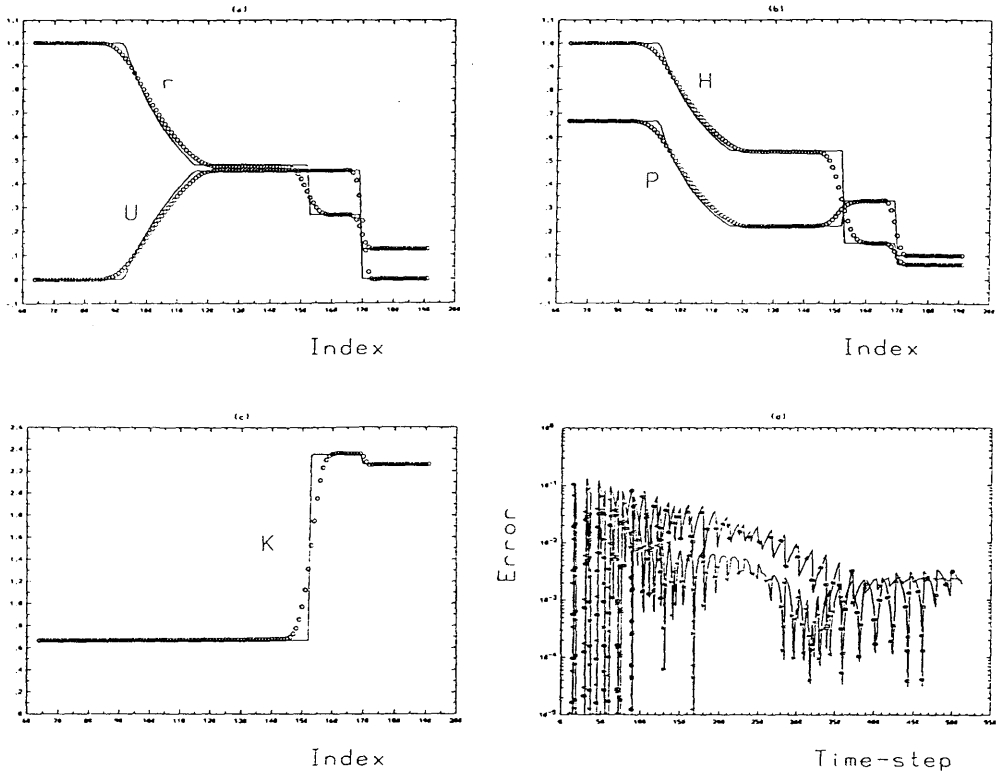

Figure 3.1: Numerical solution to shock-tube problem with purely transverse magnetic field in the pseudo-spectral method with $w = 12$. The discretization is 256 points and 512 time-steps with $\Delta t/\Delta x = 0.10$.

shock is genuinely relativistic.

We conclude that for modest shock strengths suitable choices of the parameters w and η are $10 \leq w \leq 12$ and $0.10 \leq \eta \leq 0.15$ with leapfrog time-stepping. Strong shock computations can be performed taking w large, $w \geq 12$. In all our computations, the approximation of the jump conditions across shocks shows proper convergence.

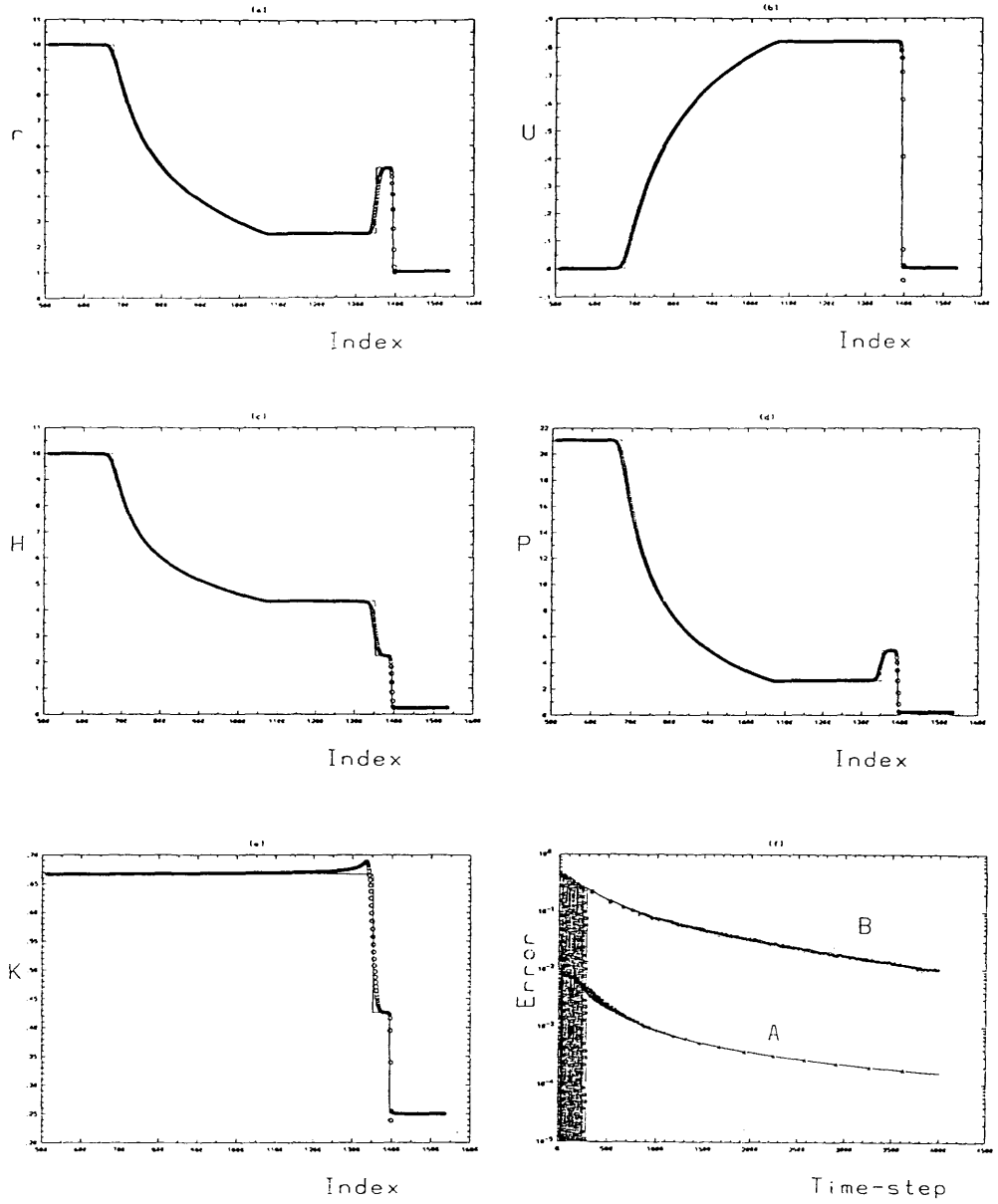

Figure 3.2: Numerical solution to shock-tube problem with relativistic shock strength in the pseudo-spectral method with $w = 12$. The discretization is 2048 points and 4000 time-steps with $\Delta t/\Delta x = 0.10$.

3.4 A coplanar MHD Riemann problem

We have computed the coplanar Riemann problem for relativistic MHD by application of the pseudo-spectral method to (3.3). In each computation, initially the velocity u^a and the transverse component h^z are zero throughout and $h_x = h_x^{(0)}\epsilon$, while $r = 1/8, P = 0.1\epsilon^2, h_y = -\epsilon$ at the right side of the discontinuity at $x = \frac{1}{2}$ and $r = 1, P = 1\epsilon^2, h_y = \epsilon$ at the left side of the discontinuity. We will consider two limiting cases of this Riemann problem. For $\epsilon \gg 1$ the resulting fluid flow has velocities approaching the speed of light, while for $\epsilon \ll 1$ the flow has low velocities, and the solutions should approach those of the nonrelativistic equations. Our choice of scaling keeps $\beta = P/h^2 = \text{const.}$ as ϵ is varied. As a check of our pseudo-spectral method (as opposed to the divergence formulation) we have also used it to solve the classical, nonrelativistic equations solved by Brio and Wu (Eqs. (16)-(22) in [37]). Our low ϵ and classical results are compared with those of [37] in Table 3.2. For this reason, we have chosen $\gamma = 2$ to facilitate comparison with results from Brio and Wu. In the coplanar Riemann problem, the magnetic field and the velocity are continuous across contact discontinuities whenever the longitudinal magnetic field, h_x, is nonzero. In contrast, $h_x^{(0)} = 0$ does allow these quantities to be discontinuous across contact discontinuities (as in Fig. 3.1). Thus, $h_x = 0$ with discontinuous magnetic field across a contact discontinuity is a singular limit in MHD. We will illustrate this numerically by consideration of $h_x^{(0)} = 1/10$ and $h_x^{(0)} = 0$.

Figs. 3.3-3.4 show the result for $\epsilon = 1$, $h_x^{(0)} = 3/4$ and $h_x^{(0)} = 1/2$, respectively, and Fig. 3.5 shows the result for $\epsilon = 0.05$, $h_x^{(0)} = 3/4$. Velocities

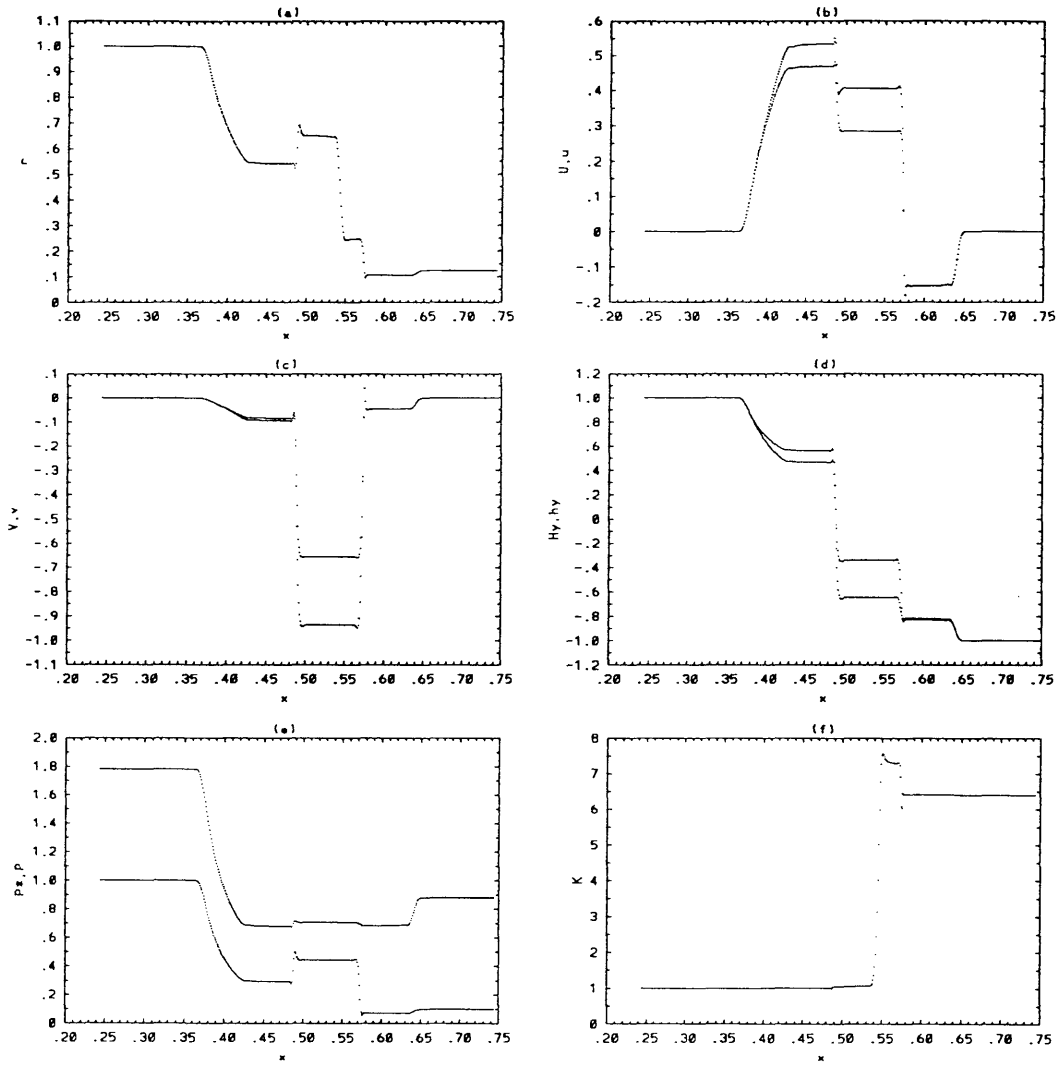

Figure 3.3: The pseudo-spectral method on the coplanar Riemann problem for relativistic MHD with $\epsilon = 1$ and $h_x^{(0)} = 3/4$. A small amplitude rarefaction wave is attached to the slow shock traveling to the left, constituting a slow compound wave. The number of time-steps is 1000 with 1024 points on the unit interval with $\Delta t/\Delta x = 0.15$. Here, smoothing is with $w = 10$.

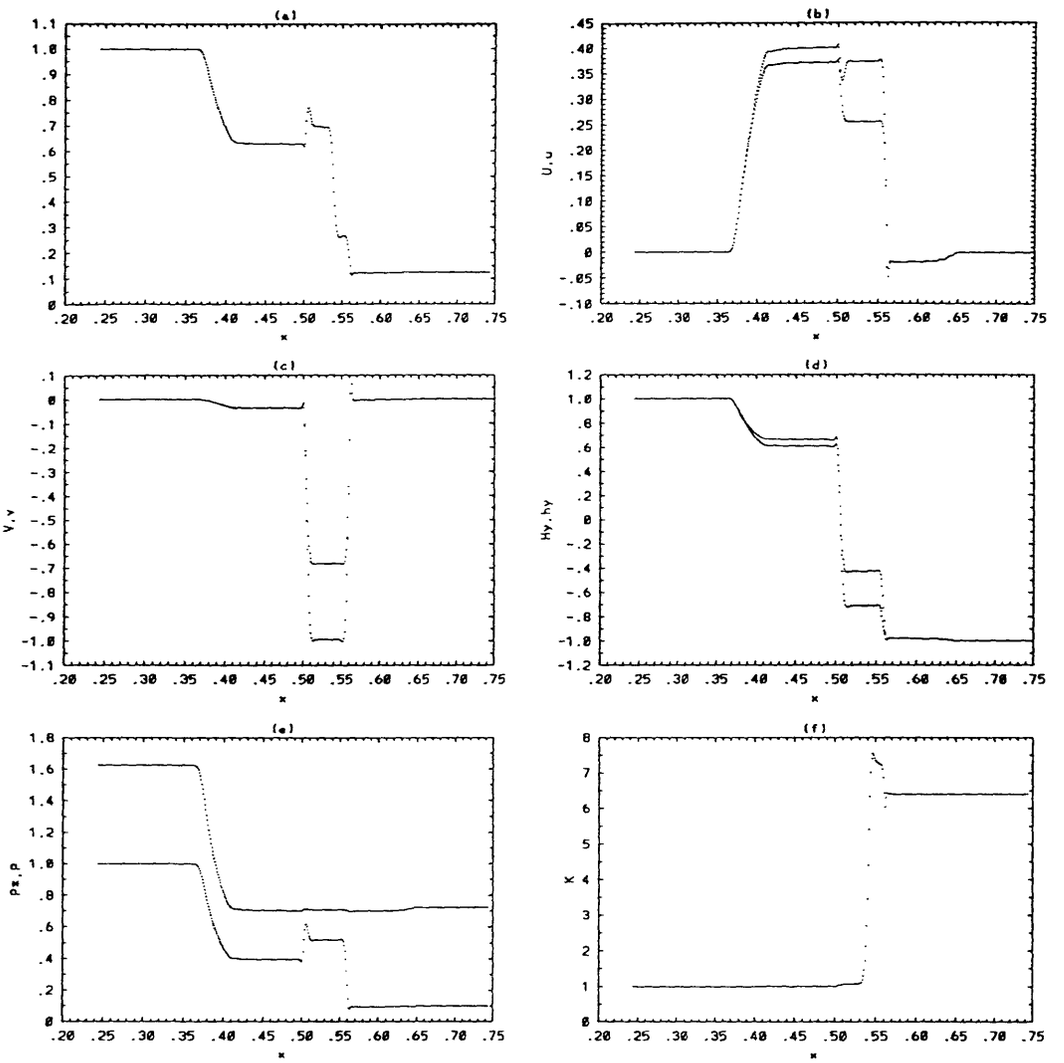

Figure 3.4: The pseudo-spectral method on the coplanar Riemann problem for relativistic MHD with $\epsilon = 1$ and $h_x^{(0)} = 1/2$. The rarefaction wave in the compound wave is now more pronounced than in Fig. 3.3. The numerical parameters are the same as in Fig. 3.3.

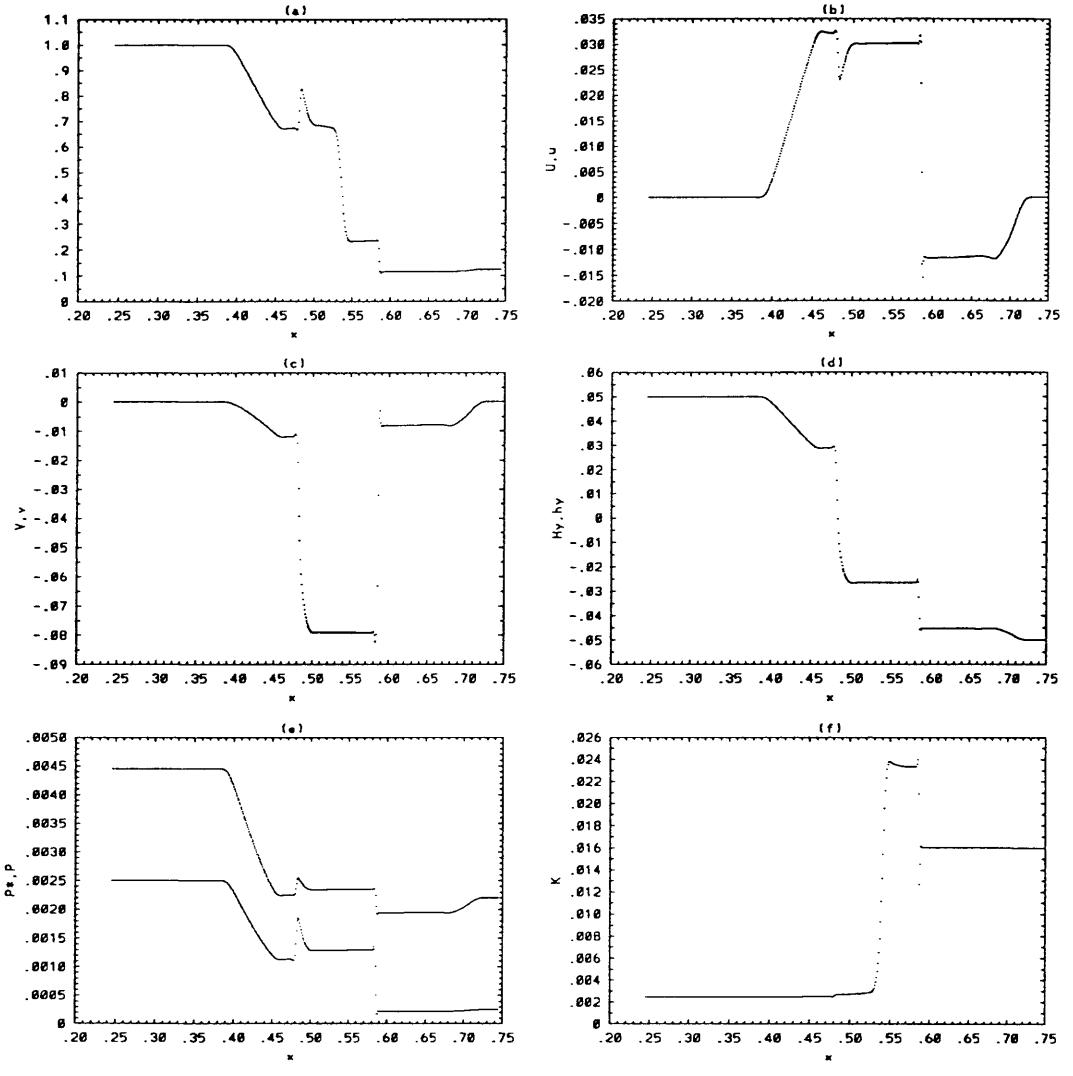

Figure 3.5: The pseudo-spectral method on the coplanar Riemann problem for relativistic MHD in the low velocity limit as with $\epsilon = 0.05$, keeping $h_x^{(0)} = 3/4$. The number of time-steps is 2400 with 1024 points on the unit interval and $\Delta t/\Delta x = 0.5$. Smoothing is obtained with $w = 10$.

and the transverse magnetic field are depicted twice in Fig. 3.3-3.4, once as physical quantities $U = u^x/u^t, V = u^y/u^t, H^y = u^t h^y - u^y h^t$ in the laboratory frame and once as tensor components u^x, u^y and h^y. The curves of the physical quantities U, V, H^y and the tensor components u^x, u^y, h^y, respectively, coincide to within 0.5% (in the order of the thickness of the lines of the figure) when $\epsilon = 0.05$. This is the nonrelativistic result of Brio and Wu and a comparison follows below. In each case, the solution consists of a fast rarefaction wave moving to the left, a slow compound wave, a contact discontinuity, and a slow shock and fast rarefaction wave moving to the right (see [37] for the discussion in nonrelativistic MHD). In Fig. 3.3 the compound wave appears most clearly in the restmass density and the tensor component u^x. Figs. 3.3-3.4 show a pronounced difference between the physical and 4-vector components of the tensors. This is due to a jump in the Lorenz factor, Γ, to $\Gamma = 1.428$ in Fig. 3.3 and to $\Gamma = 1.458$ in Fig. 3.4. This jump in Γ attenuates the jump in the physical quantities. Furthermore, the rarefaction wave in the compound wave in Fig. 3.3 is of much smaller amplitude than in Figs. 3.4-3.5; this rarefaction wave decreases in amplitude with h_x and with velocity. Finally, notice that the heating in the compound wave is negligible compared to the heating in the shock traveling to the right. This follows from the minute jump in K at $x = 0.49, x = 0.50, x = 0.48$ and the $O(1)$ jump in K at $x = 0.525, x = 0.515, x = 0.535$ in Figs. 3.3, 3.4 and 3.5, respectively. This suggests that compound waves should they occur in astrophysical flow are not likely to contribute to detectable radiation. We remark that for fluids with $\gamma = 3/2$ the numerical results show the same behavior.

3.4.1 Limit of small $h_x^{(0)}$

The problem in the limit of small $h_x^{(0)}$ is shown in Figs. 3.6-3.7 for $h_x^{(0)} = 1/10$ and $h_x^{(0)} = 0$, respectively. The other parameters are as in Section 3.4 with $\epsilon = 1$. Notice that as $h_x^{(0)} \to 0$ the transverse velocity has constant magnitude, but is captured in an ever thinner sheet bounded by two slow shocks. When $h_x^{(0)} = 0$, the sheet vanishes, but the spike in P remains. The transverse flux therefore becomes proportional to h_x in this limit, as the jump in h_y approaches finite limits across each of the two shocks. Notice that total pressure $P^* = P + h^2/2$ becomes continuous as $h_x^{(0)}$ vanishes. Next consider the limit $h_x^{(0)} = 0$. Since there is a change of sign in h_y across a contact discontinuity approximation of all quantities by smooth functions while keeping the total pressure P^* continuous necessarily requires a large spike in P at the point where h_y changes sign, *i.e.* goes through zero. Thus, transverse MHD is a singular limit when h_y changes sign across a contact discontinuity. As $h_x^{(0)}$ becomes finite two waves bifurcate from the contact discontinuity. In this problem these waves are slow shock waves. We remark that when $\gamma = 3/2$ the singular nature of this problem is also reflected numerically in a small, erroneous jump in the velocity across the contact discontinuity. The continuity of the total pressure, however, is strictly maintained. We have also considered the small $h_x^{(0)}$ limit on the test problem in Section 3.1. This yields a bifurcation of the solution near the contact discontinuity into a slow shock and a slow rarefaction wave. The result is a fast rarefaction wave followed by a slow shock traveling to the left and a fast shock followed by a slow rarefaction wave traveling to the right.

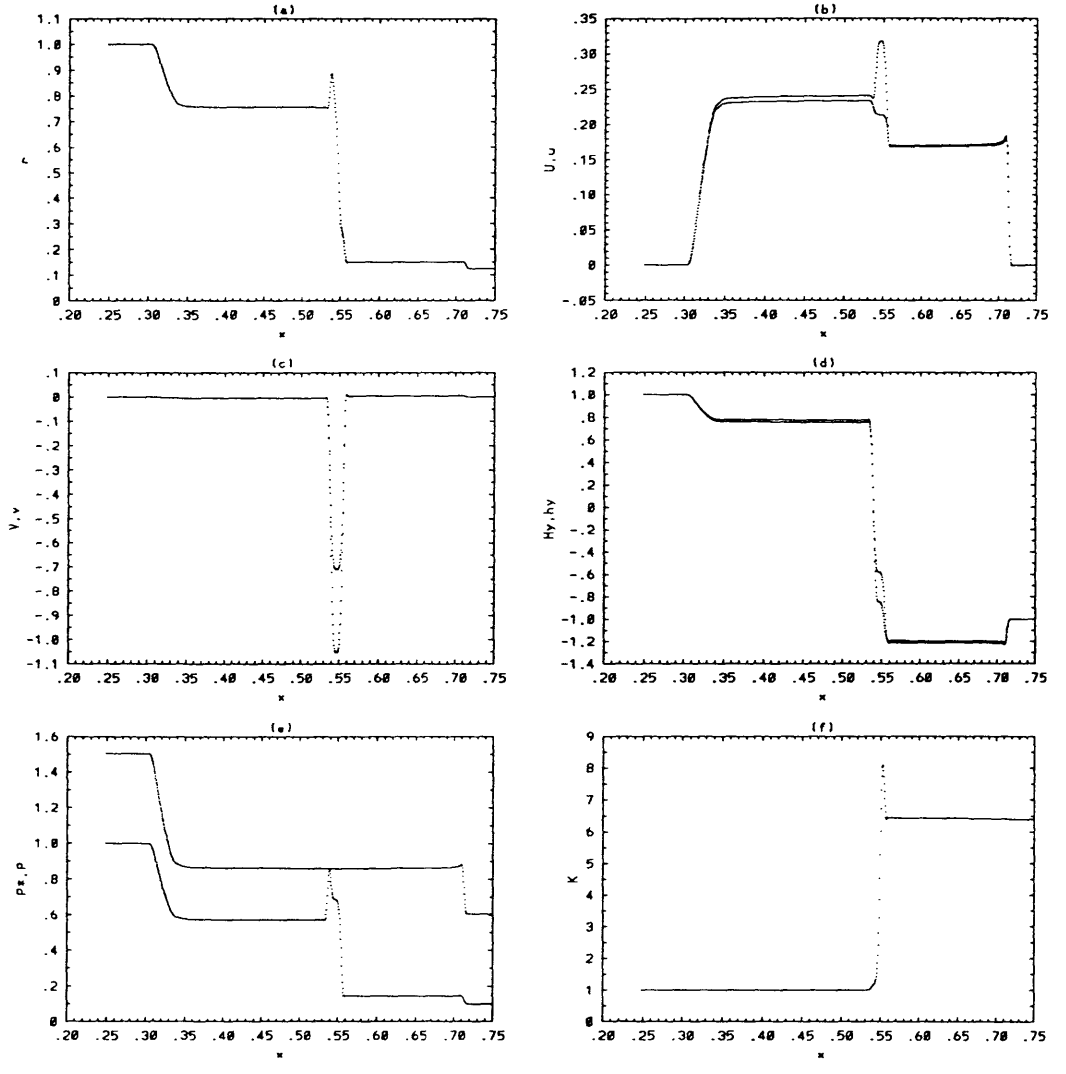

Figure 3.6: The low $h_x(0)$ limit showing a bifurcation of two slow shocks from the contact discontinuity. Here, $\epsilon = 1$ and $h_x^{(0)} = 0.10$. The number of time-steps is 3006 with 2048 points on the unit interval, $\Delta t/\Delta x = 0.15$ and $w = 10$.

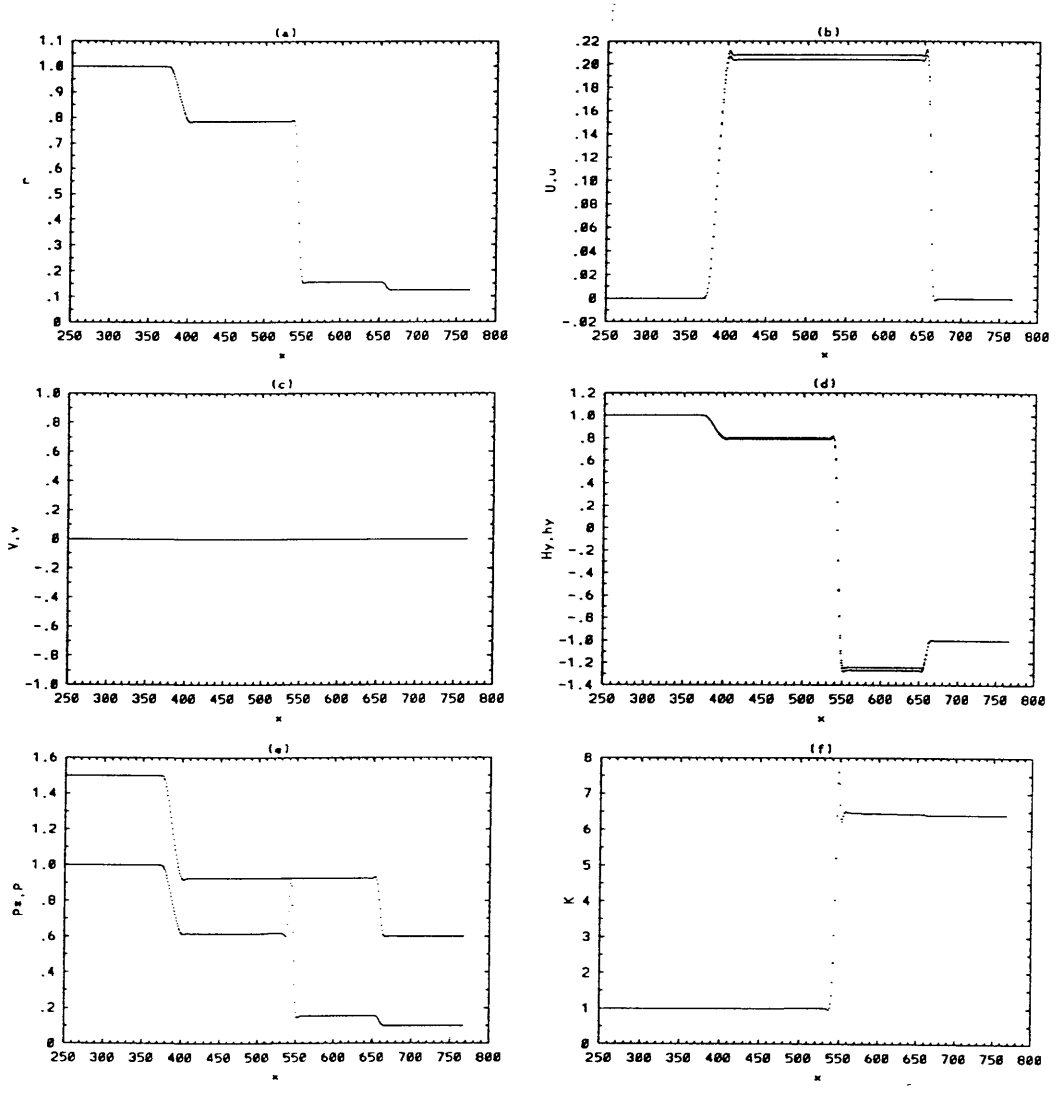

Figure 3.7: The singular Riemann problem with $\epsilon = 1$ and $h_x^{(0)} = 0$. The number of time-steps is 1000 with 1024 points on the unit interval, $\Delta t/\Delta x = 0.15$ and $w = 10$.

3.4.2 Classical limit

With nonrelativistic velocities, the system (3.4) yields the classical results. To see this, computations have been repeated with the equations of non-relativistic MHD. The difference between the 4-vector quantities u, v, h^y and physical quantities U,V and H^y, respectively, is less than 0.5% when $\epsilon = 0.05$, as mentioned before, while about 2% when $\epsilon = 0.10$ (in particular in U, u and V, v at the right side of the compound wave, where u^t is largest). As $\epsilon \to 0$, the equations of relativistic MHD reduce to their non-relativistic form [37] which for the coplanar problem amounts to:

$$\begin{cases} r_t + (rU)_x = 0, \\ (rU)_t + (rU^2 + P^*)_x = 0, \\ (rV)_t + (rUV - H_x H_y)_x = 0, \\ (H_y)_t + (H_y U - H_x V)_x = 0, \\ E_t + \{(E + P^*)U - H_x(H_x U + H_y V)\}_x = 0, \end{cases} \tag{3.17}$$

where $P^* = P + (H_x^2 + H_y^2)/2$ and H_x is constant. The solution to these equations obtained using our pseudo-spectral is shown in Fig. 3.8. We have estimated the left state before the shock, denoted by subscript L, and the right state at the tail of the rarefaction wave, denoted by subscript R, of the compound wave by taking averages over five points and compared these with data from Brio and Wu [37] and from Stone *et al.* [51]. This is listed in Table 3.2. Notice agreement typically better than 0.5%, but a 1% discrepancy in the proper restmass density on the right side, r_R. We find that this is very sensitive to to smoothing (by taking $w \to 20$ and/or smaller time-steps $\Delta t/\Delta x \leq 0.05$). This may be due to the smoothing at contact discontinuity, which our method spreads out over about 10 grid points. Interestingly, the

Quantity	$\epsilon = 1$	$\epsilon = .10$	$\epsilon = 0.05$	$\epsilon = 0$	Ref.[37]	Ref.[51]
r_L	0.5417	0.6674	0.6722	0.6762	0.6763	0.664
r_R	0.6503	0.6862	0.6844	0.6919	0.6963	0.701
U_L/ϵ	0.4680	0.6457	0.6427	0.6369	0.6366	0.662
U_R/ϵ	0.2839	0.5920	0.6002	0.6007	0.5997	0.597
V_L/ϵ	-8.318E-02	-0.2357	-0.2370	-0.2351	-0.2333	-0.248
V_R/ϵ	-0.6550	-1.545	-1.576	-1.585	-1.578	-1.58
H_L/ϵ	0.5619	0.5756	0.5791	0.5835	0.5849	0.576
H_R/ϵ	-0.3414	-0.5234	-0.5316	-0.5344	-0.5341	-0.536
P_L/ϵ^2	0.2939	0.4461	0.4528	0.4580	0.4574	0.443
P_R/ϵ^2	0.4437	0.5115	0.5152	0.5156	0.5133	0.509

Table 3.2: The low ϵ limit of the relativistic coplanar Riemann problem for MHD. Averages of the left and right constant states across the compound wave for various ϵ and the classical case. Data from Brio and Wu and from Stone *et al.* are listed here for comparison.

appearance of some oscillatory behavior at the shock shows that the classical formulation is more difficult to handle with our pseudo-spectral method than the relativistic formulation. This is probably due to a difference in the way conservation of energy is formulated. We have taken $\Delta t/\Delta x = 0.5$ in the low ϵ relativistic computations and $\Delta t/\Delta x = 0.15$ in the computation on (3.17). The spurious oscillations in classical MHD disappear when taking smaller time steps ($\Delta t/\Delta x \leq 0.05$); however, this introduces smoothing which increases the discrepancy in r_R, as mentioned before. We conclude that our implementation of MHD shows proper limiting behavior towards nonrelativistic MHD as the velocities become small.

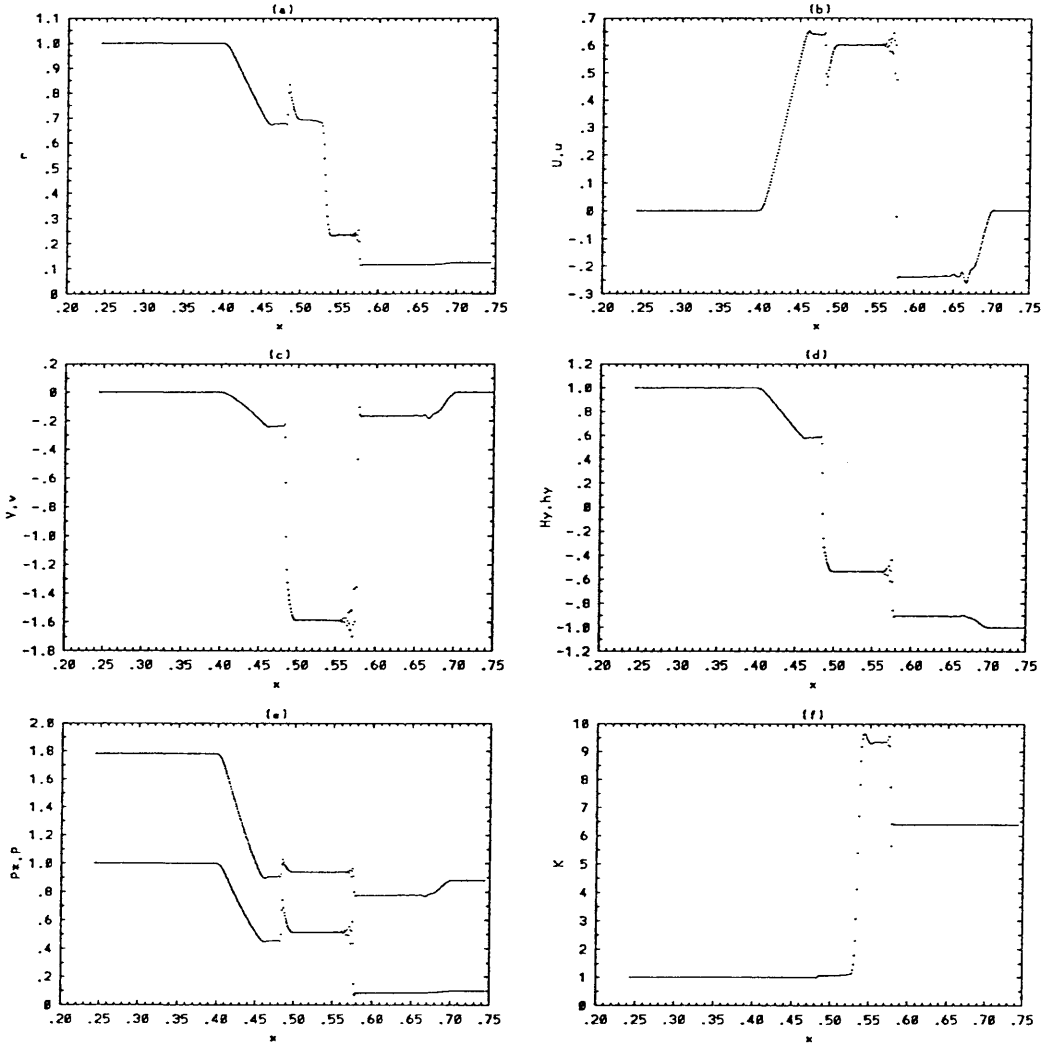

Figure 3.8: The pseudo-spectral method on classical MHD. The number of time-steps is 360 with 1024 points on the unit interval with $\Delta t/\Delta x = 0.15$. Smoothing is obtained with $w = 12$.

3.5 Discussion

The shock computations in this paper show that MHD formulated in divergence form allows stable and accurate numerical simulations. In view of astrophysical applications, emphasis has been given to the computation of the shock heating. With low discretizations the results are particularly accurate for shocks of intermediate strength. The power of the divergence formulation of MHD is brought about by

(c1) convergence of the approximations of the shock jump relations;

(c2) obtaining both relativistic and classical results in the same numerical implementation;

(c2) obtaining the above with explicit time-stepping on a uniform grid.

We wish to emphasize that the divergence form of MHD in the limit of zero magnetic field yields a divergence form of relativistic hydrodynamics. In view of the results above, this formulation may be competitive with other formulations for relativistic hydrodynamics for the purpose of numerical simulation.

Our computations show that compound waves persist in relativistic MHD. Brio and Wu [37] expressed concern as to whether the compound wave in their computations is physical or a mere artifact of numerical simulation. They do so in view of the slow shock involved being an intermediate shock. We wish to express that in the context of the coplanar Riemann problem, the results of Wu [17], Brio and Wu [37], Stone *et al.* and those contained in this paper lead us to believe that intermediate shocks should be considered natural features in numerical simulations.

Acknowledgement. With great pleasure the author wishes to acknowledge the many fruitful and stimulating discussions with Prof. E. Sterl Phinney, and his continued support during this work. The author is very grateful to Prof. John F. Hawley for drawing his attention to the work by M. Brio and C.C. Wu, and for his kind permission to include data from Ref. [51].

Chapter 4

2D SHOCK COMPUTATIONS IN MHD

(Some of this material has been presented at the "XV^{th} Annual Texas Partial Differential Equations Conference," Denton, Texas, 1992.)

4.1 Introduction

Numerical study of large scale astrophysical flows requires simulations in two or three dimensions. In the previous chapter we found that MHD in divergence form allows for accurate and stable numerical computations in one dimension. We will now turn to study MHD in divergence form in numerical applications in two dimensions. A two-dimensional numerical scheme is used based on the one-dimensional pseudo-spectral method from [55]. A sample of various problems tests the scheme on isotropy (1), independence of coordinate system (2) and convergence (3). These examples also illustrate specific aspects of jet flow. These issues will be addressed in test problems with cylindrical symmetry. The presence of cylindrical symmetry allows us

to study (1) by consideration of contour plots, (2) by comparison of the results with one-dimensional computations using polar coordinates, and (3) by variations of mesh-size and time step-size. Furthermore, an explicit proof is given to show that the two-dimensional scheme preserves divergence free magnetic fields to within arbitrary small error (in the sense of a discretized spatial derivative). This is illustrated also numerically in diverging shock problems in a uniform magnetic field in the (x,y)-plane.

4.2 A 2D numerical scheme

The 2D computations are performed on a 2D Cartesian grid with coordinates x, y and with uniform grid size, $\Delta x = \Delta y$. An immediate 2D implementation of the pseudo-spectral smoothing method in [55] is obtained as follows. At each grid point $(x, y) = (i\Delta x, j\Delta y)$ two one-dimensional problems are considered to which the method from [55] can be applied: one problem on the $x-$axis as defined by the restriction $y = \text{const.}$ and the other problem on the $y-$axis as defined by the restriction $x = \text{const.}$ The one-dimensional updates $(F^{tA}_{(y)})^{m+1}_{ij}$ and $(F^{tA}_{(x)})^{m+1}_{ij}$, respectively, thus obtained at time $t = (m+1)\Delta t$ yield an update $(F^{tA})^{m+1}_{ij}$ given by

$$(F^{tA})^{m+1}_{ij} = \frac{1}{2}[(F^{tA}_{(y)})^{m+1}_{ij} + (F^{tA}_{(x)})^{m+1}_{ij}]. \tag{4.1}$$

In terms of the smoothing operator S_w and the spatial derivative operator δ_w [56] this amounts to updates of the form

$$(F^{tA})^m = S^{2D}_w\{(F^{tA})^{m-1}\} - 2\Delta t\delta_{w,x}(F^{xA})^m - 2\Delta t\delta_{w,y}(F^{xA})^m, \tag{4.2}$$

where

$$S_w^{2D} = \frac{1}{2}(S_{w,x} + S_{w,y}). \tag{4.3}$$

Here, a subscript $,x(y)$ refers to the restriction of the argument to $y = \text{const.}$ ($x = \text{const.}$). Thus, the same smoothing is applied to each of the equations in (3.3), as before in the one-dimensional implementation by S_w. We remark that the smoothing parameter w as introduced in [55] will be fixed at 12 in all computations.

A numerical scheme of the form (4.2) conserves $c(U) \equiv u^c h_c = 0$ identically, for which a proof will be given below. Let $x_a = (t, x_\alpha)$, $\alpha = 1, 2, 3$, be a specific coordinate system with the coordinate t time-like. In this coordinate system, Maxwell's equations

$$\nabla_a\{u^{[a}h^{b]} + g^{ab}c(U)\} = 0 \tag{4.4}$$

may be written as

$$\partial_a(\sqrt{-g}u^{[a}h^{b]}) + \sqrt{-g}g^{ab}\partial_a c = 0. \tag{4.5}$$

Let δ_a be discretized time- and space-derivatives, corresponding to the coordinate derivatives ∂_a. We assume these operators to be commuting, *i.e.*, $\delta_a\delta_b = \delta_b\delta_a$. For example, δ_x can be the familiar central-differencing operator: $(\delta_x f^m)_{ijk} = [f^m_{i+1jk} - f^m_{i-1jk}]/2\Delta x$, where $f^m_{ijk} = f(t_m, x_i, y_j, z_k)$ and Δx is the grid spacing in the $x-$coordinate. Furthermore, S_w^{2D} and $\delta_{x,y}$ are assumed to be commuting, as is the case at hand with our particular smoothing (4.3).

Theorem 1 *A numerical scheme of the form (4.2) for MHD in divergence form with commuting smoothing operator S_w^{2D} and discretized derivative operators $\delta_{x,y}$ preserves the constraint $c(U) \equiv u^c h_c = 0$ identically.*

Proof: Let $\omega^{ab} = \sqrt{-g}u^{[a}h^{b]}$. Maxwell's equations (4.4) in MHD in divergence form may then be written as

$$\partial_t\omega^{tb} + \partial_x\omega^{xt} + \partial_y\omega^{yb} + \sqrt{-g}g^{tb}\partial_t c + \sqrt{-g}g^{tx}\partial_x c + \sqrt{-g}g^{ty}\partial_y c = 0. \quad (4.6)$$

Let m index time-slices $t = t_m$. Variables on $t = t_m$ will be superscripted by m. We will take the induction hypothesis $c^n = 0$ for all $n \leq m$. In two dimensions time-stepping of the form (4.2) amounts to

$$\begin{aligned}\sqrt{-g}g^{tb}c^{m+1} + (\omega^{tb})^{m+1} = \; & S_w^{2D}\{(\omega^{tb})^{m-1}\}, \\ & -2\Delta t\delta_x(\omega^{xb})^m - 2\Delta t\delta_y(\omega^{yb})^m.\end{aligned} \quad (4.7)$$

Letting $b = t, x, y$ and using $c^m = 0$ these equations amount to

$$\sqrt{-g}g^{tt}c^{m+1} + 2\Delta t\delta_x(\omega^{xt})^m + 2\Delta t(\omega^{yt})^m = 0, \quad (4.8)$$

$$(\omega^{tx})^m - S_w^{2D}\{(\omega^{tx})^{m-2}\} + 2\Delta t\delta_y(\omega^{yx})^{m-1} = 0, \quad (4.9)$$

$$(\omega^{ty})^m - S_w^{2D}\{(\omega^{ty})^{m-2}\} + 2\Delta t\delta_x(\omega^{xy})^{m-1} = 0. \quad (4.10)$$

Now apply δ_x to the second and δ_y to the third equation above, and use commutativity of the $\delta_{x,y}$ and S_w^{2D}, thereby obtaining

$$\delta_x(\omega^{tx})^m - S_w^{2D}\{(\delta_x\omega^{tx})^{m-2}\} + 2\Delta t\delta_x\delta_y(\omega^{yx})^{m-1}, \quad (4.11)$$

$$\delta_y(\omega^{ty})^m - S_w^{2D}\{(\delta_y\omega^{ty})^{m-2}\} + 2\Delta t\delta_y\delta_x(\omega^{xy})^{m-1}. \quad (4.12)$$

Notice that antisymmetry of ω and commutativity of the $\delta_{x,y}$ yields

$$\delta_x\delta_y(\omega^{yx})^{m-1} + \delta_y\delta_x(\omega^{xy})^{m-1} = 0. \quad (4.13)$$

Adding the two equations in (4.12) therefore gives

$$(\delta_x\omega^{tx} + \delta_y\omega^{ty})^m = S_w^{2D}\{\delta_x(\omega^{tx})^{m-2} + \delta_y(\omega^{ty})^{m-2}\} = 0 \quad (4.14)$$

by our induction hypothesis. It then follows from (4.8) that $c^{m+1} = 0$, which completes our induction step.□

We remark that the statement of the theorem is sharp: application of Strang's method [22] to computations of problems with nontransverse magnetic field show a drift in c away from zero. This is not necessarily dramatic, as some cases showed that c remained small ($< 10^{-3}$) without any instabilities. Smaller time-steps reduce c, so that c can still be kept small (10^{-5}) at the cost of greater computation time. It should be mentioned that in transverse MHD problems Strang's method preserves zero c and the method showed excellent isotropy.

4.3 2D shock problems in relativistic MHD

MHD in divergence form will be exemplified by several computations. First, problems with cylindrical symmetry are discussed for the purpose of testing the numerical scheme. We continue with examples of some more generality. These examples contain aspects of flow in astrophysical jets.

4.3.1 Cylindrically symmetric shock problems

The first test is on a diverging cylindrical shock problem. We consider an initially cylindrical column distribution of high density, $r = 1$, high pressure, $P = 2/3$, and strong magnetic field $h_z = 1$ in a surrounding of low density, $r = 0.125$, low pressure, $P = 0.10$ and weak magnetical field, $h_z = 0.0625$ (see Fig. 4.1). The result of this "Mexican Hat Problem" is shown in Figs. 4.2 and 4.3. The contour plots in Fig. 4.3 clearly show a high degree of isotropy

in this computation. In Fig. 4.4 we further compare this result with a one-dimensional computation using cylindrical coordinates. Notice the remarkable agreement between the two computations when the the number of radial points in the 1D simulation is the same as in the 2D simulation.

A second test on a problem with cylindrical symmetry uses the relativistic analogue of the problem as discussed in nonrelativistic hydrodynamics by Payne [49], Lapidus [5], Munz [53] and, recently, also by Zhang and So [26]. Here, the evolution of a converging shock and its reflection in its point of symmetry are studied. This is a problem of singularities, as the hydrodynamical state becomes singular at the moment of reflection.[1] The initial data for this problem are given by a column distribution of low density, $r = 1$, low pressure, $P = 1$, in a surrounding of high density, $r = 4$ and high pressure $P = 4$ (see Fig. 4.5). The magnetic field strength in this problem is zero. The result for different times $t = 30$, 57 and 120 are shown in Figs. 4.6-4.7. The time $t = 57$ is chosen to be the time at which the numerical values of the density and pressure were maximal near the origin. The contour plots in Fig. 4.7 clearly show a high degree of isentropy, limited near the origin only by grid discretization. In Fig. 4.8 we further compare the results with one-dimensional computations using cylindrical coordinates. Again, there is remarkable agreement between the 1D and 2D computations with the same number of radial points. Notice that the 1D simulation with high resolution indicates that the time at which the maximum density and pressure at the

[1] A singular perturbation analysis shows that $P(t) \sim (t^* - t)^{-\gamma}$ as $t \to t^*$, where t^* denotes the moment of reflection and γ denotes the polytropic index (see Appenix A for a complete analysis).

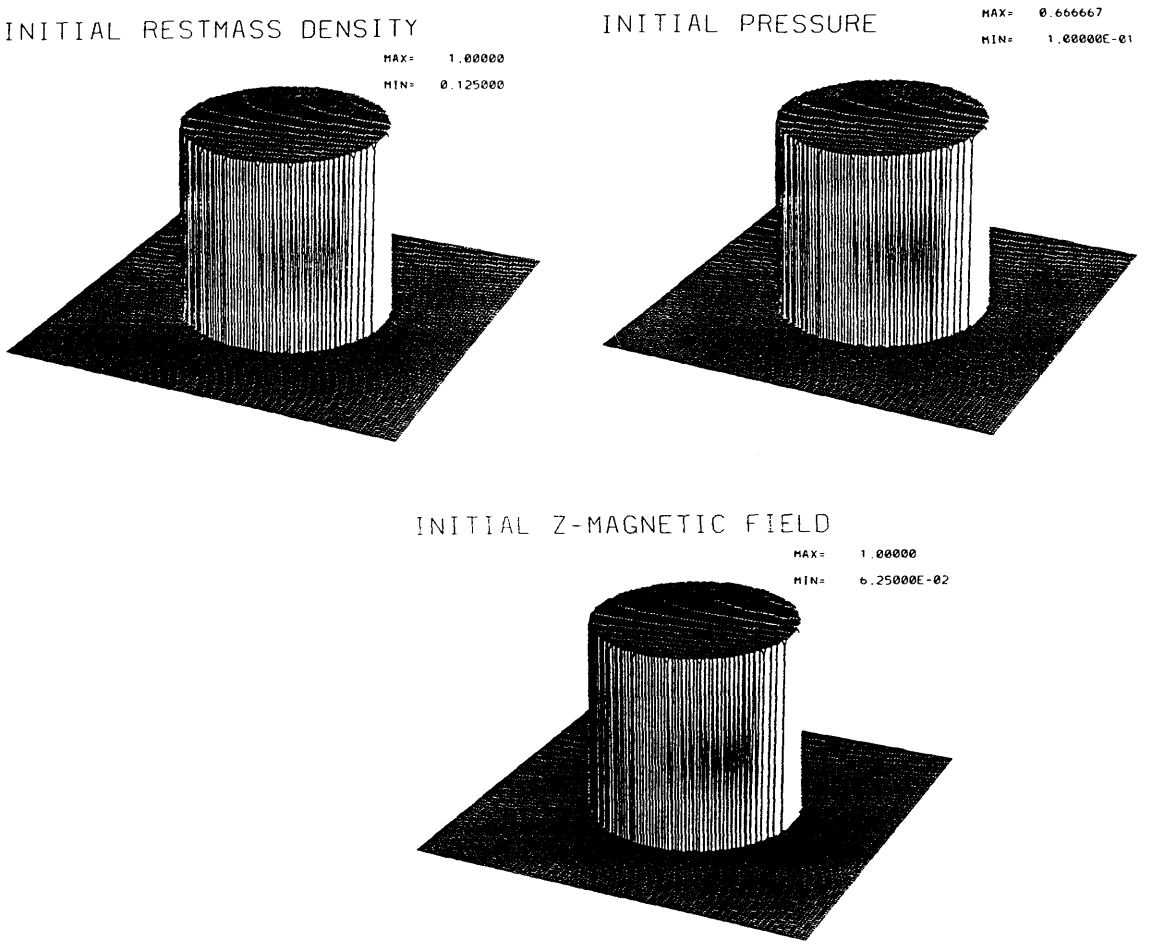

Figure 4.1: Initial density distribution in the problem of an expanding shock in transverse MHD with cylindrical symmetry. The magnetic field is alligned in the z direction along the column of high density.

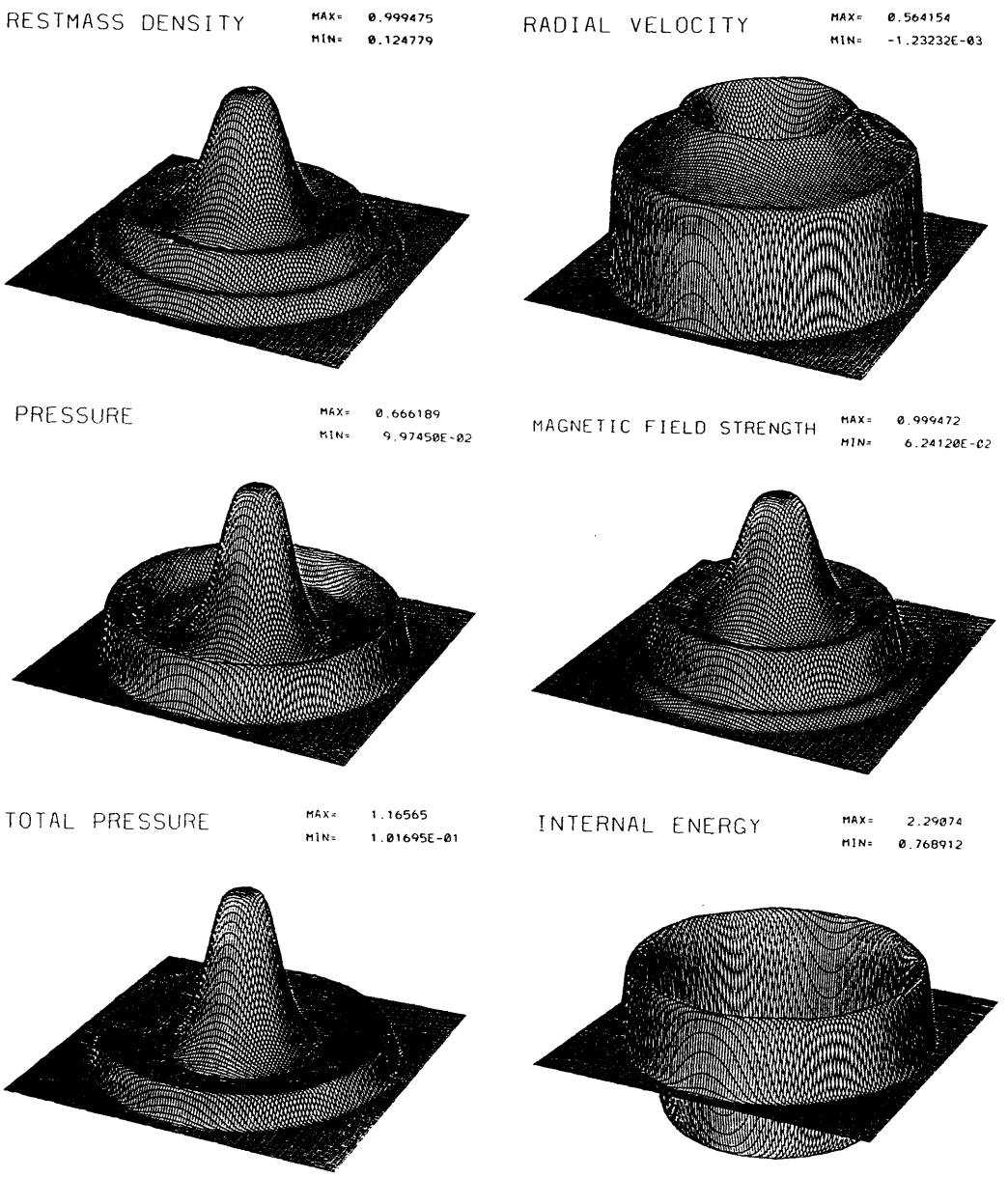

Figure 4.2: Solution of the "Mexican Hat Problem" of an expanding cylindrical shock in transverse MHD at $t = 60$ (600 time-steps).

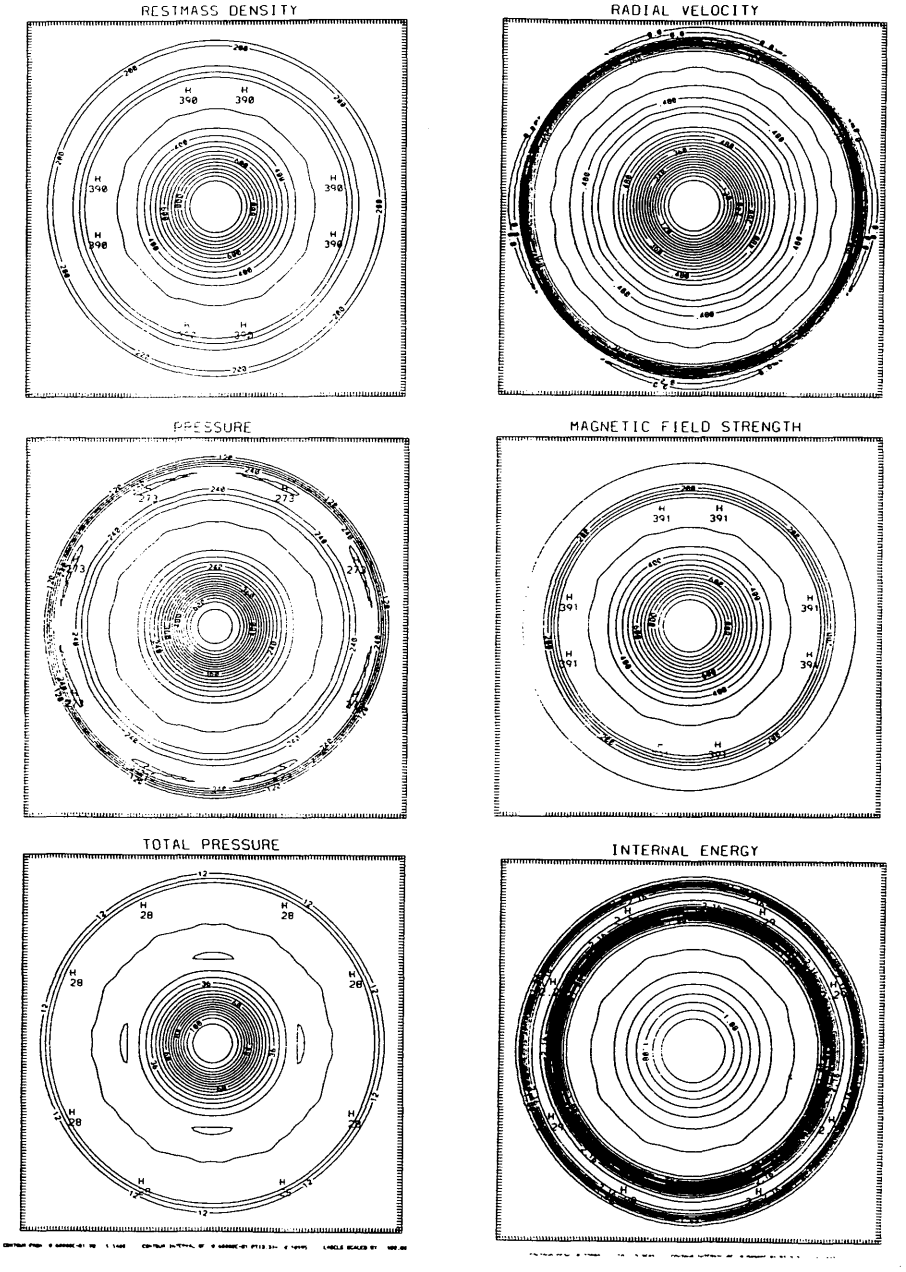

Figure 4.3: Contour plots of the solution to the problem shown in the "Mexican Hat Problem" (as in Fig. 4.2). The computation appears with high degree of isotropy.

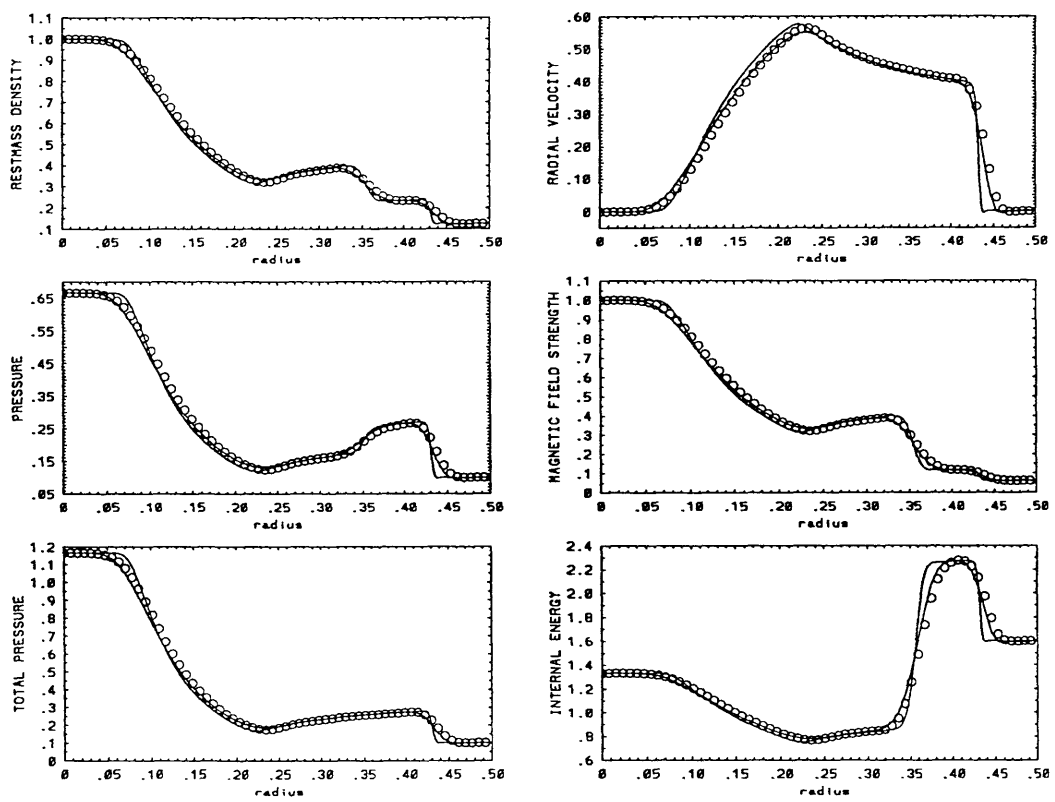

Figure 4.4: Comparison of the two-dimensional computation of the "Mexican Hat Problem" with a one-dimensional computation using polar coordinates. The dots represent the solution of the two-dimensional computation, while the two smooth curves are solutions to the one-dimensional computation in polar coordinates. The smooth curve with sharp edges represents a solution using 256 radial points, while the smooth curve with smooth edges represents a solution using 64 radial points. Notice remarkable agreement between the computations in one and two dimensions with the same number of radial points.

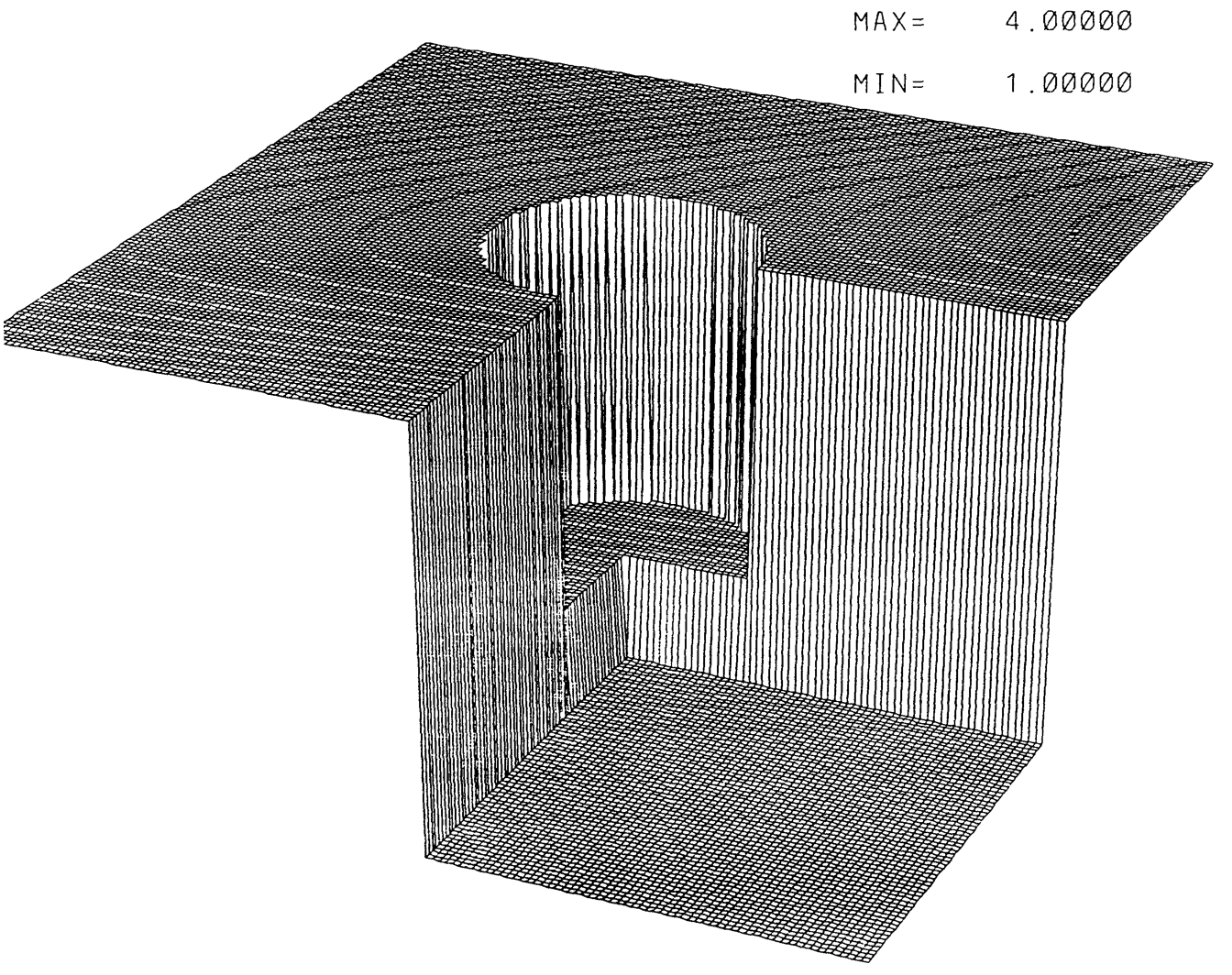

Figure 4.5: The initial density and pressure distribution in the problem of a converging cylindrical shock in relativistic hydrodynamics.

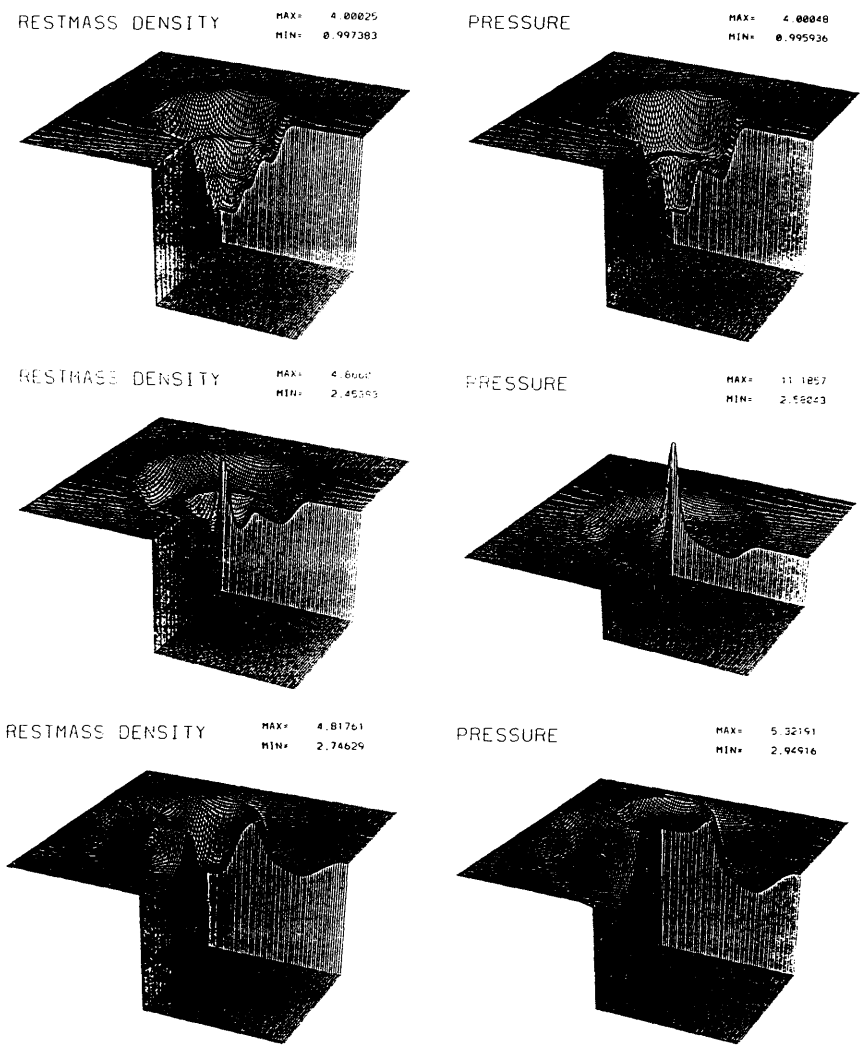

Figure 4.6: The density and pressure distributions at times $t = 30, 57, 120$ (300, 570 and 1200 time-steps) in the converging shock problem. At time $t = 57$ the numerical values of density and pressure reached their maximum in the 2D computation (theoretically both are infinite at exact time of reflection at the origin; see also Appendix A).

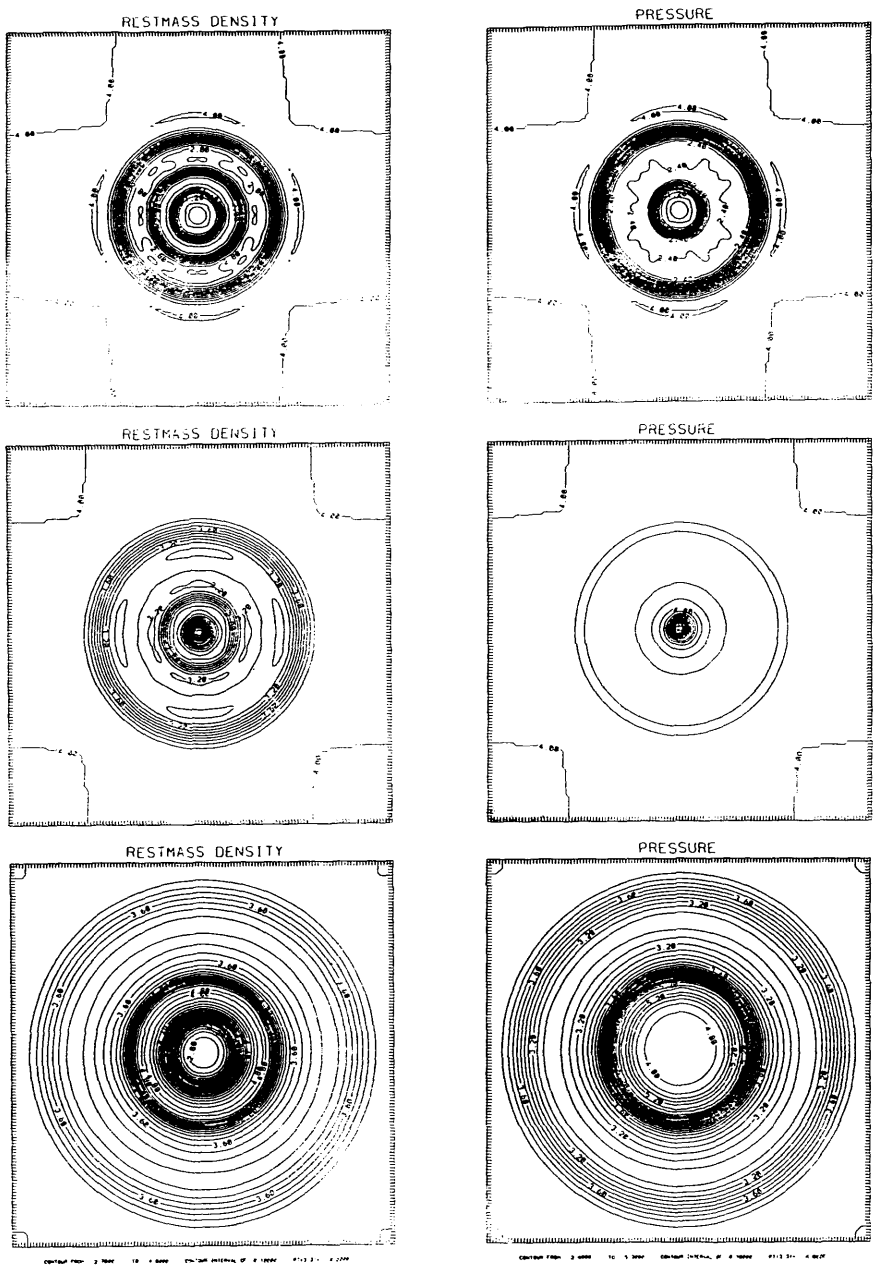

Figure 4.7: Contour plots of the solution at times $t = 30, 57, 120$ to the converging shock problem, showing high degree of isotropy.

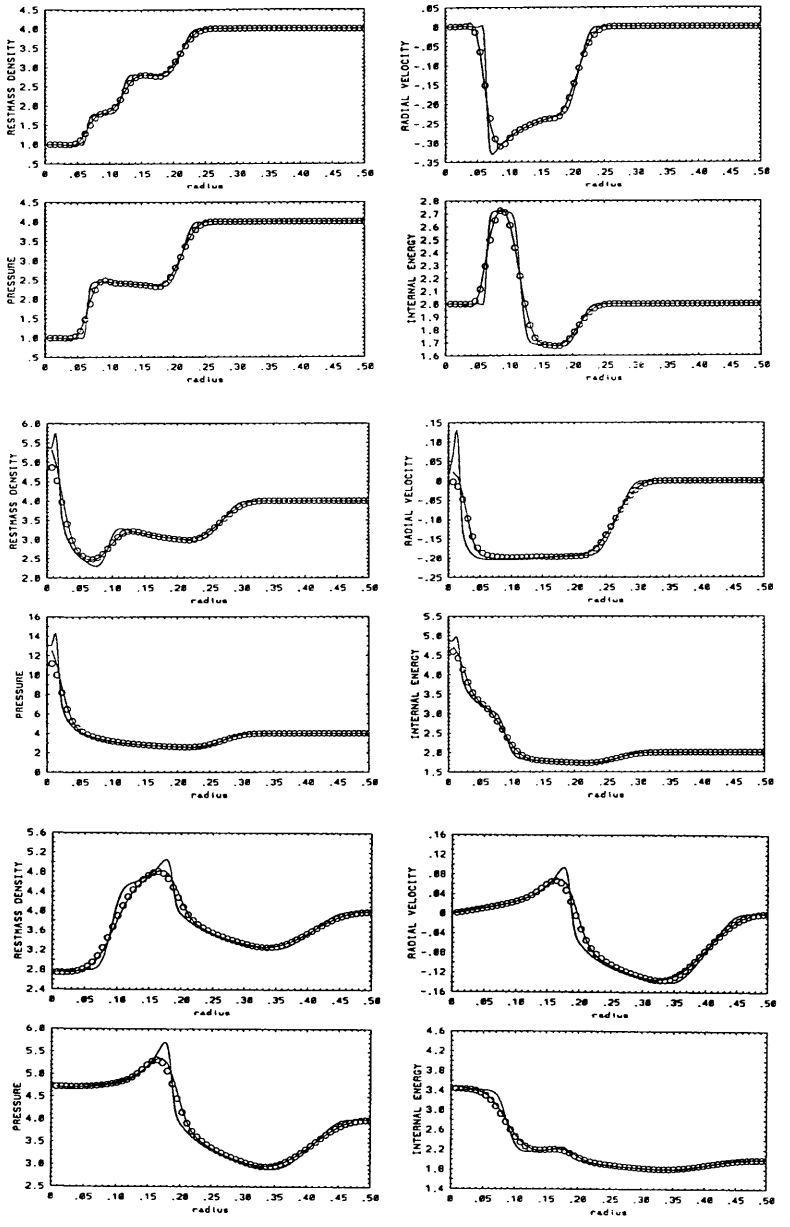

Figure 4.8: Comparison of solutions shown in Figs. 4.6-4.7 with solutions obtained in polar coordinates. The upper, mid and lower four windows correspond to times $t = 30$, 57 and 120, respectively. See caption of Fig. 4.4 for explenation of the dotted curve and the two smooth curves in each window.

origin occurs is somewhat delayed compared to the two 1D and 2D problems with lower discretizations.

These two computations indicate that the 2D implementation is highly isotropic and agrees with 1D simulations in polar coordinates. The agreement with 1D simulations suggests that convergence in the 2D simulations is no different from that reported in [55]. The standard tests of convergence by varying the mesh size and time step-size have also been performed, and no anomalies have been observed.

4.3.2 A shock induced vortex

Flow with high ram pressure, such as jets, can efficiently generate shocks. Strong shocks can further be a source of strong vorticity, as is well known in supersonic combustion theory (see, *e.g.*, [28]). We will illustrate this in the following example. Consider a relativistic flow initially moving along the positive $x-$axis (here, with $\Gamma \approx 2.35$). This flow is initially discontinuous at a sinusoidal surface, Σ, described by $(x, y) = (x, y_0 + y_1 \sin 2\pi x)$, separating the jet flow from an outer region. The fluid in the outer region is initially at rest. These initial data are shown in Fig. 4.9. Notice that some smoothing has been applied in order to prevent numerical instabilities at initial times.

A process of strong collision of gases will commence at that part of Σ which possesses a normal velocity which is ingoing, *i.e.* the "working surface" $x\epsilon(\frac{\pi}{2}, \frac{3\pi}{4})$ (in the terminology of [39]). The result is a high pressure region near this working surface bounded by two shock fronts one of which is in the jet and the other is in the outer fluid, clearly present in Fig. 4.10. This

high pressure region further possesses a contact discontinuity (a displacement of Σ) with high shear velocity as the parallel component of velocity is highly discontinuous. The high pressure fluid at the inner side of the contact discontinuity naturally possesses high parallel velocity, while the fluid at the outer side possesses low parallel velocity obtained only through expansion. The high pressure region can expand because it is localized. The parallel component of this expansion flow is highest near the edges of the contact discontinuity at $x = \frac{\pi}{2}$ and $x = \frac{3\pi}{4}$. At the edge point $x = \frac{\pi}{2}$, the expansion flow possesses a negative $x-$component of velocity and turns to join the fast jet flow at the other side of the contact discontinuity. Thus, a vortex naturally results as a mixing point for the flow from the outer region to the inner, jet flow (see Fig. 4.11).

4.3.3 An ultra-relativistic jet simulation in the hydrodynamical limit

A jet simulation in slab geometry is presented in the limit of vanishing magnetic field. The computation shows the initial evolution of a low density, $r_{jet} = 0.10$ highly supersonic jet with $\Gamma \approx 3.25$ (velocity ≈ 0.955) impinging on an outer medium of higher density, $r_{medium} = 0.5$. The jet has width W. The jet itself is in pressure equilibrium with the outer medium, $P_{jet} = P_{medium} = 0.10$. The results are shown in Figs. 4.12 -4.14. In Fig. 4.12 the jet evolution is shown at an early time (time/width=$\frac{35}{24}$), Fig. 4.13 shows the jet at three epochs time/width =$\frac{25}{24}$, $\frac{50}{24}$, $\frac{100}{24}$ and 4.14 shows the jet at time/width=$\frac{150}{24}$. In each computation $\Delta t/\Delta x = \Delta t/\Delta y = 0.10$.

These results have been obtained using a modified numerical scheme.

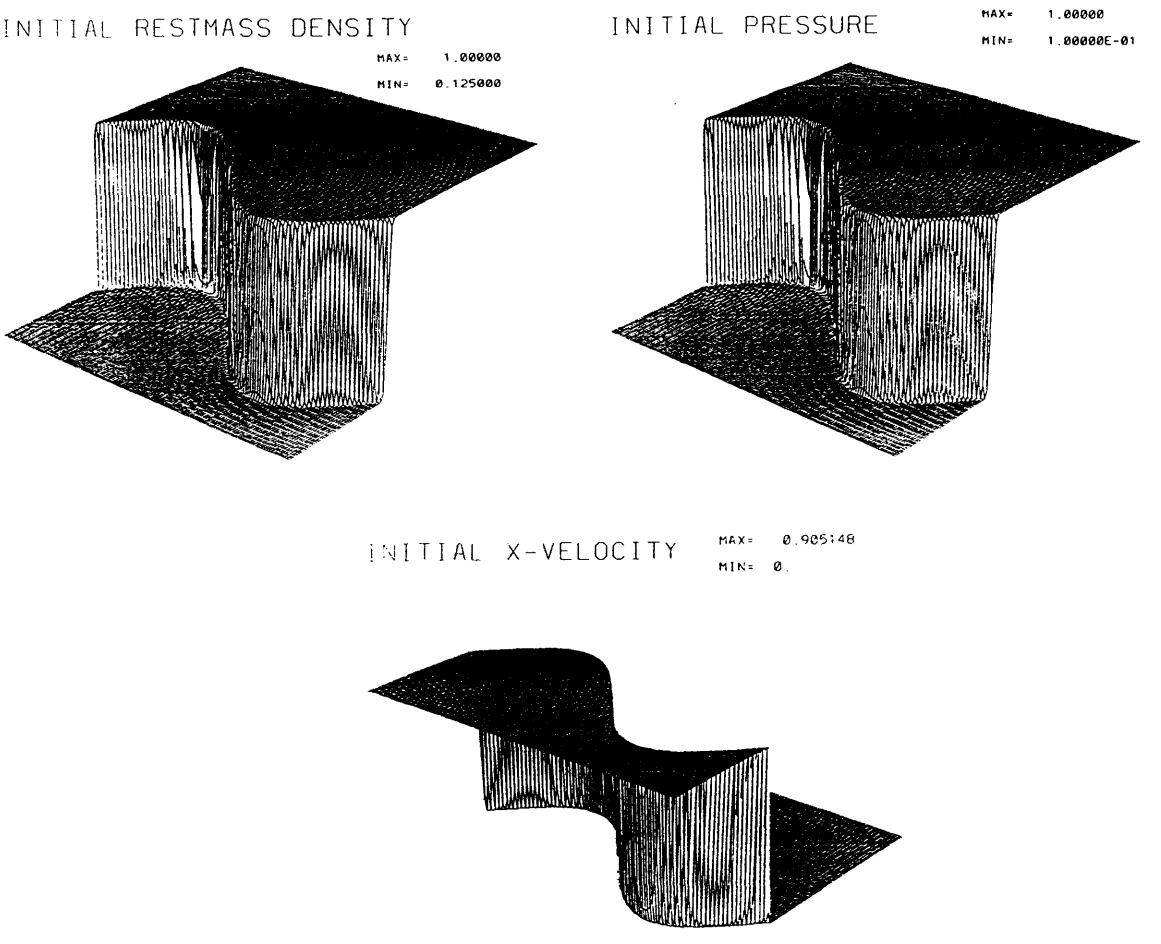

Figure 4.9: Initial data for problem of shock induced vortex by jet with $\Gamma \approx 2.35$. The jet flow is initially separated from an outer medium by a sinusoidally curved surface of discontinuity. Notice that a slight smoothing has been applied to the initial discontinuity so as to prevent initial instabilities in the computation.

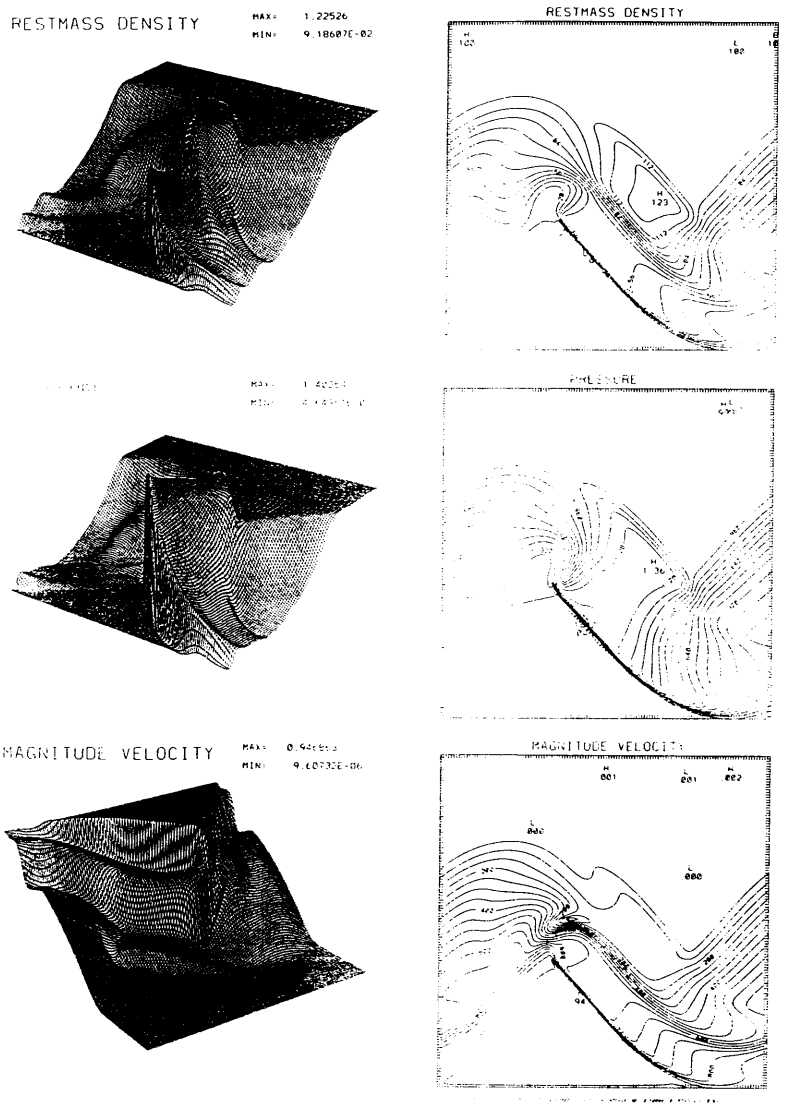

Figure 4.10: The density and pressure and velocity (magnitude) distributions at time $t = 40$ (800 time-steps). The density and pressure distributions are viewed from the the side of the jet, while the velocity distribution is viewed from the side of the outer medium. The contact discontinuity in the high pressure region clearly also appears in the distribution of magnitude of velocity due to a jump in tangential velocity.

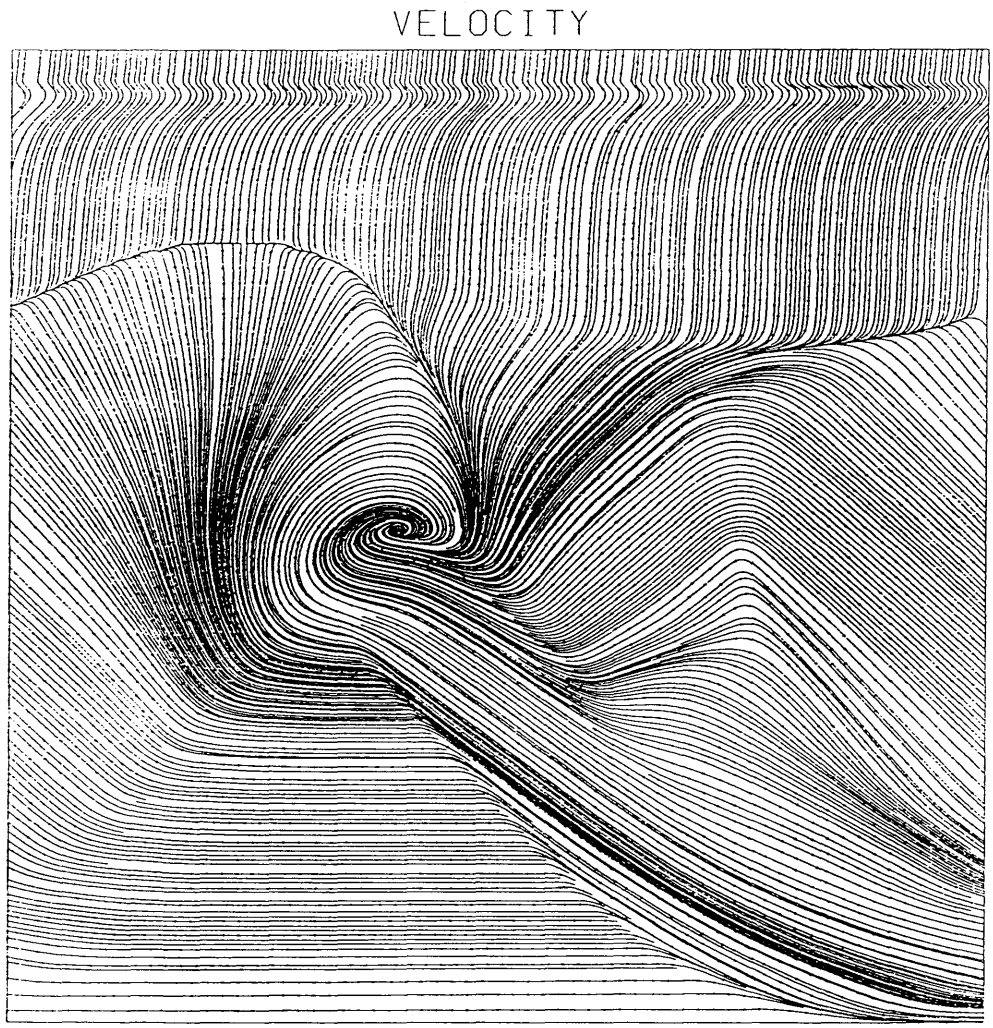

Figure 4.11: Streamline plot of problem of shock induced vortex (as in Fig. 4.10). Evidently, the vortex shows mixing of outer flow with jet flow as the flow turns clockwise here.

The smoothing S_w^{2D} was was found to give rise to artificial pressures due to the ultra-relativistic shear flow at the interface of the jet and the outer medium. As the unit velocity four-vector u^a, $u^a u_a = -1$, couples the momentum density in the y-direction to the energy equation, smoothing in the transverse, y-direction induces artificial pressures. These pressures can become significant at points where Γ possesses a large jump. This constitutes a fundamental problem with smoothing when applied uniformly to all equations. This problem has been circumvented *ad hoc* by avoiding smoothing by $S_{w,y}$ on the densities F^{tA} altogether.

The results in Fig. 4.12 are obtained on a grid with 128 by 128 points. The computation has been performed on a grid with 128 by 64 points using reflection symmetry across the axis of the jet. Fig. 4.12 clearly shows an instability arising at the contact surface between the shocked jet fluid and the shocked outer medium. Two dark points on this contact surface represent low density regions which numerically run away to negative densities and prohibit further computation. Notice also the curving of the shock surface in the jet flow, most clearly in the pressure distribution; expansion of the shocked jet fluid sidewards decreases pressure and accelerates the shock in the jet. For the purpose of long-time integration the jet flow has been given a smooth profile across, thereby preventing this instability from arising. The results are shown in Figs. 4.13-4.14. These computations have been performed on a grid with 256 by 128 points, and the results are shown after reflection across the $x-$axis. Notice flaring of the shocked outer medium in the extended region behind the bow shock in the extended region away from the jet. It

requires further numerical study to distinguish whether this is physical or numerical[2]; it clearly originates at the head of the bow shock. Notice also the two small strike-features in the pressure distribution at time/width=$\frac{50}{24}$. This discontinuity is an acoustic wave in the jet with small opening angle, θ, due to relativistic beaming, $\tan\frac{\theta}{2} = \frac{1}{\Gamma}\frac{\alpha}{v_{jet}}$. Here, α is the local sound speed, $\alpha^2 = \frac{\gamma\frac{P}{\rho}}{1+\frac{\gamma}{\gamma-1}\frac{P}{\rho}}$ [20]. This amounts to a small opening angle, $\tan\frac{\theta}{2} \approx 0.19$.

These relativistic jet computations are to be regarded as indicative for future work on relativistic jet simulations. It would be of interest to apply Roe's method on the equations of relativistic hydrodynamics (using the equations for hydrodynamics in divergence form as they follow from MHD in divergence form with vanishing magnetic field (see [55])) for reasons of comparison.

4.3.4 Magnetic pressure dominated stagnation points

Three problems in nontransverse MHD are considered to illustrate MHD in divergence form and the computational method in some more generality. These problems also serve to illustrate the fact that the computational method preserves divergence free magnetic fields to within arbitrarily small error. The problems have an initially cylindrical column distribution of high density and high pressure (Fig. 4.15). Three computations are presented,

[2]Improved results have been obtained using the 2D smoothing operator defined by $S_w^{2D}\{F^{tA}\} = \frac{1}{2}(S_{w,x} + S_{w,y})\{F^{tA}\}$ if $A = y$ and $S_w^{2D}\{F^{tA}\} = \frac{1}{2}(S_{w,x} + id)\{F^{tA}\}$ if $A \neq y$. This construction is based on the observation that the primary jet flow is ram pressure dominated, while the shocked jet flow and the shocked ambient flow are both hydrostatic pressure dominated. This S_w^{2D} applies strong smoothing along the field parallel to the jet axis and mild smoothing along the field transverse to the jet, and, importantly, shows no flaring.

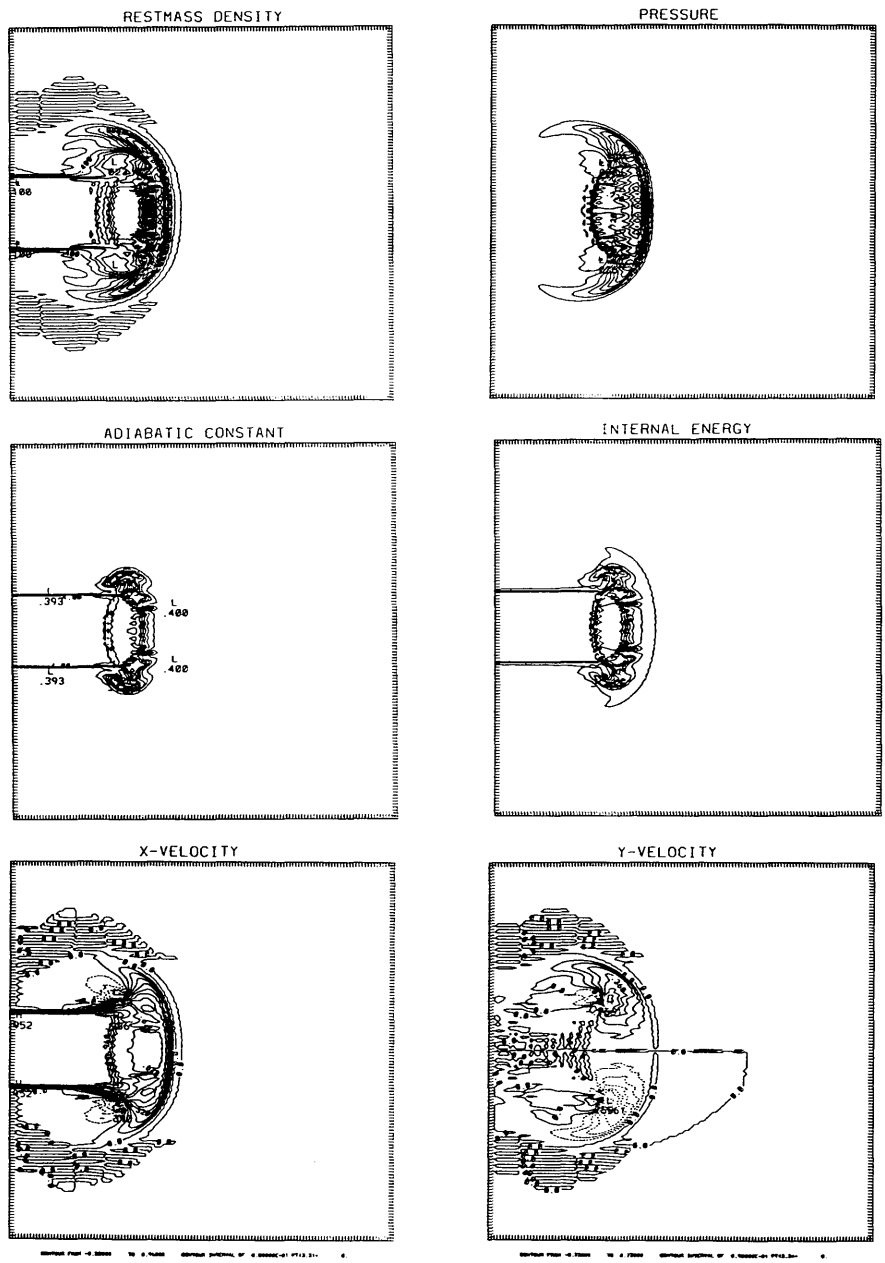

Figure 4.12: The initial evolution of the relativistic hydrodynamical jet with $\Gamma \approx 3.25$. The two sharp features in the contact surface between the shocked jet fluid and the shocked outer medium are points of instability in this computation. The time/width = $\frac{35}{24}$.

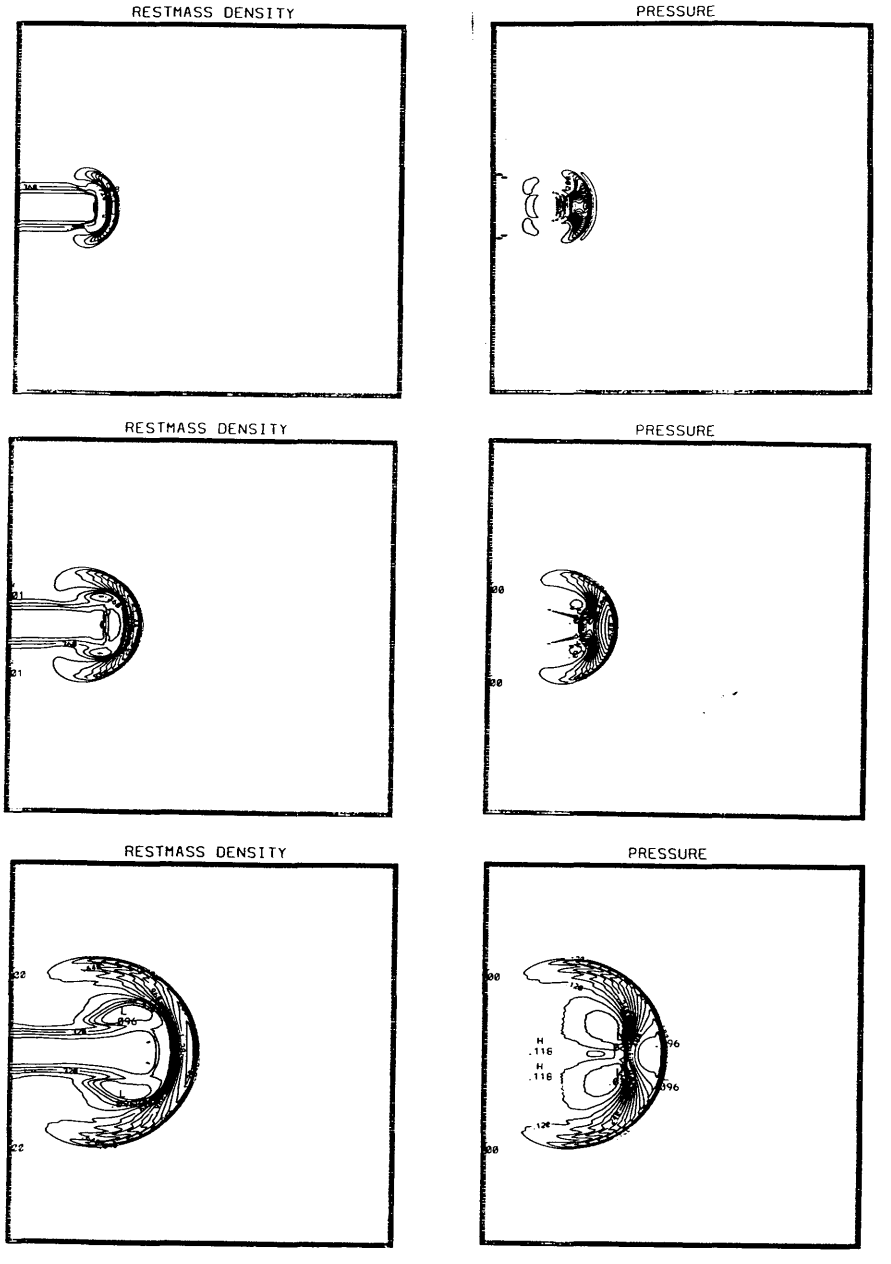

Figure 4.13: The jet at three epochs at time/width=$\frac{25}{24}, \frac{50}{24}, \frac{100}{24}$. The jet has been given a smooth profile across so as to avoid any initial instabilities on the contact surface. Notice flaring of the shocked outer medium behind the bow shock in the extended region away from the jet.

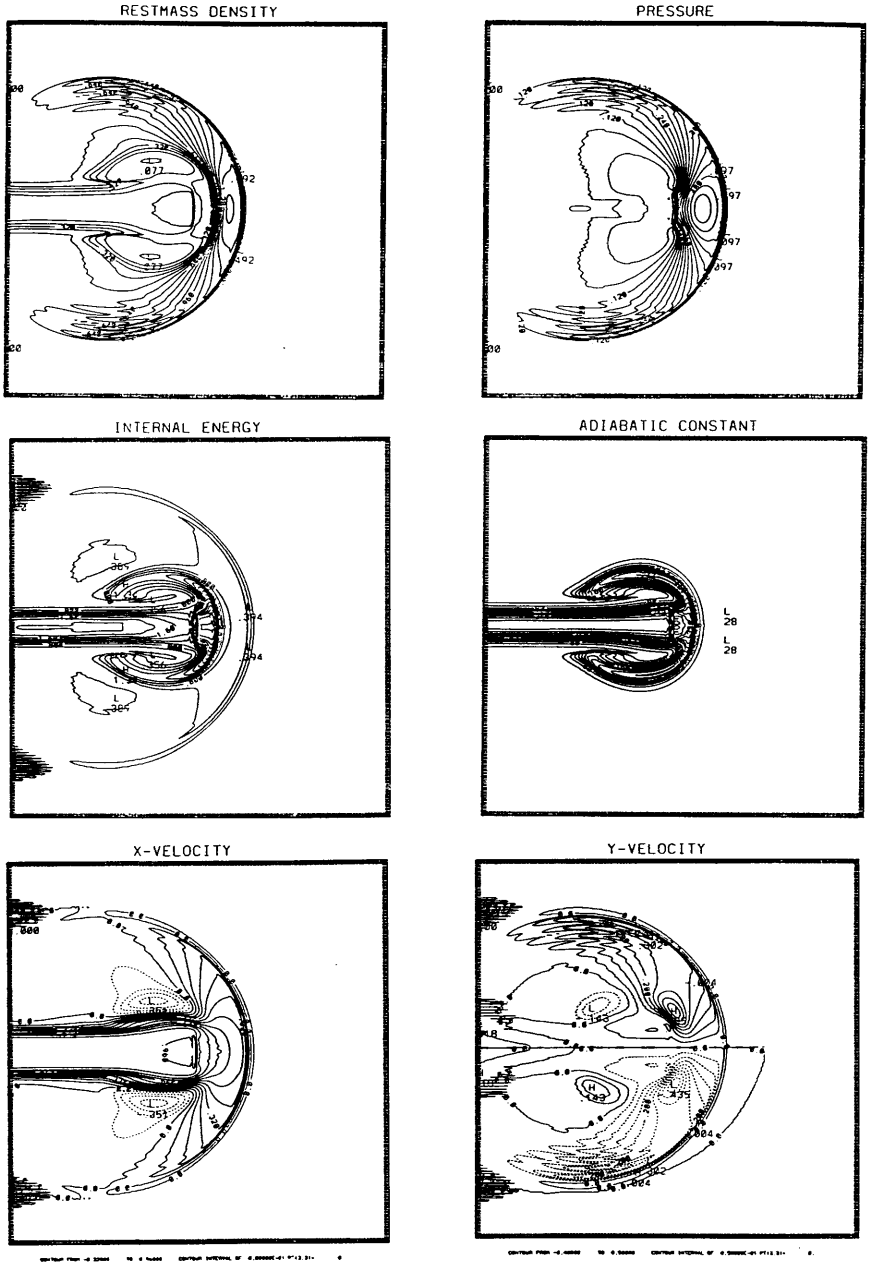

Figure 4.14: The jet at time/width=$\frac{150}{24}$.

Problem	Quantity	Column	Environment
(a)	density	1	0.125
	pressure	2/3	0.100
(b)	density	4	1
	pressure	4	1
(c)	density	10	1
	pressure	$\frac{2}{3}10^{3/2}$	1

Table 4.1: Initial data in the three test problems in nontransverse MHD.

showing cases for various $\beta = P/h^2$. Initially, the density and pressure in the column are taken to be as in Table 4.1. The problem is considered in an initially uniform magnetic field in the (x,y)-plane of strength $\sqrt{2}$ and aligned along the main diagonal of the grid. The results are shown in Figs. 4.16-4.22. Each of the results may (somewhat loosely) be interpreted as a symbiosis of two one-dimensional problems, one a shock-tube problem in transverse MHD and the other a shock-tube problem in MHD with longitudinal magnetic field. One-dimensional simulations (in simple planar geometry) of the associated longitudinal and transverse MHD problems show remarkable agreement with the respective longitudinal and transverse intersections of the distributions in the 2D problem. The 2D problem only differs in a jump in the magnetic field at the shock-front in the longitudinal intersection, which is due to the cylindrical geometry (in planar geometry there would be no such discontinuity). The results have also been computed with 400 time-steps ($\eta = \Delta t/\Delta x = 0.15$). This results in a slight overshoot at the shock, but otherwise identical distributions. Furthermore, the computation shows

Two nearly perfect stagnation points appear in the streamline plot of the velocity (Fig. 4.22(a)). These stagnation points also appear clearly as two local maxima in the total pressure, $P + h^2/2$ on the line through the origin perpendicular to the magnetic field. Furthermore, the pressure at these stagnation points is *predominantly magnetic pressure*, as follows from comparison of the distributions of pressure, magnetic field strength and total pressure in Fig. 4.16.

The decreasing importance of the magnetic field in these three problems is apparent from the three respective total pressure distributions in Figs. 4.16-4.21 and the plots of velocity streamlines and magnetic field lines in Fig. 4.22. The shock strength in these problems clearly increases in going from Problem (a) to Problem (c). Finally, we remark that in these test problems the absolute value of $c_1(U)$ was kept below 10^{-6}.

4.4 Conclusions

Some test 2D shock computations in MHD in divergence form have been performed using an extension of the pseudo-spectral method from [56]. The numerical results show that

(a) convergence and accuracy are consistent with one-dimensional simulations;

(b) the results are highly isotropic;

(c) the computational method preserves divergence free magnetic fields (in the sense of the discretized spatial derivative) to within arbitrarily small error, even when shocks are present.

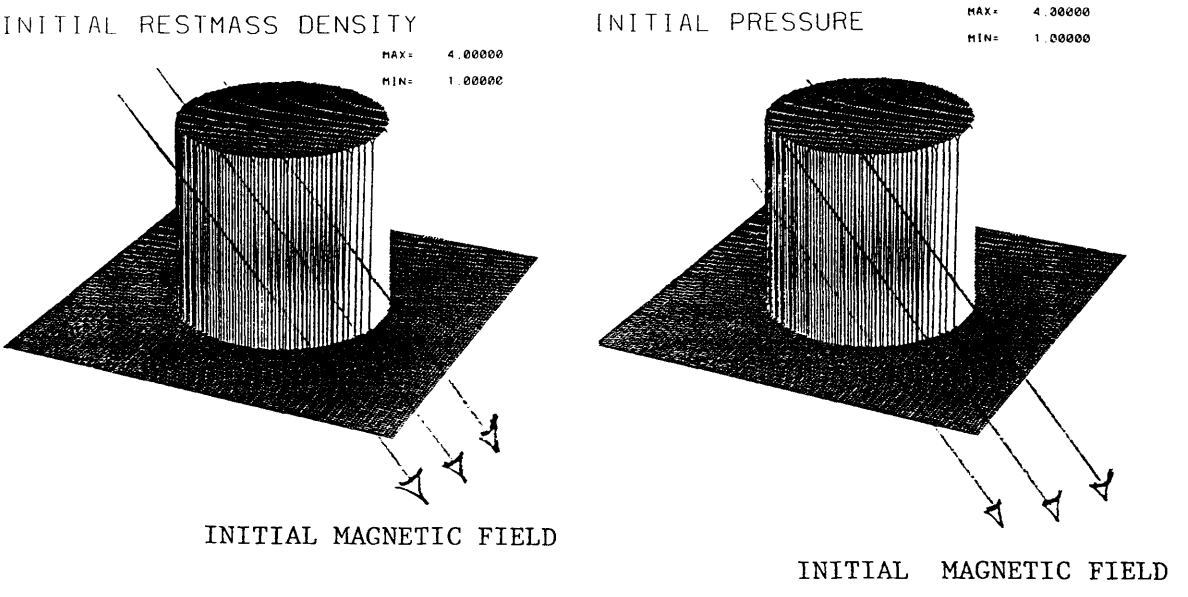

Figure 4.15: The initial density and pressure distribution in the problem of an expanding shock in nontransverse MHD. The magnetic field is initially uniform and aligned along the main diagonal of the Cartesian grid.

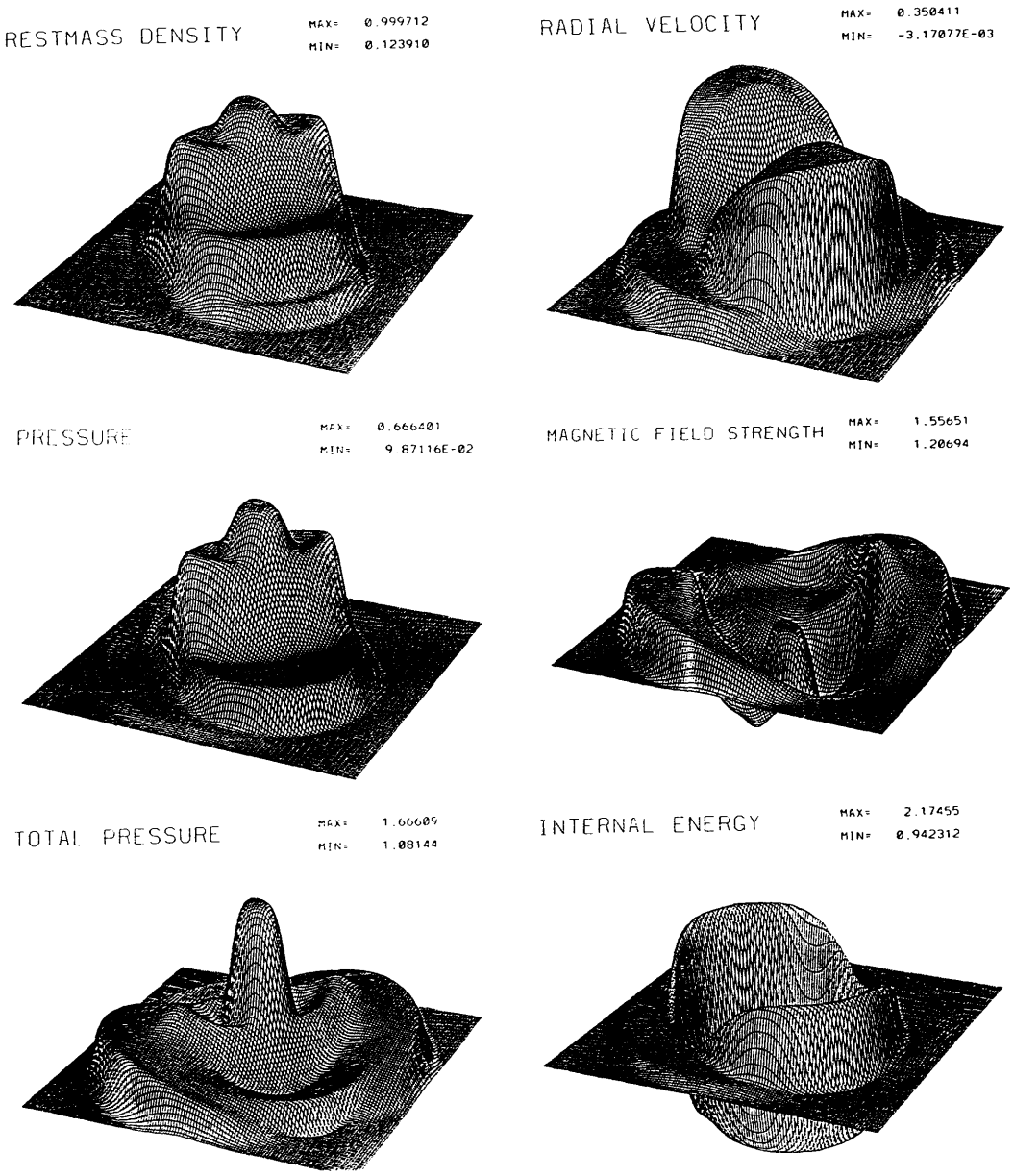

Figure 4.16: The solution to the shock problem with initial conditions as given in (a) of Table 4.1. at $t = 60$ (600 time-steps). The solution may be interpreted as an intrigate symbiosis of two one-dimensional problems one of which is a shock-tube problem in transverse MHD while the other is a shock-tube problem in MHD with longitudinal magnetic field.

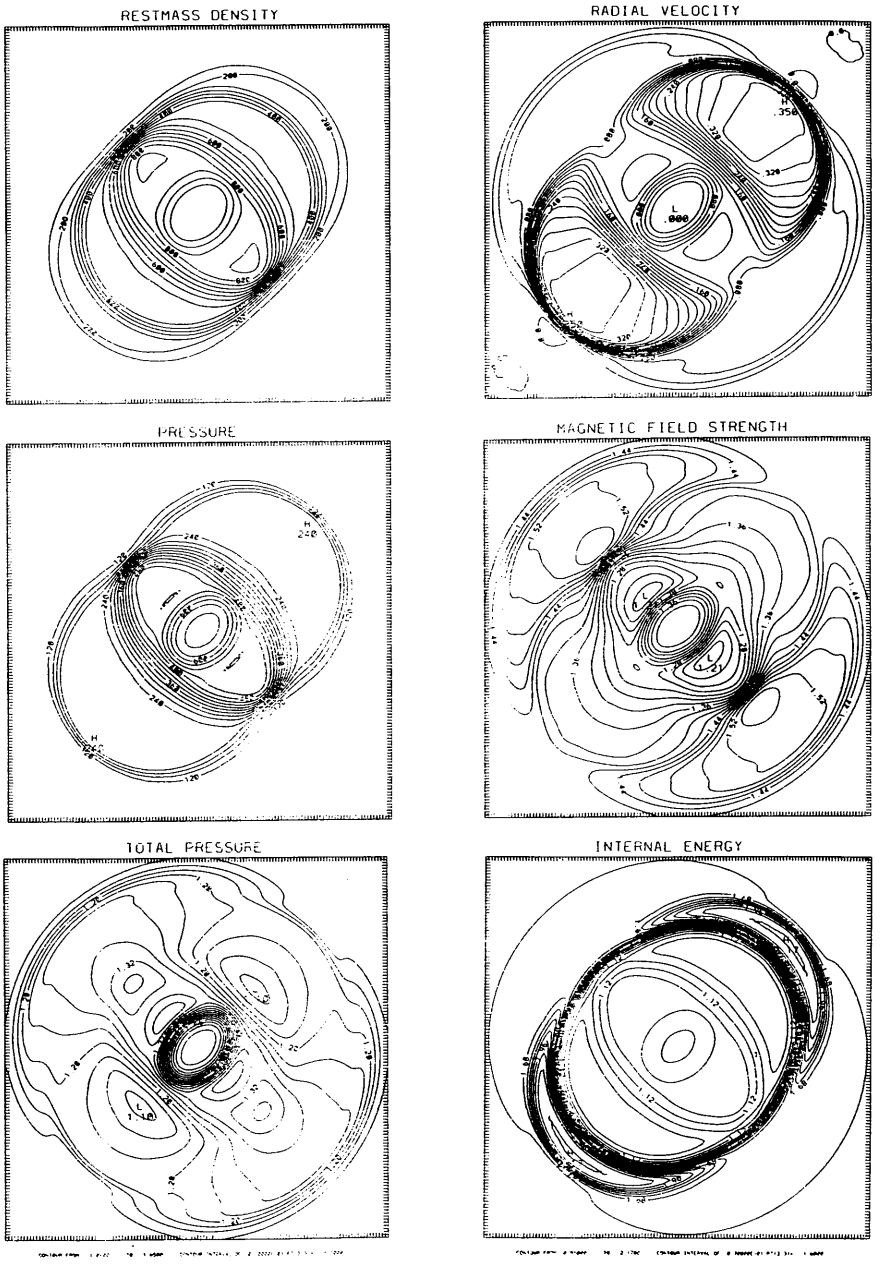

Figure 4.17: Contour plots of the solution to nontransverse MHD Problem (a).

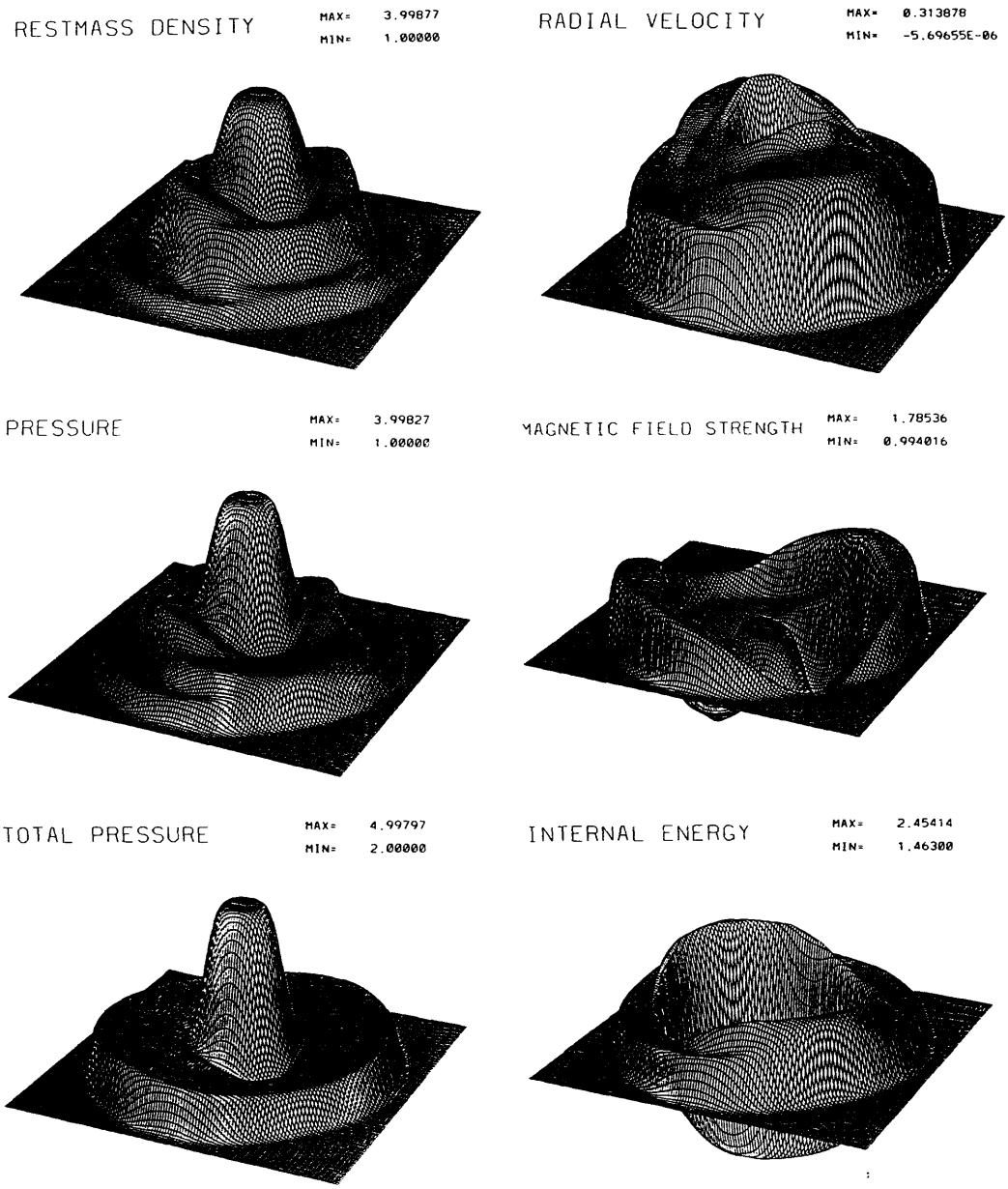

Figure 4.18: The solution to the shock Problem (b) in nontransverse MHD at $t = 60$.

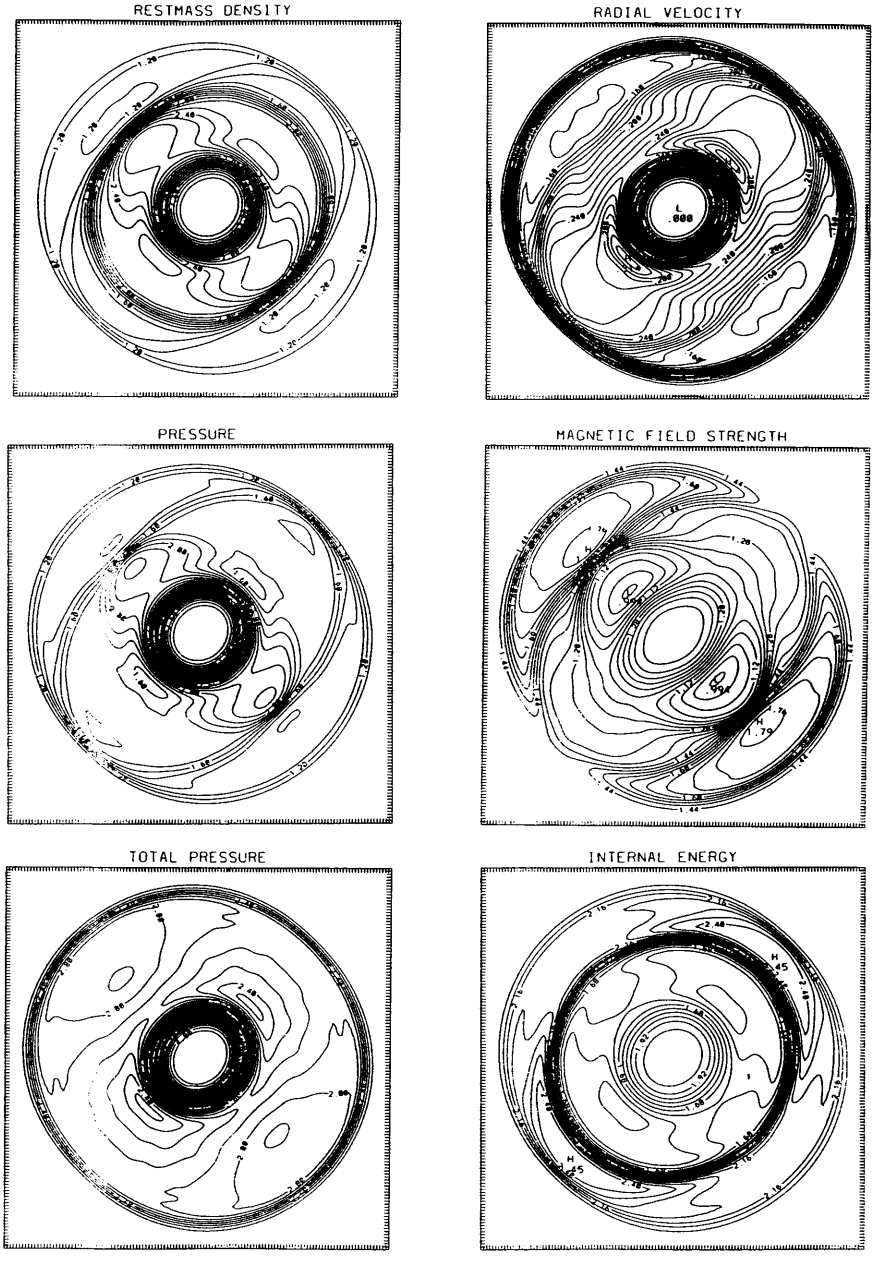

Figure 4.19: Contour plots of the solution to nontransverse MHD Problem (b).

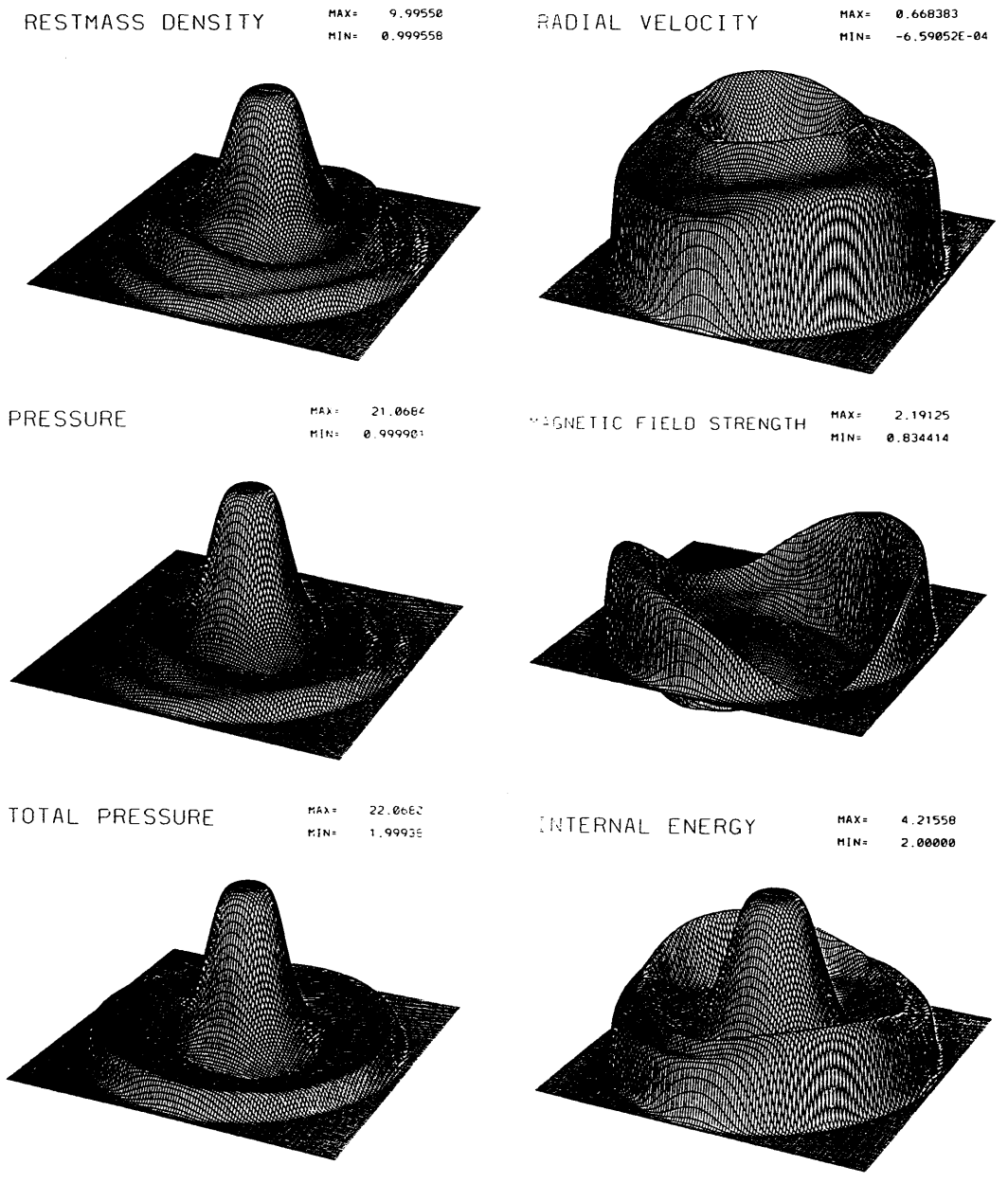

Figure 4.20: The solution to the shock Problem (c) in nontransverse MHD at $t = 60$.

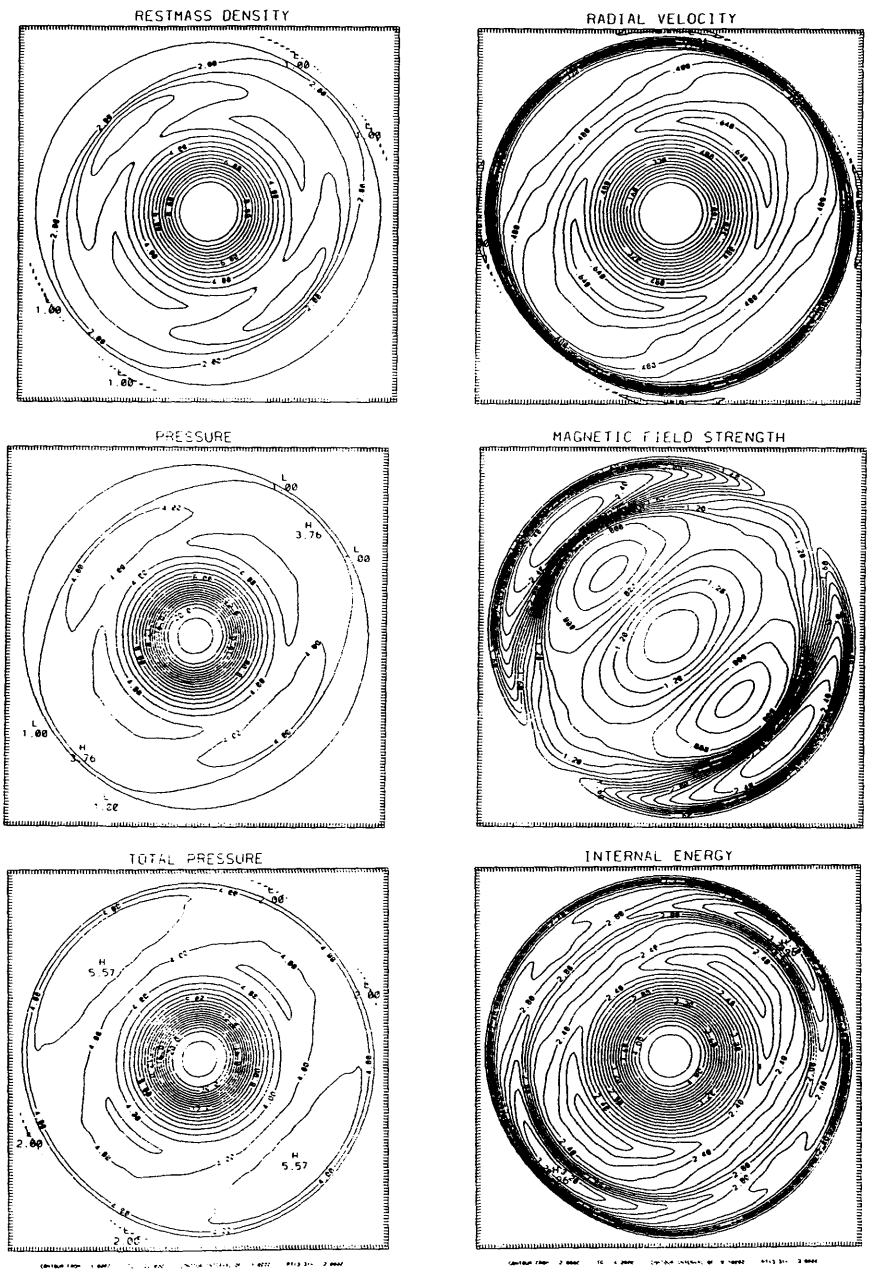

Figure 4.21: Contour plots of the solution to nontransverse MHD Problem (c).

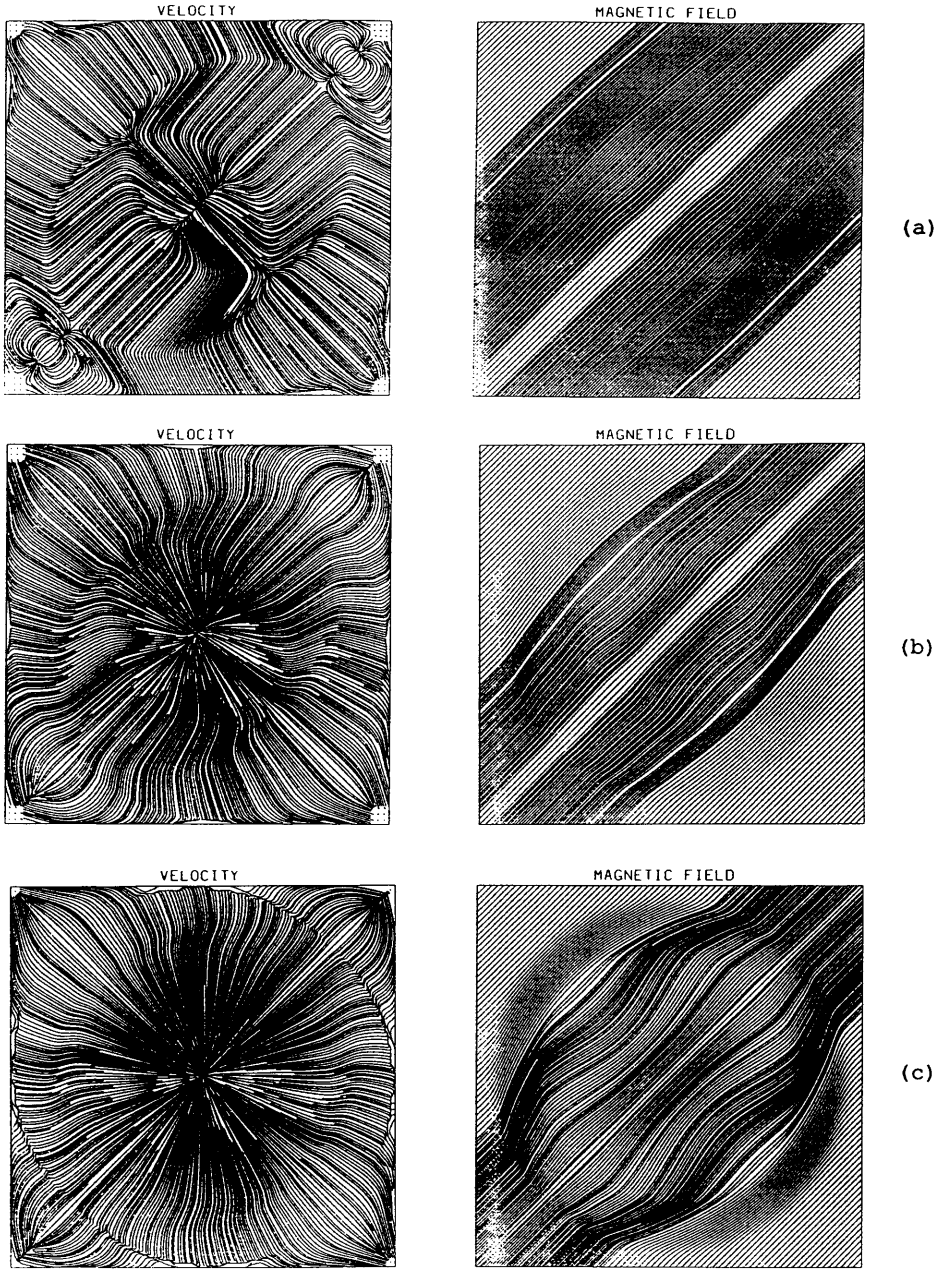

Figure 4.22: Streamline plots of velocity and magnetic field lines in the rest-frame of the grid of Problems (a)-(c).

The power of this numerical implementation is further brought about by obtaining these results on a two-dimensional Cartesian grid with uniform spacing and explicit time-stepping.

The difficulties of the smoothing method (4.2) in hydrodynamical problems with ultra-relativistic shear flow indicate that *Riemann problems with relativistic shear flow* are the appropriate test problems for numerical hydrodynamics in the ultra-relativistic limit.

The results on the magnetic pressure dominated stagnation points demonstrate that MHD in divergence form allows for accurate and stable numerical simulations of two-dimensional shock problems.

Acknowledgement The author wishes to express his gratitute to Prof. Sterl E. Phinney for his support and to Dr. Tasso J. Kaper for his many constructive comments during this work.

Appendix A

A note on rotational discontinuities

In this note we will illustrate numerically rotational disontinuities, which did not arise in the coplanar Riemann problem discussed in Chapter 3. Rotational discontinuities travel at intermediate velocities: faster than slow rarefaction waves and slower than fast rarefaction waves. They can be introduced by perturbing the coplanar Riemann problem into a noncoplanar Riemann problem, for example, by taking initially

$$\begin{cases} h_z = 0 (x < \frac{1}{2}), \\ h_z = h_z^{(0)} (x > \frac{1}{2}), \end{cases} \tag{A.1}$$

while maintaining the initial condition $u^z \equiv 0$. This introduces two rotational discontinuities, traveling in opposite directions. We will consider a perturbed case of that shown in Fig. 3.3. With $h_z^{(0)} = 0.0025$ this is illustrated for the relativistic case $\epsilon = 0.5$ in Fig. A.1 and the nonrelativistic case $\epsilon = 0$ in Fig. A.2. Clearly, a rotational discontinuity resides between the slow shock and the fast rarefaction wave traveling to the right. Notice that the velocity of the slow shock is close to the velocity of the rotational discontinuity in the

Quantity	$\epsilon = 0.50$	$\epsilon = 0$
$(v_A)_L$	-0.0838	-0.2761
v_{shock}	-0.0752 ± 0.0025	-0.2958 ± 0.010
$(v_A)_R$	-0.0949	-0.2997

Table A.1: The Alfven and shock velocities in the compound wave. $(v_A)_L$ denotes the Alfven velocity ahead and $(v_A)_R$ denotes the Alfven velocity behind the shock. The data are listed for both the relativistic case $\epsilon = 0.50$ and the classical case $\epsilon = 0$.

relativistic case. With $\epsilon = 1$ numerical results indicate that they are almost equal. This limiting case is related to the problem of intermediate shock waves discussed below (see also Lichnerowicz [7, 8] for theoretical results).

In the case of classical MHD the change of sign of h_y indicate that this shock is intermediate (the argument used by Brio and Wu [37]). That is, the velocity of the rotational discontinuity is less than the shock speed ahead of the shock and larger than the shock speed behind the shock. We have computed the Alfven wave speeds using the relations (*cf.* [6, 50])

$$\begin{array}{ll} \text{relativistic MHD:} & (rf + h^2)(u^a \nu_a)^2 - (h^a \nu_a)^2 = 0, \\ \text{nonrelativistic MHD:} & v_A = v - H_x/\sqrt{r}, \end{array} \tag{A.2}$$

and the shock speed by taking the center point on the jump as the shock position. The results are listed in Table A.1. The uncertainty in the shock velocity due to the finite grid resolution of 2048 points is also listed. Thus, Table A.1 indicates that the relativistic shock is not intermediate, while alone it leaves open whether the classical shock is intermediate (which illustrates a limit of our numerical implementation).

Notice peaks at the shock in the compound wave. In the relativistic case

the relative velocities of the shock and the Alfven waves at either side of it are so small that the rotational wave does not separate from it given the limit of our resolution. In the classical case the rotational wave remains "captured" at the shock. In both cases this results numerically in a nonstationary shock region of finite thickness. Because intermediate waves leave the thermodynamical state of the fluid unchanged, this shock persists for longer time even as the peak becomes large.

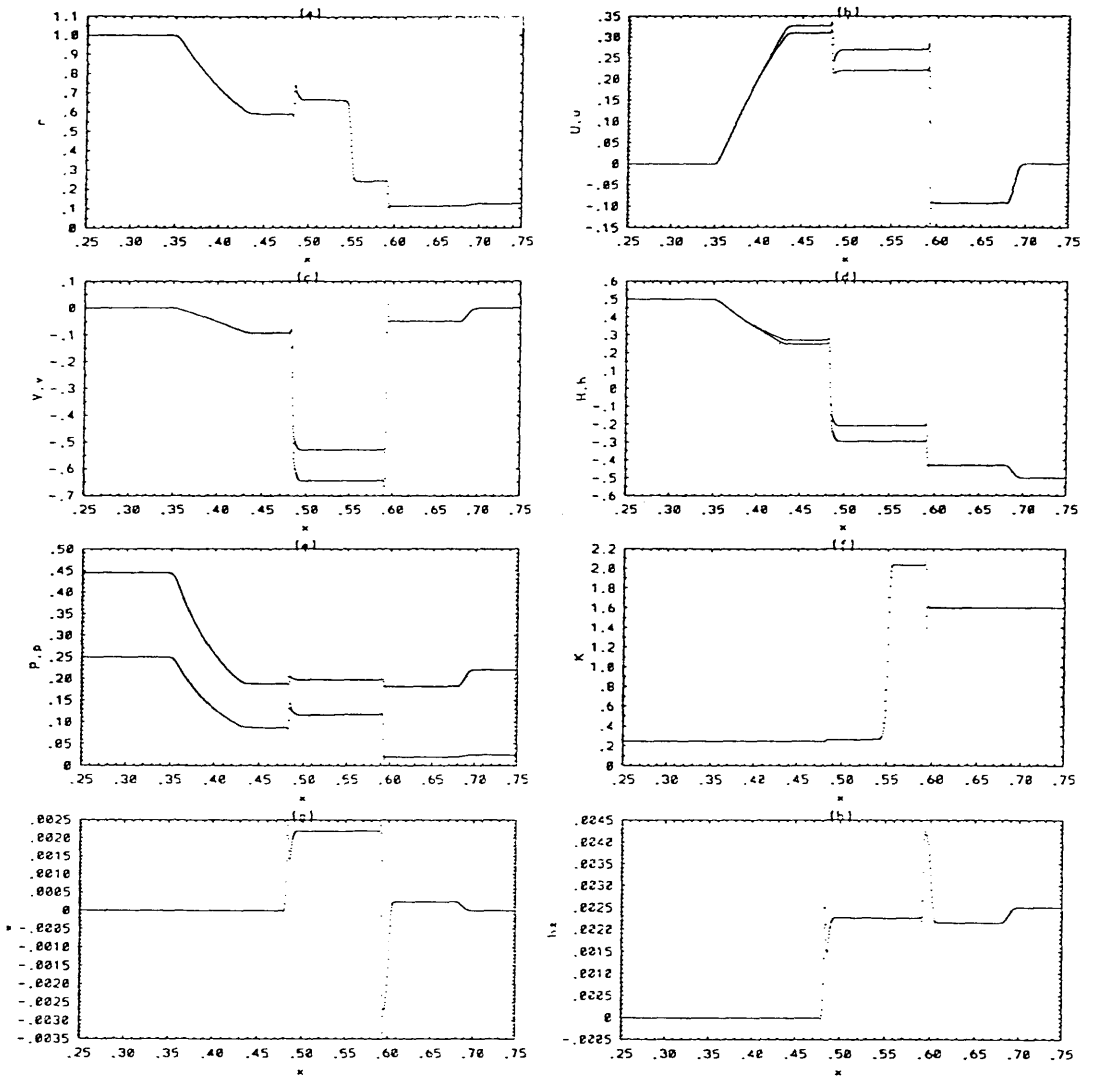

Figure A.1: The rotational discontinuity between the slow shock and the fast rarefaction wave travelling to the right in the relativistic problem $\epsilon = 0.50$. Here, $h_z^{(0)} = 0.0025$. Notice that the shock speed is close to the Alfven wave speed. The peak in the slow shock in the compound wave is due to the rotational discontinuity which travels to the left. The number of grid points is 2048 and the number of time-steps is 3000 with $\Delta t/\Delta x = 0.15$. and $w = 10$.

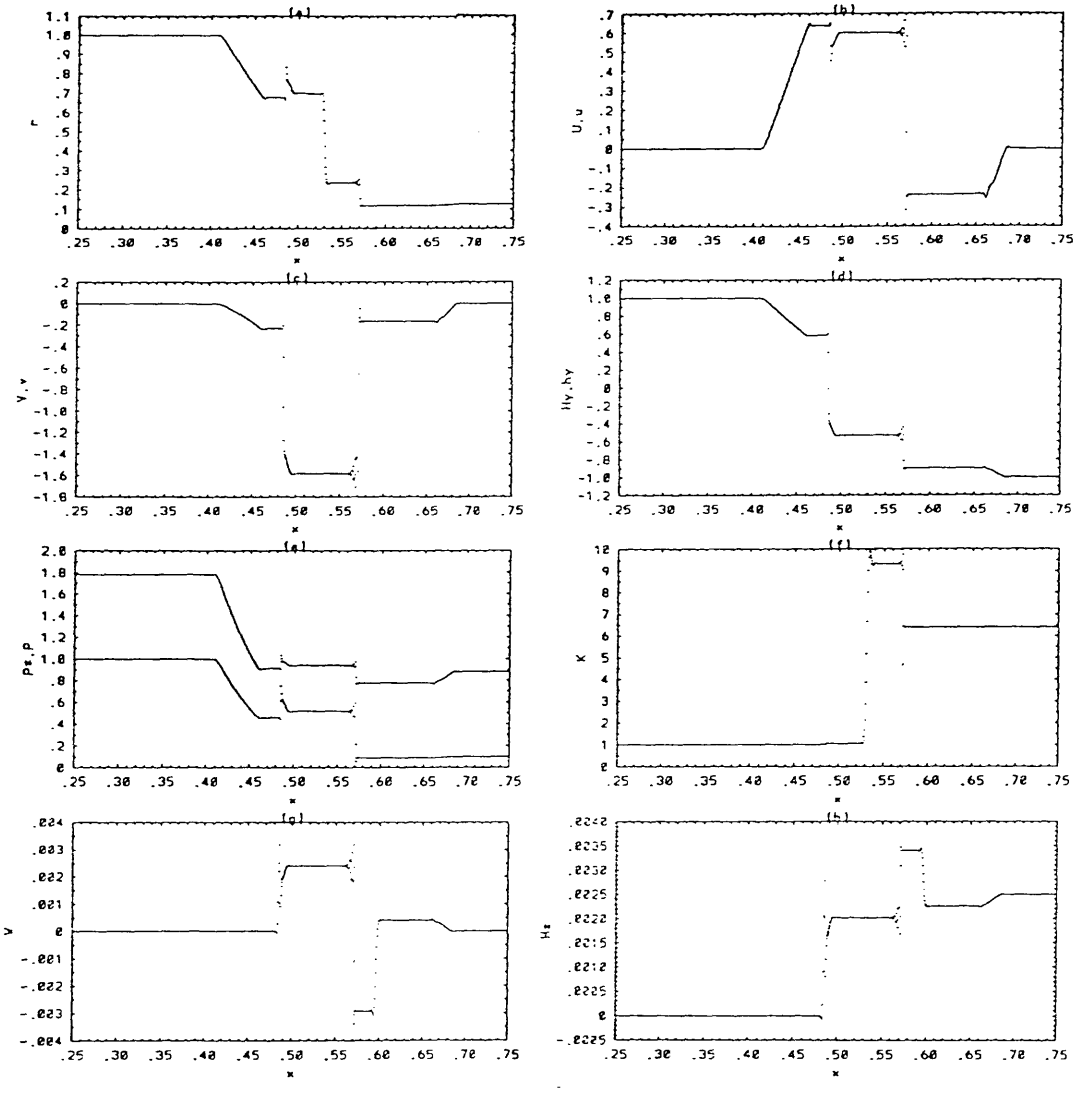

Figure A.2: The same prolem is in Figure A.1, but now for the nonrelativistic case $\epsilon = 0$ with $h_z^{(0)} = 0.0025$. The number of grid points is 2048 and the number of time-steps is 676 with $\Delta t/\Delta x = 0.15$ and $w = 12$.

Appendix B

Asymptotics of shock strength

An asymptotic analysis of the shock strength in the converging shock problem in Chapter 4 is given. Introduce the shock strength, z, as the ratio of the post- and pre-shock pressure, P and P_0, respectively, and denote by R the ratio of the post- and pre-shock restmass densities, r and r_0, respectively. We will analyze the problem in a frame comoving with the shock. Let (t, σ, ϕ) denote polar coordinates in the laboratory frame such that the shock front corresponds to $(t, \Sigma(t), \phi)$. The transformation $\sigma = \frac{\bar{\sigma}+\Sigma'(t)\bar{t}}{\alpha}$, $t = \frac{\bar{t}+\bar{\sigma}\Sigma'(t)}{\alpha}$ with $\alpha = (1 - \Sigma'(t))^{\frac{1}{2}}$ further introduces the coordinates $(\bar{t}, \bar{\sigma}, \phi)$ such that the shock surface corresponds to $(\bar{t}, 0, \phi)$. The line element for this coordinate system is given by

$$ds^2 = -d\bar{t}^2 + d\bar{\sigma}^2 + \sigma^2 d\phi^2. \tag{B.1}$$

We will describe the evolution of the shock first in this comoving coordinate system.

The Rankine-Hugoniot relations for relativistic hydromagnetics are given

by [20],

$$f^2 - f_0^2 = (P - P_0)(\frac{f}{r} + \frac{f_0}{r_0}) \tag{B.2}$$

with $f = 1 + \frac{\gamma}{\gamma-1}\frac{P}{r}$ and $f_0 = 1 + \frac{\gamma}{\gamma-1}\frac{P_0}{r_0}$. Notice that we assume the polytropic index γ to be the same in the pre- and post-shock region. Let $v = \tanh\lambda$ and v_0 denote the fluid velocities behind and ahead of the shock. Notice that $\Sigma'(t) = -v_0$, as the shock moves into fluid which is at rest with respect to the laboratory frame. The Rankine-Hugoniot relations yield

$$\begin{aligned} R &\sim R_1 z^{\frac{1}{2}}, \\ \lambda &\sim \lambda_0 + \lambda_1 z^{-\frac{1}{2}}, \\ v &\sim \gamma - 1, \\ v_0 &\sim 1, \end{aligned} \tag{B.3}$$

as $z \to \infty$.

The equations of relativistic hydrodynamics which govern the fluid in the post-shock region are those of conservation of energy-momentum, baryon number and entropy

$$\begin{aligned} &\nabla_a(rfu^a u^b + g^{ab}P) = 0, \\ &\nabla_a(ru^a) = 0, \\ &u^a\partial_a(P/r^\gamma) = 0. \end{aligned} \tag{B.4}$$

In our coordinate system these equations take the form

$$\begin{aligned} &rfu^a\partial_a\lambda + v^a\partial_a P = 0, \\ &u^a\partial_a r + rv^a\partial_a\lambda = -r\frac{u^a\sqrt{g}_{,a}}{\sqrt{g}}, \\ &u^a\partial_a r - \tfrac{1}{a^2}u^a\partial_a P = 0. \end{aligned} \tag{B.5}$$

Here, we have used the parametrization $u^a = (\cosh\lambda, \sinh\lambda, 0)$, and $v^a = (\sinh\lambda, \cosh\lambda, 0)$. Notice that

$$u^{\bar{t}}j \equiv u^a\sqrt{g}_a = u^{\bar{t}}\sigma_{\bar{t}} + u^{\bar{\sigma}}\sigma_{\bar{\sigma}} = u^{\bar{t}}(-v_0 + v)\alpha^{-1} \sim u^{\bar{t}}(\gamma - 2)\alpha^{-1}. \tag{B.6}$$

Use the third equation in (B.5) to write the first two equations therein in terms of λ and P. The first two equations in (B.5) may then be written as

$$\begin{array}{ll}(\partial_{\bar{t}} + w^+\partial_{\bar{\sigma}})\lambda + \frac{1}{A}(\partial_{\bar{t}} + w^+\partial_{\bar{\sigma}})P & = -\frac{\beta}{1+\beta v}\frac{j}{\sigma}, \\ (\partial_{\bar{t}} + w^-\partial_{\bar{\sigma}})\lambda - \frac{1}{A}(\partial_{\bar{t}} + w^-\partial_{\bar{\sigma}})P & = +\frac{\beta}{1-\beta v}\frac{j}{\sigma}, \end{array} \tag{B.7}$$

where $w^{\pm} = \frac{v\pm\beta}{1\pm\beta v}$, $\beta = \frac{a}{\sqrt{f}}$ and $A = a\sqrt{f}r$ with $a^2 = \gamma P/r$. Notice that $A \sim \frac{\sqrt{\gamma-1}}{\gamma P}$ and $\partial_{\bar{t}}\lambda|_{\bar{\sigma}=0} \sim -\frac{\lambda_1}{2z^{3/2}}\frac{dz}{d\bar{t}}$ (on the shock surface $(\bar{t}, 0, \phi)$) as $z \to \infty$. Consequently, the term $\partial_{\bar{t}}\lambda$ is of higher order in (B.7). We are therefore left with

$$\begin{array}{ll} w^+\partial_{\bar{\sigma}}\lambda + \frac{1}{A}(\partial_{\bar{t}} + w^+\partial_{\bar{\sigma}})P & = -\frac{\beta}{1+\beta v}\frac{j}{\sigma}, \\ w^-\partial_{\bar{\sigma}}\lambda - \frac{1}{A}(\partial_{\bar{t}} + w^-\partial_{\bar{\sigma}})P & = +\frac{\beta}{1-\beta v}\frac{j}{\sigma}. \end{array} \tag{B.8}$$

Combining these two equations yields an equation for $\partial_{\bar{t}}P$:

$$\frac{w^+ + w^-}{2}\frac{1}{A}\partial_{\bar{t}}P \sim -\frac{\beta}{\sigma}\frac{1}{2}\left(\frac{w^-}{1+\beta v} + \frac{w^-}{1-\beta v}\right)j \tag{B.9}$$

on the shock surface $\bar{\sigma} = 0$. Using the identities $\frac{w^+ + w^-}{2} = v\frac{1-\beta^2}{1-\beta^2 v^2}$ and $\frac{1}{2}\left(\frac{w^-}{1+\beta v} + \frac{w^+}{1-\beta v}\right) = \frac{v}{1-\beta^2 v^2}$ this last equation amounts to

$$\frac{1}{P}\partial_{\bar{t}}P \equiv \frac{1}{\alpha}\frac{1}{P}\partial_t P \sim -\frac{\gamma}{2-\gamma}\frac{j}{\sigma}, \tag{B.10}$$

where we have used $A \sim \gamma P/\sqrt{\gamma-1}$ and $\beta \sim \sqrt{\gamma-1}$ as $z \to \infty$. It follows that

$$\frac{1}{P}\partial_t P \sim \frac{\gamma}{2-\gamma}\frac{\alpha j}{\sigma} \sim \frac{\gamma}{\sigma} \tag{B.11}$$

in the shock surface in the limit as z tends to infinity, and the shock evolves as

$$\frac{P}{P_0} \sim \Sigma(t)^{\gamma}. \tag{B.12}$$

Finally, $\lambda(\bar{t},\bar{\sigma})$ of the form $\lambda \sim \lambda_0+\lambda_1 P^{-\frac{1}{2}}+j\frac{\bar{\sigma}}{\sigma}$ shows existence for solving the asymptotic equations (B.8) by suitable choice of λ_2, as $\partial_{\bar{t}}\lambda = \lambda_2\frac{j}{\sigma} = \lambda_2\frac{j}{\Sigma(t)}$ at $\bar{\sigma} = 0$. Now let t^* denote the moment of reflection of the shock at the origin, so that $\Sigma(t) \sim t^* - t$ as a consequence of (B.3).

The asymptotic solutions can now be given as

$$\begin{aligned} &\tfrac{P}{P_0} \sim (t^* + x - t)^{-\gamma}, \\ &\lambda \sim \lambda_0 + \lambda_1(t^* + x - t)^{\frac{\gamma}{2}} + \lambda_2\tfrac{x}{t^*+x-t}, \end{aligned} \tag{B.13}$$

as z tends to ∞, valid in a layer $\frac{x}{t^*-t} \ll 1$, where x denotes the distance to the shock surface.

Appendix C

On the structure of Einstein's tensor

An algebraic proof is given on the structure of Einstein's tensor. These results are familiar in particular in a space-time split $\{x^a\} = \{t, x^\alpha\}$ with lapse function N and shift functions N_α. However, we wish to emphasize that the results can also be viewed as an algebraic rather than a geometric property of Einstein's tensor. The purpose of this treatment lies in its possible applications towards numerical integration of the initial value problem in relativity. We begin with the structure of the Ricci tensor.

Lemma C.1 *The Ricci tensor R^a_b is of the form*

$$R^a_b = L^a_b(g_{cd})(\partial_c\partial_d g_{uv}) + P^{ai_1\ldots i_5}(g)Q_{bi_1\ldots i_5}(\partial_c g_{uv}), \tag{C.1}$$

where $P^{ai_1\ldots i_5} = g^{ai_1}g^{i_2i_3}g^{i_4i_5}$ and $Q_{ai_1\ldots i_5}$ is quadratic in its arguments.

Proof. Introduce $P^{ai_1\ldots i_5} = g^{ai_1}g^{i_2i_3}g^{i_4i_5}$. We will analyze R^a_b,

$$R^a_b = g^{ae}\partial_c\Gamma^c_{eb} - g^{ae}\partial_e\Gamma^d_{db} + g^{ae}\Gamma^c_{eb}\Gamma^d_{cd} - g^{ae}\Gamma^c_{ed}\Gamma^d_{cb}. \tag{C.2}$$

The terms containing the first partial derivatives of g_{cd} will be factorized over P. We will do so in three steps.

Step(a): The terms containing the first partial derivatives of g_{cd} in the first two terms of R^a_b will be evaluated using the identity

$$-g^{ad}g^{cu}\partial_e g_{uv}\Gamma^v_{db} \equiv -\frac{1}{2}P^{adcuvw}\partial_e g_{uv}\gamma_{dbw}. \tag{C.3}$$

Using the relations $\partial_c g^{ab} = -g^{au}\partial_c g_{uv}g^{vb}$ and $\Gamma^c_{ab} = \frac{1}{2}g^{cd}[g_{db,a}+g_{ad,b}-g_{ab,d}] \equiv \frac{1}{2}g^{cd}\gamma_{abd}$, it follows that the first partial derivatives of g_{cd} in the first two terms of R^a_b are contained in

$$-\frac{1}{2}P^{adcuvw}(\partial_c g_{uv}\gamma_{dbw} - \partial_d g_{uv}\gamma_{cbw}) \equiv P^{adcuvw}A_{bdcuvw}. \tag{C.4}$$

Continuing this expansion, we find

$$\begin{aligned} A_{bdcuvw} &= -\tfrac{1}{2}g_{uv,c}(g_{wb,d}+g_{dw,b}-g_{db,w}) + \tfrac{1}{2}g_{uv,d}(g_{wb,c}+g_{cw,b}-g_{cb,w}) \\ &= -g_{uv,c}g_{b[w,d]} + g_{uv,d}g_{b[w,c]} - \tfrac{1}{2}g_{uv,c}g_{dw,b} + \tfrac{1}{2}g_{uv,d}g_{cw,b}. \end{aligned} \tag{C.5}$$

Step (b): The terms containing the first derivatives of g_{cd} in the last two terms of R^a_b follow from expanding

$$g^{ad}\Gamma^c_{db}\Gamma^v_{vc} = \frac{1}{4}P^{adcuvw}\gamma_{dbu}g_{vw,c} \tag{C.6}$$

$$g^{ad}\Gamma^c_{dv}\Gamma^v_{bc} = \frac{1}{4}P^{adcuvw}\gamma_{dvu}\gamma_{bcw} \tag{C.7}$$

with

$$\begin{aligned} \tfrac{1}{4}\gamma_{dbu}g_{vw,c} &= \tfrac{1}{4}[g_{ub,d}+g_{du,b}-g_{db,u}]g_{vw,c} = \tfrac{1}{2}g_{vw,c}g_{b[u,d]} + \tfrac{1}{4}g_{vw,c}g_{du,b} \\ \tfrac{1}{4}\gamma_{dvu}\gamma_{bcw} &= \tfrac{1}{4}[g_{uv,d}+g_{du,v}-g_{dv,u}][g_{wc,b}+g_{bw,c}-g_{bc,w}] \\ &= \tfrac{1}{4}g_{uv,d}g_{wc,b} + \tfrac{1}{2}g_{uv,d}g_{b[w,c]} + \tfrac{1}{2}g_{d[u,v]}g_{wc,b} + g_{d[u,v]}g_{b[w,c]}. \end{aligned}$$

Step (c): Thus, Q_{bdcuvw} is obtained by adding the results from Step (a) and Step (b) as

$$Q_{bdcuvw} = Q^{(1)}_{bdcuvw} + Q^{(2)}_{bdcuvw} \tag{C.8}$$

with

$$\begin{aligned} Q^{(1)}_{bdcuvw} &= -g_{uv,c}g_{b[w,d]} + \tfrac{1}{2}g_{uv,d}g_{b[w,c]} + \tfrac{1}{2}g_{vw,c}g_{b[u,d]} - g_{d[u,v]}g_{b[w,c]}, \\ Q^{(2)}_{bdcuvw} &= -\tfrac{1}{2}g_{uv,c}g_{dw,b} + \tfrac{1}{4}g_{uv,d}g_{cw,b} + \tfrac{1}{4}g_{vw,c}g_{du,b}. \end{aligned} \tag{C.9}$$

Here, we have used $g_{cw,b}g_{d[u,v]}P^{adcuvw} = 0$ in view of the symmetry $g_{[cw],b} = 0$. Define the quantities I^{uv}_b and J^{uv}_b by

$$\begin{aligned} I^{uv}_b &:= g_{cd,b}g^{uc}g^{vd}, \\ J^{uv}_b &:= g_{b[c,d]}g^{uc}g^{vd}. \end{aligned}$$

Notice that I^{uv}_b is symmetric and J^{uv}_b is antisymmetric in u and v. Notice also that neither I^{uv}_b nor J^{uv}_b contains $\partial_a g_{a*}$ whenever $b \neq a$. Using this, we obtain

$$\begin{aligned} P^a Q^{(1)}_b &= -g_{uv,c}J^{va}_b g^{cu} + \tfrac{1}{2}g_{vw,c}J^{ca}_b g^{vw} - g_{d[u,v]}J^{vu}_b g^{ad}, \\ P^a Q^{(2)}_b &= -\tfrac{1}{2}g_{uv,c}I^{av}_b g^{cu} + \tfrac{1}{2}g_{vw,c}I^{ac}_b g^{vw} + \tfrac{1}{4}g_{uv,d}I^{uv}_b g^{ad}. \end{aligned}$$

Here, we have used $g_{uv,d}J^{uv}_b = 0$ by symmetry of $g_{uv,d}$ in u and v. This completes the representation of Q.□

The full factorization of the first derivatives in R^a_b we will refer to as the PQ factorization.

Lemma C.2 *The component R^a_b of the Ricci tensor does not depend on*

(i) $\partial_c\partial_c g_{cd}$ for all c, d,

(ii) $\partial_a g_{ab}$ whenever $b \neq a$.

Proof of Part (i): The first part follows from analyzing the second derivatives in R^p_b. An easy calculation shows that R^p_b contains no second derivatives of the form $\partial_a\partial_a g_{a*}$ (all p, b): the second derivatives of the metric in R^p_b are contained in

$$g^{pe}\partial_c\Gamma^c_{eb} - g^{pe}\partial_b\Gamma^c_{ec} \tag{C.10}$$

and, therefore, in

$$\frac{1}{2}g^{pe}g^{cu}[g_{ub,e}+g_{eu,b}-g_{eb,u}]_{,c}-\frac{1}{2}g^{pe}g^{cu}g_{uc,eb}. \tag{C.11}$$

Derivatives of the form $\partial_a\partial_a g_{a*}$ therein appear as

$$\frac{1}{2}g^{pa}g^{au}g_{ub,aa}+\frac{1}{2}g^{pe}g^{au}g_{eu,ba}-\frac{1}{2}g^{pe}g^{aa}g_{eb,aa}-\frac{1}{2}g^{pa}g^{cu}g_{uc,ab}. \tag{C.12}$$

When $b\neq a$, these terms contain $\partial_a\partial_a g_{a*}$ necessarily in the first and third terms as

$$\frac{1}{2}g^{pa}g^{aa}g_{ab,aa}-\frac{1}{2}g^{pa}g^{au}g_{au,aa}=0, \tag{C.13}$$

while when $b=a$ these derivatives are contained in all four terms as

$$\begin{array}{ll} & \frac{1}{2}g^{pa}g^{au}g_{ua,aa}+\frac{1}{2}g^{pe}g^{au}g_{eu,aa}-\frac{1}{2}g^{pe}g^{aa}g_{ea,aa}-\frac{1}{2}g^{pa}g^{cu}g_{uc,aa} \\ = & \frac{1}{2}g^{pa}g^{au}g_{ua,aa}+\frac{1}{2}g^{pa}g^{au}g_{au,aa}+\frac{1}{2}g^{pe}g^{aa}g_{ea,aa}-\frac{1}{2}g^{pa}g^{aa}g_{aa,aa} \\ & -\frac{1}{2}g^{pe}g^{aa}g_{ea,aa}-g^{pa}g^{ac}g_{ac,aa}+\frac{1}{2}g^{pa}g^{aa}g_{aa,aa} \\ = & 0. \end{array} \tag{C.14}$$

Proof of Part (ii): To obtain (ii) $PQ^{(1)}$ and $PQ^{(2)}$ will be analyzed in two steps. We emphasize that in what follows a and b are fixed. In particular, no sum is taken over a as an index.

Step (a): We will now analyze $PQ^{(1)}$ in its dependency on $\partial_a g_{a*}$. We consider the case $b\neq a$. In seeking terms $\partial_a g_{**}$, the relevant terms in $P^aQ_b^{(1)}$ are

$$-g_{uv,a}J_b^{va}g^{au}-\frac{1}{2}g_{du,a}J_b^{au}g^{ad}+\frac{1}{2}g_{dv,a}J_b^{va}g^{ad}. \tag{C.15}$$

Here, we have used $J_b^{aa}=0$. In seeking terms $\partial_a g_{a*}$, conclude

$$-g_{av,a}J_b^{va}g^{aa}-\frac{1}{2}g_{au,a}J_b^{au}g^{aa}+\frac{1}{2}g_{av,a}J_b^{va}g^{ad}=0. \tag{C.16}$$

It follows that no terms of the form $\partial_a g_{a*}$ are present in $P^a Q_b^{(1)}, b \neq a$.

Step (b): In this step we will analyze $PQ^{(2)}$ in its dependence on $\partial_a g_{a*}$. Again, we consider the case $b \neq a$. The terms containing $\partial_a g_{**}$ in $PQ^{(2)}$ are then given by

$$-\tfrac{1}{2} g_{uv,a} I_b^{av} g^{au} + \tfrac{1}{4} g_{uv,a} I_b^{uv} g^{aa} + \tfrac{1}{4} g_{vw,a} I_b^{aa} g^{vw}. \tag{C.17}$$

In seeking terms of the form $\partial_a g_{a*}$, we encounter the terms

$$-\frac{1}{2} g_{av,a} I_b^{av} g^{aa} - \frac{1}{2} g_{ua,a} I_b^{aa} g^{au} + \frac{1}{2} g_{av,a} I_b^{av} g^{aa} + \frac{1}{2} g_{aw,a} I_b^{aa} g^{aw} = 0, \tag{C.18}$$

where we have used the symmetry $I_b^{[uv]} = 0$. It follows that no terms of the form $\partial_a g_{a*}$ are present in $P^a Q_b^{(2)}, b \neq a$. □

We will now turn to the dependency of the components G_b^a of Einstein's tensor,

$$G_b^a = R_b^a - \frac{1}{2} \delta_b^a R_d^d \tag{C.19}$$

on $\partial_a g_{ac}$. Here, δ_b^a is the Kronecker delta-function. Using the previous Lemma, we find

Theorem C.1 *The components G_b^a of Einstein's tensor do not depend on*

(i) $\partial_a \partial_a g_{cd}$ for all c, d,

(ii) $\partial_a g_{ab}$ for all b.

Proof: The first part is well known. As to the second part, clearly we only need to assert that

$$G_a^a = R_a^a - \frac{1}{2} R_d^d \tag{C.20}$$

has no dependency on $\partial_a g_{a*}$, as the result immediately follows for $G^a_b = R^a_b$ by the previous Lemma whenever $b \neq a$. Here, no sum is taken over a. The Bianchi identity,

$$\nabla_d R^d_a - \frac{1}{2}\nabla_a R^d_d \equiv 0, \tag{C.21}$$

yields

$$\partial_a(R^a_a - \frac{1}{2}R^d_d) \equiv -\Gamma^a_{ac}R^c_a + \Gamma^c_{aa}R^a_c - \sum_{c\neq a}\partial_c R^c_a. \tag{C.22}$$

Consequently, the right-hand side in this equation (C.22) contains no dependency on $\partial_a\partial_a g_{a*}$ by the previous Lemma on R^a_b. Conclude that

$$G^a_a = R^a_a - \frac{1}{2}R^d_d \tag{C.23}$$

possesses no dependency on $\partial_a g_{a*}$. This completes the proof of the Theorem. □

The dependency of G^a_b on its arguments can be summarized as follows. Let $\{x^a\}$ be a coordinate system. Fix a coordinate a^* and denote by $\cdot$ the derivative ∂_{a^*} (for example, a^* denotes a time-like coordinate, t). Then the dependency of G^a_b on its arguments g_{cd}, $\dot{g}_{cd}$ and $\ddot{g}_{cd}$ is as follows:

$$G^a_b = \begin{cases} \phi_b(g_{cd}, \dot{g}_{\alpha\beta}) \text{ if } a = a^*, \\ G^\alpha_b(\dot{g}_{cd}, \ddot{g}_{\alpha\beta}) \text{ if } a = \alpha \neq a^*, \end{cases} \tag{C.24}$$

where only dependence on the highest appearing a^*−derivatives has been made explicit.

Bibliography

[1] Anile A. *Relativistic Fluids and Magneto-Fluids.* Cambridge University Press, Cambridge, 1989.

[2] Anile A. and Bruhat Y. (eds.). *Lecture Notes in Mathematics: Relativistic Fluid Dynamics.* Springer-Verlag, Hamburg, 1987.

[3] Canuto C. Hussaini M.Y. Quarteroni A. and Zang T.A. *Spectral methods in fluid mechanics.* Springer-Verlag, Berlin, 1988.

[4] Harten A. Eno schemes with subcell resolution. *J. Comp. Phys.*, 54:148–184, 1984.

[5] Lapidus A. Computation of radially symmetric shocked flows. *J. Comp. Phys.*, 8:106–118, 1971.

[6] Lichnerowicz A. Etudes mathematique des fluides thermodynamique relativiste. *Comm. Math. Phys.*, 1:328–373, 1966.

[7] Lichnerowicz A. *Relativistic Hydrodynamics and Magnetodynamics.* W. A. Benjamin Inc., New York, 1967.

[8] Lichnerowicz A. Shock waves in relativistic magnetohydrodynamics under general assumptions. *J. Math. Phys.*, 17:2135–2142, 1976.

[9] Eringen A.C. and Maugin G.A. *Electrodynamics of Continua II.* Springer-Verlag, New York, 1990.

[10] Fischer A.E. and Marsden J.E. The Einstein evolution equations as a first-order quasi-linear symmetric hyperbolic system. *Comm. Math. Phys.*, 28:1–38, 1972.

[11] Sod A.G. A survey of several finite difference methods for systems of nonlinear hyperbolic conservation laws. *J. Comp. Phys.*, 27:1–31, 1978.

[12] Carter B. and Gaffet B. Standard covariant formulation for perfect-fluid dynamics. *J. Fluid. Mech.*, 186, 1988.

[13] Orszag B. and Tang M.C. Small-scale structure of two-dimensional magnetohydrodynamic turbulence. *J. Fluid Mech.*, 90:129–143, 1979.

[14] Fanaroff B.L. and Riley J.M. The morphology of extragalactic radio sources of high and low luminosity. *Mon. Not. R. astr. Soc.*, 167:31p–35p, 1974.

[15] Choquet Bruhat Y. DeWitt-Morette C. and Dillard-Bleick M. *Analysis, Manifolds and Physics, Part I:Basics.* North-Holland, Amsterdam, 1982.

[16] Evans R. C. and Hawley J. F. Simulation of magnetohydrodynamic flows: a constrained transport method. *AP. J.*, 332:659–677, 1988.

[17] Courant and Hilbert. *Partial Differential Equations.* Interscience Publications, New York, 1967.

[18] Shu C.W. and Osher S. Efficient implementation of essentially non-oscilatory shock-capturing schemes ii. *J. Comp. Phys.*, 54:32–78, 1984.

[19] Taub A.H. Relativistic Rankine-Hugoniot equations. *Phys. Review*, 74:328–334, 1948.

[20] Phinney E.S. A theory of radio sources. *Ph.D. Thesis*, Cambridge, 1983.

[21] Strang G. On the construction and comparison of difference schemes. *SIAM J. Numer. Anal.*, 5:506–517, 1968.

[22] Eulderink F. A general relativistic Roe solver. *(unfinished Ph.D. thesis).*

[23] Witham G.R. *Linear and Nonlinear Waves.* J. Wiley and Sons, New York, 1974.

[24] Bethe H.A. Supernova mechanisms. *Rev. Mod. Phys.*, 62:801–866, 1990.

[25] Zhang H.S. and So R.M. A flux-coordinate-splitting technique for flows with shocks and contact discontinuities. *Computers Fluids*, 20:421–442, 1991.

[26] Wu C.C. On MHD intermediate shocks. *Geophys. Res. Lett.*, 14:668–671, 1987.

[27] Bazer J. and Ericson W.B. Hydromagnetic shocks. *Ap. J.*, 129:758–785, 1959.

[28] Yang J. *An analytical and computational investigation of shock-induced vortical flows with applications to supersonic combustion.* Ph.D. Thesis, California Institute of Technology, Pasadena, 1991.

[29] Lind K.R. Numerical jet simulations and parsec-scale jets, in *Parsec – Scale Radio Jets.* Zensus J.A. and Pearson T.J. (eds.), Cambridge Univ. Press, New York, 1990.

[30] Marti J.M. Ibanez J.M. and Mirallos J.A. Numerical relativistic hydrodynamics: local characteristic approach. *Physical Review D*, 43:3794–3801, 1991.

[31] Friedrichs K.O. On the laws of relativistic electro-magneto-fluid dynamics. *Comm. Pure and Appl. Math.*, 28:749–808, 1974.

[32] Misner C.W. Thorne K.S. and Wheeler J.A. *Gravitation.* Freeman and Company, San Fransisco, 1973.

[33] Herrera L. and Nunez L.A. Luminosity profiles and the evolution of shock waves in general-relativistic radiating spheres. *Ap. J.*, 364:212–221, 1990.

[34] Hawley J.F. Smarr L.L., Wilson J.R. A numerical study of nonspherical black hole accretion. I. Equations, and test problems. *Ap. J.*, 55:211–246, 1984.

[35] Hawley J.F. Smarr L.L., Wilson J.R. A numerical study of nonspherical black hole accretion. II. Finite differencing, and code calibration. *Ap. J.*, 55:211–246, 1984.

[36] Anile A. M. and Pennisi S. On the mathematical structure of test relativistic magnetohydrodynamics. *Ann. Inst. H. Poincare*, 46:27–44, 1987.

[37] Brio M. and Wu C.C. An upwind differencing scheme for the equations of ideal magnetohydromagnetics. *J. Comp. Phys.*, 75:400–422, 1988.

[38] Wald R. M. *General Relativity.* University of Chicago Press, Chicago, 1984.

[39] Burns J.O. Norman M.L. and Clarke D.A. Numerical models of extragalactic radio sources. *Science*, 253:522–530, 1991.

[40] Dubal M.R. Numerical simulations of special relativistic, magnetic gasflows. *Comput. Phys.*, 64(2):221–234, 1991.

[41] Muscato O. Breaking of relativistic simple waves. *J. Fluid Mech.*, 196:223–239, 1988.

[42] Warner F.W. Foundations of Differential Manifolds and Lie Groups. Springer-Verlag, New York, 1983.

[43] Colella P. and Woodward P. The piecewise parabolic method (ppm) for gas-dynamical simulations. *J. Comp. Phys.*, 54:174–201, 1984.

[44] Garabedian P. *Partial Differential Equations.* Chelsea, New York, 1986.

[45] Meszaros P. and Ostriker J.P. Shocks in spherically accreting black holes: a model for classical quasars. *Ap. J.*, 273:L59–L63, 1983.

[46] Woodward P. and Colella P. The numerical simulation of two-dimensional fluid flow with strong shocks. *J. Comp. Phys.*, 54:115–173, 1984.

[47] Scheuer P.A.G. Models of extragalactic radio sources with a continuous energy supply from a central object. *Mon. Not. R. Astr. Soc.*, 166:513–528, 1974.

[48] Peyret R. and Taylor T.D. *Computational Methods for Fluid Flow.* Springer Verlag, New York, 1983.

[49] Payne R.B. A numerical method for a converging cylindrical shock. *J. Fluid Mechanics*, 2:185–200, 1957.

[50] Kennel C.F. Blandford R.D. and Coppi P. MHD intermediate shock discontinuities. Part I. Rankine-Hugoniot conditions. *J. Plasma Physics*, 42:299–319, 1989.

[51] Stone J.M. Hawley J.F. Charles R.E. and Norman M.L. A test suite for magnetohydrodynamical simulations. *Ap. J.*, 388:415–437, 1992.

[52] Roe P.L. Approximate Riemann solvers, parameter vectors and difference schemes. *J. Comp. Phys.*, 43:357–372, 1981.

[53] Munz C.D. Two step schemes for the Euler equations and numerical experiments on the stability of converging cylindrical shock waves. *Shock Tubes and Waves*, Sixteenth Int. Symp. Shock Tubes and Waves, Aachen, West Germany, July 26-31, 1987.

[54] van Dijk R. The general relativistic Riemann problem. *private communication*, 1990.

[55] van Putten M.H.P.M. A numerical implementation of MHD in divergence form. *(submitted to J. Comp. Phys.)*.

[56] van Putten M.H.P.M. Maxwell's equations in divergence form with applications to MHD. *Commun. Math. Phys.*, 141:63–77, 1991.

[57] Bruhat Y. Fluides relativiste de conductibilite infinie. *Acta Astronautica*, 6:354–363, 1960.

[58] Bruhat Y. Etudes des equations des fluides relativistes charges et inductive conducteurs. *Commun. Math. Physics*, 3:334–357, 1966.

[59] Muller zum Hagen H. and Seifert H.J. On characteristic initial-value and mixed problems. *General Relativity and Gravitation*, 8:259–301, 1977.